Apatite Formation on Organic-inorganic Composites Modified with Phosphorus- or Sulfur-containing Functional Groups in Simulated Body Environment

(リンもしくは硫黄含有官能基で修飾した有機-無機複合体での擬似体液環境下におけるアパタイト形成)

Ryo Hamai

2018

Contents

General Introduction

1. Bone-bonding bioactivity materials and organic-inorganic composites

Bone substitutes have been clinically employed for repairing bone defect caused by serious accidents or diseases. Implantation of the artificial materials would contribute to keeping quality of our life (QOL) after healing the damage due to replacing the lost function of bone. Moreover, it can decrease the risks of infection and injury of the healthy bone occurred by allogenic and autogenous bone grafts. However, artificial materials are encapsulated and isolated from surrounding the living bone with fibrous tissue, when they are implanted into the part of bone defect [1]. This encapsulation is a drawback to fixation of the implants for long-term.

Hench *et al.* first discovered that Bioglass® (CaO-Na_2O-P_2O_5-SiO_2) [2-3] could bond with bone tissue directly. Contentiously, glass-ceramic A-W was developed by Kokubo *et al.* [4-7]. It improved the mechanical properties of bone-bonding bioactive glass as a result of MgO-CaO-SiO_2 including crystalline phases of oxyfluorapatite and β-wollastonite. They showed that bending strength of it is higher than that of human cortical bone. In addition, sintered hydroxyapatite ($Ca_{10}(PO_4)_6(OH)_2$), which has composition similar to inorganic component of living bone, was fabricated [7-10]. These bioactive ceramics have been already applied as bone substitute owing to their anomalous bone-bonding ability [12-14].

However, these bioactive ceramics show higher Young's moduli as compared with natural bone. The moduli of cortical and cancellous bone of are about 7-30 and 0.05-0.5 GPa, respectively [15-16]. On the other hand, the moduli of glass-ceramic A-W and sintered hydroxyapatite are more than that of cortical bone [10, 17]. This mismatch of Young's moduli blocks the transmission of the loading to bone tissue surrounding the implantation part, i.e. stress-shielding [18]. Generally, mechanical stimulus against bone cells is one of the factors for bone metabolism. The stress-shielding causes the inhabitation of the remodeling of healthy bone tissue, and subsequent bone adsorption

[19]. In addition, the bending and compressive strength of some kind of bone-bonding bioactive ceramics are higher than that of cortical bone, but their low toughness is concerned about fracture of the implant in living body [10]. In contrast, natural bone consists collagen fiber and calcium-deficient carbonate apatite [20] oriented c-axis toward the direction of the fiber length [21-22]. Such organic-inorganic composite structures are arranged and assembled hierarchically to construct our bone [23-24]. It is a reason of mechanical properties of the living bone which has the higher fracture toughness, bending strength and flexibility. Therefore, fabrication of artificial bioactive organic-inorganic composite materials has been used to solve these problems.

According to the previous studies, bioactive ceramics formed Ca-P-rich layer as low crystalline apatite on their surface [6,25-28], and then osteoblasts modeling the new bone matrix attach on the layer to bond with living bone [28-29]. Thus, ability to form the apatite layer is one of the key factors to make the bonding between artificial materials and bone tissue. The mechanism of the apatite layer formation on the surface of glass-type bioactive ceramics were also examined in simulated body fluid (SBF) [30]. SBF has component of inorganic ions analogous to human blood plasma without proteins [31-32]. Currently, using SBF is a method for assessment of apatite-forming ability *in vitro* to develop the bioactive materials [32]. Ohtsuki *et al.* revealed that hydrated $CaO\text{-}SiO_2$ glass surface and Ca^{2+} release from the glass into the fluid take an important role to induce heterogeneous nucleation of apatite in SBF [33]. Contentiously, it was found that Si-OH groups in the hydrated glass surface induce the heterogeneous nucleation of apatite [34].

Since these discoveries, some researchers found other kinds of functional groups contributing to apatite formation in SBF, for example Ti-OH [35], $-PO_3H_2$ [36], -COOH[36], Zr-OH [37], Ta-OH[38], Nb-OH [39] and $-SO_3H$[40] groups, by using the model surface such as the metal oxide hydrogel and the self-assembly monolayer. These fundamental results have been giving the motivation of preparation the novel bone-bonding bioactive materials, which show the high toughness and flexibility, based on organic-inorganic composites. In fact, Tsuru *et al.* fabricated polydimethylsiloxane-CaO-

SiO_2 nanocomposites forming apatite layer due to the presence of Si-OH groups and Ca release in SBF [41]. Kamitakahara *et al.* achieved preparation of nanocomposites of Si-polytetramethyleneoxide-TiO_2 and -Ta_2O_5 exhibiting apatite-forming ability and Young's moduli similar to the cancellous bone [42-43].

2. Modification with phosphorus- sulfur-containing functional groups to fabricate the bioactive composites

Phosphate (-PO_3H_2) group has been attracted attention for improving the ability of implants repairing the bone defects. They have two types of molecular structure: phosphoric acid (-O-PO_3H_2) and phosphonic (-C-PO_3H_2) acid [44]. For example, Tanahashi *et al*. revealed that the -O-PO_3H_2 on the self-assembly monolayer formed more amount of apatite rapidly as compared with -COOH and -OH groups in SBF [36]. Datta *et al.* reported that modification with the -O-PO_3H_2 *via* phosphorylation reaction affected increase in proliferation of osteoblast-like cells, and induced calcium phosphate formation on the poly(vinyl alcohol) film and fiber *in vitro* [45]. Recently, Huang *et al*. reported that modification of -O-PO_3H_2 promoted the differentiation of mesenchymal stem cells which subsequently caused the mineralization on the poly(sebacoyl diglyceride) [46]. Furthermore, the activities of osteoblast-like cells on the poly(vinylphosphonic acid (VPA)-acrylamide) hydrogel were improved as number of -C-PO_3H_2 units in the gel increased [47]. Grafting of the poly(VPA) using plasma induced polymerization also could enhance the affinity for osteoblast on the biodegradable polymers such as chitosan and ε-polycaprolactone [48-49].

Modification with sulfonic acid (-SO_3H) groups also has been tried to fabricate the implants showing bone-bonding ability. Sulfuric acid treatment was carried out for incorporation of these groups on the surface of the high molecular weight polyethylene [50] and polyetheretherketone (PEEK) [51]. These polymers modified with -SO_3H and treated with calcium salt solution could form bone-like apatite in SBF. Polysaccharide of λ- and κ-carrageenan delivers the organic matrix consisting a lot of -SO_3H groups. Nakata

et al. and Kim *et al.* prepared organic-inorganic composite [52] and thermoreversible hydrogel [53], respectively, by using carrageenan modified with Ca^{2+}. They also had a potential to deposit the apatite layer. On the other hand, sodium *p*-toluene sulfinate (*p*-TSS) is a compound of sulfinic acid derivative. In dental field, the compound has been clinically applied as the radical polymerization accelerators to set the self-adhesive dental resin [54]. Sulfonic acid and sulfinic acid ($-SO_2H$) groups are composed of the same element, but bone-bonding ability of latter has been remained unclear.

These previous studies indicate that incorporation of phosphorus- or sulfur-containing acidic functional groups into the polymer has a potential to fabricate organic matrix of composites, which have biocompatibility and apatite-forming ability to bond with bone tissue.

3. Purpose of this study

The purpose of the study in this thesis is examination of the apatite-forming ability of polymer-$CaCl_2$ composites modified with phosphorus- or sulfur-containing acidic functional groups in SBF, to establish the guideline to design the polymer as organic matrix of the composites showing bone-bonding ability in terms interaction with Ca^{2+}.

Apatite deposition on the material is governed by surface condition and supersaturation degree with respect to apatite in the physiological condition, suggested by the equation giving activation free energy to induce heterogeneous nucleation [33, 55]. Especially, Ca^{2+} adsorption on the surface is considered as a trigger to induce the heterogeneous nucleation of the apatite on the surface in SBF [36, 56-57]. The surface after adsorption of Ca^{2+} allows adsorption of phosphate ion in SBF to form precursor of apatite. Miyazaki *et al.* reported that density of apatite was increased as number of -COOH groups on the polyamide film increased, because much $-COO^{-}\cdots Ca^{2+}$ ion-ion interaction occurred on the film following soaking in simulated body environment [58]. Moreover, it was also reported that Ca^{2+} release to increase the supersaturation degree in

SBF was suppressed by increase in amount of $-SO_3^-\cdots Ca^{2+}$ formation in the composites [59].

Thus, content of phosphate group in the polymer chain also would influence the condition of composite surface and surrounding fluid to form apatite in terms of Ca^{2+} interaction. Although calcification on the copolymer incorporated different amount of phosphate groups was investigated in SBF [60], the detail of surface condition changed by the different content related to the apatite-forming behavior has been not presented. Furthermore, it is assumed that the difference in specific molecular structure in phosphorus- or sulfur-containing acidic functional groups also affects apatite-forming behavior. Stability of ionized acidic functional groups is increased by electron delocalization depend on the some factor such as electronegativity of element in the acid [61-62]. It would lead to the change in binding state between Ca^{2+} and functional group which subsequently impact the surface condition and Ca^{2+} release behavior of the composites. Consequently, to clarify of these points fundamentally is important issue to select the structure of polymer in the composites exhibiting high ability to form apatite in physiological condition.

Radical polymerization is one of the conventional methods to incorporate the functional groups. Gemeinhart *et al.* carried out this method to obtain the copolymer with different ratio of phosphate or sulfonate groups units against other monomers [46, 63-64]. Therefore, they showed definitely that these groups were able to enhance the osteoblast activity *in vitro*. It is expected that radical polymerization is able to synthesize the model of composites to determine the suitable structure modified with these acidic functional groups to achieve the high apatite-forming ability. However, phosphate-containing vinyl monomer sometime inhibits radical polymerization reaction using tertiary amine as initiator system [65-66]. It would cause the dissolution of the unreacted monomers and/or low molecular weight polymer from the substrate, and subsequent decrease in pH in the fluid. Thus, approach to improve the chemical durability of phosphate-containing copolymer also should be examined to evaluate the apatite-forming ability of composites

for achievement of aims in this study.

In Chapter 1, the phosphate groups-containing copolymer were prepared from VPA and triethylene glycol dimethacrylate (TEGDMA) *via* radical polymerization. Different amount of *p*-TSS as polymerization accelerator was added during the polymerization reaction. The chemical durability and apatite-forming ability of different copolymer were investigated in SBF. Change in the degradation behavior of the copolymer was discussed by the hydrophilic property depend on the phosphate group content and molecular weight cross-linking density.

In Chapter 2, the apatite-forming ability on the polymer-$CaCl_2$ composites consisting different amount of phosphate groups were examined in SBF. The composites were prepared through the polymerization of VPA, 2-hydroxyethylmethacrylate (HEMA) and TEGDMA and treatment with $CaCl_2$ solution. The surface condition and Ca^{2+} release of composites were measured to discuss the reason why different apatite-forming behavior occurred by change in phosphate content in terms of Ca^{2+} interaction.

In Chapter 3, the behavior of apatite formation on the polymer-$CaCl_2$ composites modified with -C-PO_3H_2 and that with -O-PO_3H_2 prepared from VPA and methacryloyloxyethyl phosphate, respectively, were compared in SBF. The stability of interaction between Ca^{2+} and each type of phosphate was evaluated quantitatively and mechanism of the apatite formation on the surface was discussed by using chemical analysis and computational approach.

In Chapter 4, -SO_2H groups on the surface were investigated whether they are able to induce heterogeneous nucleation of apatite in SBF. The morphology and adhesive strength of apatite formed on the polymer-$CaCl_2$ composites prepared form sodium 4-vinylbenzene sulfinate ($NaVBSO_2$) and HEMA were evaluated. These results were compared with the composites prepared from poly(HEMA) or other materials inducing apatite formation reported in previous research to determine the ability of -SO_2H groups in SBF.

In Chapter 5, the apatite-forming ability of polymer-$CaCl_2$ composites modified

with -SO_2H or -SO_3H prepared using $NaVBSO_2$ or sodium 4-vinylbenzene sulfonate, respectively, were examined. The release amount of Ca^{2+} into SBF with soaking of each composites and stability of Ca^{2+} complex consisting of each structure of acid under physiological condition were determined to discuss the structural effects of sulfur-containing acidic functional groups on apatite formation.

In General Summary, the result of each Chapter described above were summarized and discussed the relationship between the structure of polymer in the composites consisting of these acidic functional groups and apatite-forming ability in SBF.

Reference

[1] S.F. Hulbert, "The use of alumina and zirconia in surgical implant", *An introduction to bioceramics*, ed. by L.L Hench, J. Wilson, Word Scientific Publishing, Singapore, 25-40 (1993).

[2] L.L. Henchi, R.J. Splinter, W.C. Allen, T.K. Greenlee, "Bonding mechanism at the interface of ceramic prosthetic materials," *J. Biomed. Mater. Res.*, **2**, 117-142 (1972).

[3] LL. Hench, "Bioceramics," *J. Am. Ceram. Soc.*, **81**, 1705-1728 (1998).

[4] T. Kokubo, M. Shigematsu, Y. Nagashima, M. Tashiro, T. Nakamure, T. Yamamuro, S. Higashi, "Apatite- and wollstonite-containing glass-ceramics for prosthetic application," *Bull. Inst. Chem. Res., Kyoto Univ.*, **60**, 260-268 (1982).

[5] T. Kokubo, "Bioactive glass ceramics: properties and applications" *Biomaterials*, **12**, 155-163 (1991).

[6] T. Kokubo, "Bioactive glass ceramics," *Bioceramics and their clinical applications*, ed. by T. Kokubo, Wooden Publishing, Cambridge, 284-301 (2008).

[7] M. Jarcho, C.H. Bolen, M.B. Thomas, J. Bobick, J.F. Kay, R.H. Doremus, "Hydroxyapatite synthesis and characterization in dense polycrystalline forms," *J. Mater. Sci.*, **11**, 2161-2175 (1976).

[8] M. Jacho, J.L. Kay, R.H. Gumaer, H.P. Drobeck, "Tissue, cellular and subcellular events at bone-ceramics hydroxyapatite interface," *J. Bioeng.*, **1**, 79-92 (1977).

[9] H. Aoki, K. Kato, T. Tabata, "Osteocompatibility of apatite ceramics in dog's mandibles," *Rep. Inst. Med. Dent. Eng. Japan*, **11**, 33-35, (1977).

[10] H. Aoki, K. Kato, M. Ogiso, T. Tabata, "Sintered hydroxyapatite as a new dental implant materials," *J. Dnt. Outlook*, **49**, 567-575 (1977).

[11] T. Kokubo, H.-M. Kim, M. Kawashita, "Novel bioactive materials with different mechanical properties," *Biomaterials*, **24**, 2161-2175 (2003).

[12] L.L. Hench, "Bioceramics; From Concept to Clinic," *J. Am. Ceram Soc.*, **74**, 1487-1510 (1991).

[13] T. Yamamuro, "Clinical application of bioactive glass ceramics," *Bioceramics and their clinical applications*, ed. by T. Kokubo, Wooden Publishing, Cambridge, 583-605 (2008).

[14] R.Z. LeGeros, "Hydroxyapatite," *An introduction to bioceramics*, ed. by L.L Hench, J. Wilson, Word Scientific Publishing, Singapore, 139-180 (1993).

[15]J.Y. Rho, R.B. Ashman, C.H. Turner, "Young's modulus of trabecular and cortical bone material: ultrasonic and microtensile measurements," *J. Biomech.*, **26**, 111-119 (1993).

[16] J.Y. Rho, L.K. Spearing, P.Z. Ziupos, "Mechanical properties and the hierarchical structure of bone," *Med. Eng. Phys.*, **20**, 92-102 (1998).

[17] M. Akao, H. Aoki, K. Kato, "Mechanical properties of sintered hydroxyapatite for prosthetic applications," *J. Mater. Sci.*, **16**, 809-812 (1981).

[18] M. Niinomi, T. Hattori, K. Morikawa, T. Kasuga, A. Suzuki, H. Fukui, S. Niwa, "Development of low rigidity β-type titanium alloy for biomedical applications," *Mater. Trans.*, **43**, 2970-2977 (2002).

[19] Y. Noyama, T. Miura, T. Ishimoto, T. Itaya, M. Niinomi, T. Nakano, "Bone loss and reduced bone quality of the human femur after Total hip arthroplasty under stress-shielding effects by titanium-based implant," *Mater. Trans.*, **53**, 565-570 (2012).

[20] R.Z. LeGeros, J.P. LeGeros, "Hydroxyapatite," *Bioceramics and their clinical applications*, ed. by T. Kokubo, Wooden Publishing, Cambridge, 367-394 (2008).

[21] W.J. Landis, K.J. Hodgens, J. Arena, M.J. Song, B.F. McEwen, "Structure Relation between collagen and mineral in bone as determined by high voltage electron microscopic tomography," *Micros. Res. Tech.*, **33**, 192-202 (1996).

[22] T. Nakano, K. Kaibara, Y. Tabata, N. Nagata, S. Enomoto, E. Marukawa, Y. Umakoshi, "Unique alignment and texture of biological apatite crystallites in typical calcified tissues analyzed by microbeam X-ray diffractometer system," *Bone*, **31**, 479-487 (2002).

[23] W.J. Landis, "The strength of a calcified tissue depends in part on the molecular structure and organization of its constituent mineral crystal in their organic matrix," *Bone*, **16**, 533-544 (1995).

[24] S. Weiner, H.D. Wagner, "The material bone: structure mechanical function relation," *Annu. Rev. Mater. Sci.*, **28**, 271-298 (1998).

[25] T. Kitsugi, T. Nakamura, T. Yamamuro, T. Kokubo, T. Shibuya, M. Takagi, "SEM-EPMA observation of three types of apatite-containing glass-ceramics implanted in bone: The variance of a Ca-P-rich layer," *J. Biomed. Mater. Res.*, **21**, 1255-1271 (1987).

[26] T. Kokubo, S. Ito, Z.T. Huang, T. Hayashi, S. Sakka, T. Kitsugi and T. Yamamuro, "Ca, P-rich layer fromed on the high-strength bioactive glass-ceramic A-W," *J. Biomed. Mater. Res.*, **24**, 331-343 (1990).

[27] M. Neo, S. Kotani, T. Nakamura, T. Yamamuro, C. Ohtsuki, T. Kokubo, Y. Bando, "A comparative study of ultrastructures of the interfaces between four kinds of surface-active ceramic and bone," *J. Biomed. Mater. Res.*, **26**, 1419-1432 (1992).

[28] M. Neo, T. Nakamura, T. Yamamuro, C. Ohtsuki, T. Kokubo, "Apatite formation on three kinds of bioactive material at an early stage in vivo: A comparative study by transmission electron microscopy," *J. Biomed. Mater, Res.*, **27**, 999-1006 (1993).

[29] L.L. Hench, O. Anderson, "Bioactive glass," *An introduction to bioceramics*, ed. by L.L Hench, J. Wilson, Word Scientific Publishing, Singapore, 41-62 (1993).

[30] T. Kokubo, H. Kushitani, S. Sakka, T. Kitsugi, T. Yamamuro, "Solution able to reproduce in vivo surface-structure change in bioactive glass-ceramic A-W," *J. Biomed.*

Mater. Res., **24**, 721-734 (1990).

[31] S.B. Cho, T. Kokubo, K. Nakanishi, N. Soga, C. Ohtsuki, T. Nakamura, T. Kitsugi, T. Yamamuro, "Dependence of apatite formation on silica gel on its structure: Effect of heat treatment," *J. Am. Ceram. Soc.*, **78**, 1769-1774 (1995).

[32] T. Kokubo, H. Takadama, "How useful is SBF in predicting in vivo bone bioactivity?" *Biomaterials*, **27**, 2907-2915 (2006).

[33] C. Ohtsuki, T. Kokubo, T. Yamamuro, "Mechanism of apatite formation on CaO-SiO_2-P_2O_5 glass in a simulated body fluid," *J. Non-Cryst. Sol.*, **143**, 84-92 (1992).

[34] P. Li, C. Ohtsuki, T. Kokubo, K. Nakanishi, N. Soga, T. Nakamura, T. Yamamuro, "Apatite formation induced by silica gel in a simulated fluid," *J. Am. Ceram. Soc.*, **75** 2094-2097 (1992).

[35] R. Li, C. Ohtsuki, T. Kokubo, K. Nakanishi, N. Soga, K. Groot, "The Role of hydrated silica, titania, and alumina in inducing apatite on implants," *J. Biomed. Mater. Res.*, **28**, 7-15 (1995).

[36] M. Tanahashi, T. Matsuda, "Surface functional group dependence on apatite formation on self-assembled monolayers in a simulated body fluid," *J. Biomed. Mater. Res.*, **34**, 305-315 (1997).

[37] M. Uchida, H.-M. Kim, T. Kokubo, T. Namura, "Bonelike apatite formation induced on zirconia gel in simulated body fluid and its modified solution," *J. Am. Ceram. Soc.*, **84**, 2041-2044 (2001).

[38] T. Miyazaki, H.-M. Kim, T. Kokubo, H. Kato, T. Nakamura, "Induction and acceleration of bonelike apatite formation on tantalum oxide gel in simulated body fluid," *J. Sol-gel. Sci. Tech.*, **21**, 83-88 (2001).

[39] T. Miyazaki, H.-M. Kim, T. Kokubo, C. Ohtsuki, T. Nakamura, "Apatite-forming ability of niobium oxide gels in a simulated body fluid," *J. Ceram. Soc. Japan.*, **109**, 934-938 (2001).

[40] T. Kawai, C. Ohtsuki, M. Kamitakahara, T. Miyazaki, M. Tanihara, Y. Sakaguchi, S. Konagaya, "Coating of an apatite layer on polyamide films containing sulfonic groups by

a biomimetic process. *Biomaterials*, **25**, 4529-4534 (2004).

[41] K. Tsuru, C. Ohtsuki, A. Osaka, T. Iwamoto, J.D. Mackenzie, "Bioactivity of sol-gel derived organically modified silicates: Part I: *In vitro* examination," *J. Mater. Sci.: Mater. Med.*, **8**, 157-161 (1997).

[42] M. Kamitakahara, M. Kawashita, N. Miyata, T. Kokubo, T. Nakamura, "Apatite-forming ability and mechanical properties of CaO-free poly(tetramethylene oxide) (PTMO)-TiO_2 hybrids treated with hot water," *Biomaterials*, **24**, 1357-1363 (2003).

[43] M. Kamitakahara, M. Kawashita, N. Miyata, T. Kokubo, T. Nakamura, "Preparation of bioactive flexible poly(tetramethylene oxide) (PTMO)-CaO-Ta_2O_5 hybrids," *J. Mater. Sci.: Mater. Med.*, **18**, 1117-1124 (2007).

[44] N. Moszner, U. Salz, J. Zimmermann, "Chemical aspects of self-etching enamel-dentin adhesives: A systematic review," *Dent. Mater.*, **21**, 895-910 (2005).

[45] P. Datta, J. Chatterjee, S. Dhara, "Electrospun nanofibers of a phosphorylated polymer -A bioinspired approach for bone graft applications," *Colloids Surf. B: Biointerface*, **94**, 177-183 (2012).

[46] P. Huang, X. Bi, J. Gao, L. Sun, S. Wang, S. Chen, X. Fan, Z. You, Y. Wang, "Phosphorylated poly(sebacoyl diglyceride) - a phosphate functionalized biodegradable polymer for bone tissue engineering," *J. Mater. Chem. B*, **4**, 2090-2101 (2016).

[47] J. Tan, R.A. Gemeinhart, M. Ma, W.M. Saltzman, "Improved cell adhesion and proliferation on synthetic phosphonic acid-containing hydrogels," *Biomaterials*, **26**, 3663-3671 (2005).

[48] P.M. López-Pérez, R.M. Silva, C. Serra, I. Pashkuleva, R.L. Reis, "Surface phosphorylation of chitosan significantly improves osteoblast cell viability, attachment and proliferation," *J. Mater. Chem.*, **20**, 483-491 (2010).

[49] P.M. López-Pérez, R.M. Silva, R.A. Sousa, I. Pashkuleva, R.L. Reis, "Plasma-induced polymerization as a tool for surface functionalization of polymer scaffolds for bone tissue engineering: An in vitro study," *Acta Biomater.*, **6**, 3704-3712 (2010).

[50] I.B. Leonor, H.-M. Kim, F. Balas, M. Kawashita, R.L. Reis, T. Kokubo, T. Nakamura,

"Surface potential change in bioactive polymer during the process of biomimetic apatite formation in a simulated body fluid," *J. Mater. Chem.*, **17**, 4057-4063 (2007).

[51] T. Miyazaki, C. Matsunami and Y. Shirosaki, "Bioactive carbon-PEEK composites prepared by chemical surface treatment", *Mater. Sci. Eng. C*, **70**, 71-75 (2017).

[52] R. Nakata, T. Miyazaki, Y. Morita, E. Ishida, R. Iwatsuki, C. Ohtsuki, "Apatite formation abilities of various carrageenan gels in simulated body environment," *J. Ceram. Soc. Japan,* **118**, 487–90 (2010).

[53] I.Y. Kim, R. Iwatsuki, K. Kikuta, Y. Marita, T. Miyazaki, C. Ohtsuki, "Thermoreversible behavior of κ-carrageenan and its apatite-forming ability in simulated body fluid," *Mater. Sci. Eng. C*, **31**, 1472-1476 (2011).

[54] J. Yamauchi, "Study of dental adhesive resin containing phosphoric acid methacrylate monomer," *J. Jpn. Soc. Den. Mater. Devi.*, **5**, 144-154 (1986).

[55] T. Kawai, C. Ohtsuki, M. Kamitakahara, M. Tanihara, T. Miyazaki, Y. Sakaguchi, S. Konagaya, "A comparative study of apatite deposition on polyamide films containing different functional groups under a biomimetic condition," *J. Ceram. Soc. Japan.*, **113**, 588-592 (2005).

[56] H.-M. Kim, T. Himeno, M. Kawashita, J.H. Lee, T. Kokubo, T. Nakamura, "Surface potential change in bioactive titanium metal during the process of apatite formation in simulated body fluid," *J. Biomed. Mater. Res. A.*, **67A**, 1350-1309 (2003).

[57] H.-M. Kim, T. Himeno, T. Kokubo, T. Nakamura, "Process and kinetics of bonelike apatite formation on sintered hydroxyapatite in a simulated body fluid," *Biomaterials*, **26**, 4366-4373 (2005).

[58] T. Miyazaki, C. Ohtsuki, Y. Akioka, M. Tanihara, J. Nakao, Y. Sakaguchi and S. Konagaya, "Apatite deposition on polyamide films containing carboxyl group in a biomimetic solution," *J. Mater. Sci.: Mater. Med.*, **14**, 569-574 (2003).

[59] T. Miyazaki, M. Imamura, E. Ishida, M. Ashizuka and C. Ohtsuki, "Apatite formation abilities and mechanical properties of hydroxyethylmethacrylate-based organic-inorganic hybrids incorporated with sulfonic groups and calcium Ions," *J. Mater.*

Sci.: Mater. Med., **20**, 157-161 (2009).

[60] I.C. Stancu, R. Filmon, C. Cincu, B. Marculescu, C. Zaharia, Y. Tourmen, M.F. Basle, D. Chappard, "Synthesis of methacryloyloxyethyl phosphate copolymers and in vitro calcification capacity", *Biomaterials*, **25**, 205-213 (2004).

[61] O. Exner, "The inductive effect: theory and quantitative assessment," *J. Phys. Org. Chem.*, **12**, 265-274 (1999).

[62] D.D. Perrin, B. Dempesy, E.P. Sejeant, "Molecular factor that modify pK_a value," *pK_a prediction for organic acid and base*s ed. by DD. Perrin, B. Dempsey E.P. Serlent, Springer, Berlin, 12-20 (1981).

[63] R.A. Gemeinhart, C. M. Mare, R.T. Haasch, E.J. Gemeinhart, "Osteoblast-like cell attachment to and calcification of novel phosphonate-containing polymeric substrates," *J. Biomed. Mater. Res. A*., **78A**, 433-440 (2006).

[64] S. Chaterji, R.A. Gemeinhart, "Enhanced osteoblast-like cell adhesion and proliferation using sulfonate-bearing polymeric scaffold," *J. Biomed. Mater. Res. A*., **83A**, 990-998 (2007).

[65] R.L Bowen, E.N, Cobb, J.E Rapson, "Adhesive bonding of various materials to hard tooth tissues: improvement in bond strength to dentin," *J. Dent. Res.*, **61**, 1070-1076 (1982).

[66] F.R Tay, N.M King, B.I. Suh, D.H. Pashley, "Effect of delayed light-cured activation on bond-strengths between composites and adhesives" *Arch. Orofac. Sci.,* **1**, 36-41 (2006).

Chapter 1

Effects of Polymerization Accelerator on Biomineralization and Chemical Durability of Vinylphosphonic Acid-based Copolymer in Simulated Body Fluid

1. Introduction

Bone-bonding ability is one of the essential properties to fix the bone substitute stably in the bone defect for long periods. Bioglass® [1], glass-ceramic A-W [2], and sintered hydroxyapatite [3] exhibit bone-bonding ability through the formation of the low crystalline apatite layer on their surface in living body. However, they might cause the bone adsorption around the implantation part, because their Young's moduli are higher than living bone. Organic inorganic-composites have been expected to show the Young's moduli similar to natural bone. Therefore, such composites would solve the problem occurred by the difference in the mechanical properties.

Modification with the functional groups inducing formation of bone-like apatite in simulated body fluid (SBF), such as Si-OH [4] and Ti-OH [5] groups, have attracted for improving the bone-bonding ability of the materials. Phosphate groups ($-PO_3H$) have been also reported to form of apatite layer faster than carboxyl hydroxyl groups on the surface of the self-assembly monolayer in SBF [6]. It suggests that incorporation of the phosphate groups into the polymer has effective to obtain the composites showing bone-bonding property.

As a conventional precursor of such polymer, phosphate-containing vinyl monomers such as vinylphosphonic acid (VPA) are often used for biomaterial applications. VPA-acrylamide copolymer shows the enhancement of adhesion and growth rate of the osteoblast-like cells [7]. Stancu *et al.* prepared copolymers from methacryloyloxyethyl phosphate and (diethylamino)ethyl methacrylate [8]. They showed the calcium phosphate formation in SBF, although it was not spectroscopically confirmed

with the apatite.

The phosphate-containing monomers inhibit the radical polymerization initiated by the combination of peroxide or camphor quinone, and tertiary amine, because the monomer and the amine form the salt [9, 10]. In order to solve these problems, sodium *p*-toluenesulfinate (*p*-TSS) has been reported to promote radical polymerization of the phosphate-containing monomer applied as a self-adhesive dental resin [11].

On the other hand, dissolution of monomer or polymer with low molecular weight would be the unfavorable phenomena for the apatite formation, because the phosphate groups in the eluted materials decrease in pH of the SBF. The several factors such as molecular weight, crosslink density, hydrophilicity and so on affect dissolution and degradation of polymer [11, 13]. However, effects of the accelerator addition on chemical durability and apatite-forming ability of the polymers in simulated body environment have been remained unclear.

In this Chapter, the copolymers from VPA and triethylene glycol dimethacrylate (TEGDMA) were prepared through the radical polymerization added with various amount of *p*-TSS. The apatite-forming ability and degradation of these copolymers were investigated in SBF. TEGDMA is a bifunctional vinyl monomer and provides a polymer with high crosslink density and strength. The behavior of the degradation and biomineralization changed by the additive were discussed in terms of hydrophilicity and molecular weight/crosslink density of the copolymer.

2. Materials and methods

2.1 Preparation of specimen

VPA (95%, Tokyo Chemical Industry Co., Ltd., Japan) and TEGDMA (90%, Wako pure Chemical Industries, Ltd., Japan) were used as monomer at molar ratio of VPA : TEGDMA = 40 : 60 in the 10 g of mixture of monomers. Various amount of *p*-TSS (98%, Tokyo Chemical Industry Co., Ltd., Japan) was dispersed in the mixture of those monomer at 0 to 5.0 wt% to the total of VPA and TEGDMA by using an ultrasonic

cleaner. Then as a photo polymerization initiator, *N*,*N*'-dimethyl-*p*-toluidine (97%, Wako pure Chemical Industries, Ltd., Japan) and (±)-camphorquinone (97%, Wako pure Chemical Industries, Ltd., Japan) were added at 2 wt% and 0.77 wt%, respectively, to the total amount of the monomer mixture.

These mixtures were stirred under the light shielding for 1 hour. Blue light (460 nm) was exposed to the mixtures for 1 hour to progress the polymerization. The obtained copolymer was dried at 60°C for 1 day and soaked in ultra-pure water to remove unreacted monomers at room temperature for 1 day. After the drying, the obtained copolymer was cut into rectangular specimens 10 mm × 10 mm × 1 mm in size and polished using waterproof abrasive paper (SiC #1000).

2.2 Preparation of SBF and soaking specimen in SBF

SBF (Na^+ 142.0, K^+ 5.0, Mg^{2+} 1.5, Ca^{2+} 2.5, Cl^- 147.8, HCO_3^- 4.2, HPO_4^{2-} 1.0, SO_4^{2-} 0.5 mol·m^{-3}) was prepared by addition of NaCl, $NaHCO_3$, KCl, $K_2HPO_4 \cdot 3H_2O$, $MgCl_2 \cdot 6H_2O$, $CaCl_2$, Na_2SO_4 (Nacalai Tesque, Inc., Japan) into the ultra-pure water. pH of the solution was adjusted at 7.40 by tris(hydroxymethyl) aminomethane (Nacalai Tesque, Inc., Japan) and appropriate volume of 1 kmol·m^{-3} HCl solution [14]. The obtained specimens were soaked in 30 cm^3 of SBF at 36.5°C for various periods within 7 days.

2.3 Characterization

The specimens were analyzed by scanning electron microscopy (SEM; S-3500N, Hitachi Co., Japan) attached with energy dispersive X-ray analysis (EDX; EMAX Energy, Horiba Ltd., Japan), thin-film X-ray diffraction (TF-XRD; MXP3V, Mac Science, Co., Japan) and Fourier transform infrared spectroscopy (FT-IR; FT/IR-6100, JASCO Co., Japan) using attenuated total reflectance method and. In the TF-XRD, the angle of the X-ray (CuKα) was fixed at 1° against the specimen surface. In SEM-EDX, carbon was coated on the surfaces of the specimens using a carbon coater (CADE, Meiwafosis Co.,

Ltd., Japan). The water-contact angle against the specimen surface was measured by water-contact angle gauge (DMe-200, Kyowa Interface Science, Co., Ltd., Japan). In addition, the glass-transition temperature of specimen was measured by differential scanning calorimetry (DSC; DSC 3100S, Mac Science, Co., Japan). In the DSC measurement, the specimens were heated from room temperature to 200°C at a rate of 10°C/min.

Moreover, Ca and P concentration and pH of SBF after soaking in specimen by inductively coupled plasma optical emission spectrometry (ICP-OES; Optima 4300DV CYCLON, Perkin-Elmer Inc., UK) and pH electrode (6261-10C, Horiba Ltd., Kyoto, Japan).

3. Results

Figure 1 shows FT-IR spectra of the specimens before soaking SBF. The peaks

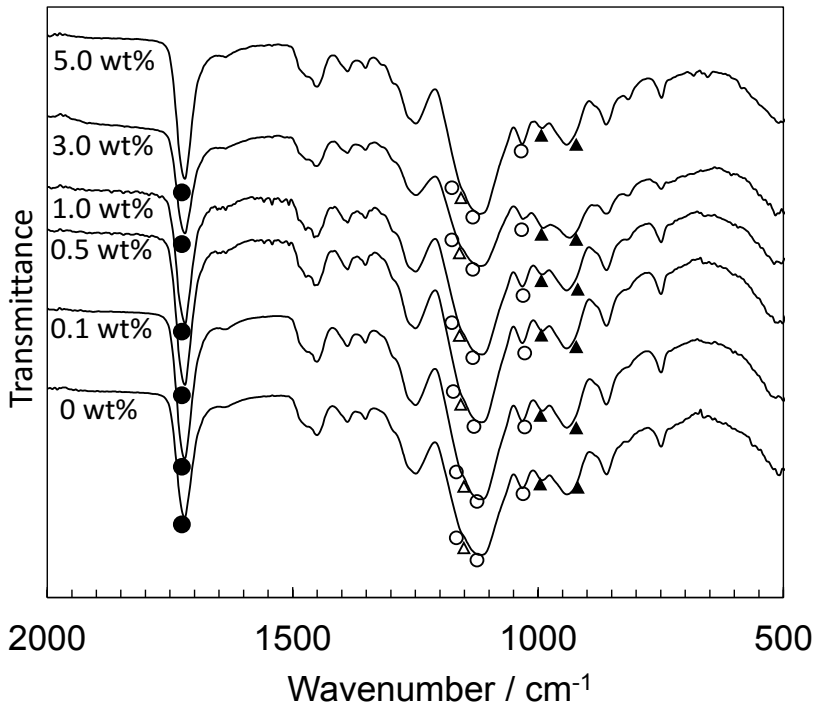

Figure 1 FT-IR spectra of the specimens added with *p*-TSS before soaking SBF (▲ : P-O bond of VPA , △ : P=O bond of VPA, ○ : C-O-C bond of TEGDMA, ● : C=O bond of TEGDMA).

assigned to P-O were observed at 930 and 990 cm^{-1} and those assigned to P=O peak at 1150 cm^{-1} for all the specimens. In addition, the peaks assigned to C-O-C stretching were observed at 1030, 1130, 1160 cm^{-1}, and those assigned to C=O stretching at 1720 cm^{-1}. Moreover, the no peaks of C=C bond derived from uncured VPA and TEGDMA were detected.

Figure 2 shows phosphorus content and water contact angle on the surface of specimens added with various amount of *p*-TSS. The P content was increased, and contact angle was decreased as the *p*-TSS amount increases.

.

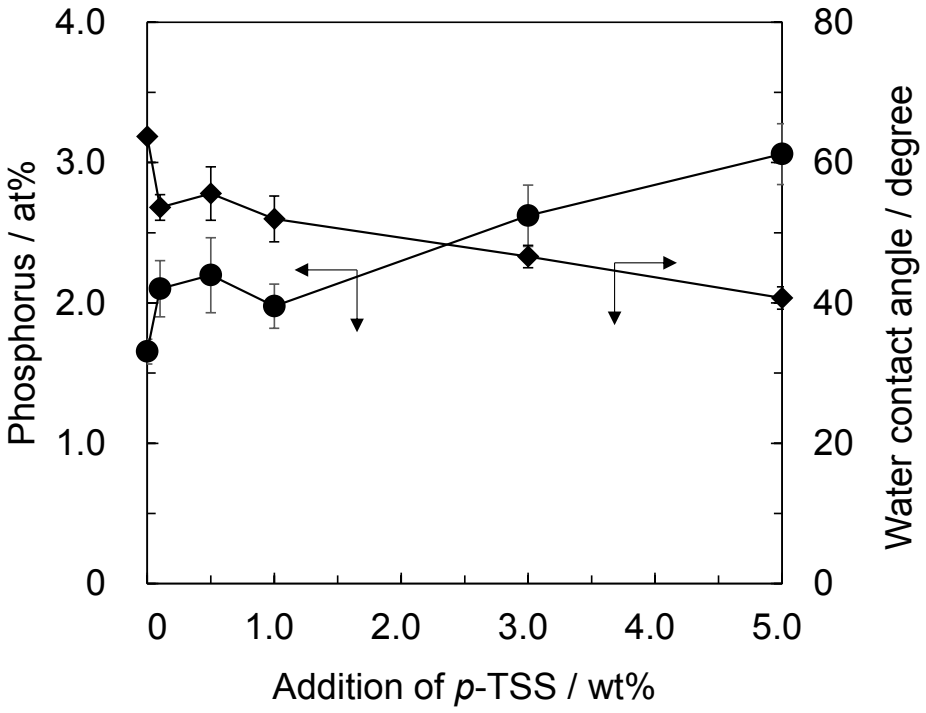

Figure 2 Change in phosphorus content and water contact angle on the surfaces of the samples added with *p*-TSS (n = 3).

Figure 3 shows DSC curve of specimen and glass transition temperature (T_g). The exothermic peak corresponding to crystallization was observed around the 130˚C for all specimens. The T_g was slightly sifted to the higher temperature with

increase in additive amount of *p*-TSS.

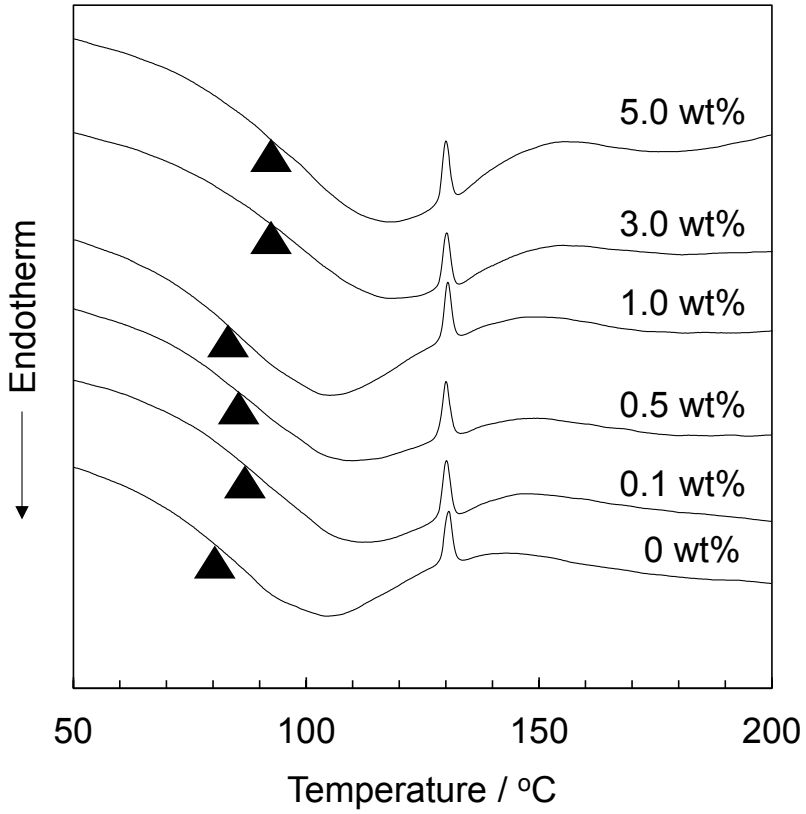

Figure 3 DSC curves and glass-transition temperatures (▲) of the different copolymer samples treated with *p*-TSS .

Figure 4 shows SEM images of surface of specimen after soaking in SBF for 7 days. Depositions were observed on the specimens with 0.5 wt% or more of *p*-TSS. Area of the surface covered with depositions was increased as *p*-TSS amount increases. In the higher magnification images of the depositions, the spherical particles with diameter range of 0.3 - 1 μm were aggregated. This morphology of the depositions was different from that of the apatite formed on the organic polymer in simulated body environment [15].

Figure 5 shows EDX spectra of deposition on the surface of different specimens after soaking in SBF for 7 days. EDX analysis revealed that deposition consisted Ca and P, and that Ca/P molar ratio was about 1.5 for all the specimens.

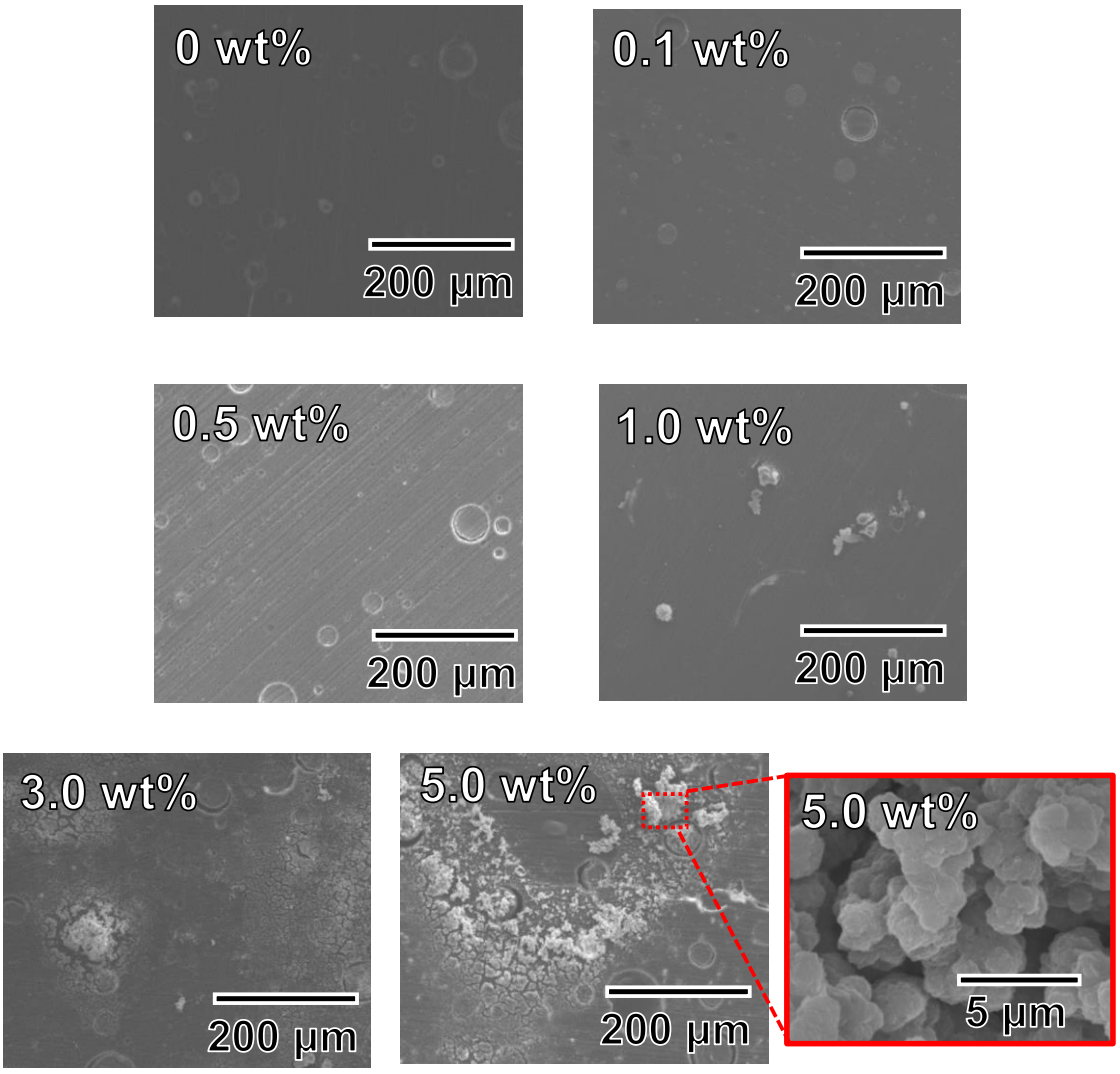

Figure 4 SEM images of the surfaces of the different copolymer samples after they had been soaked in SBF for 7 days.

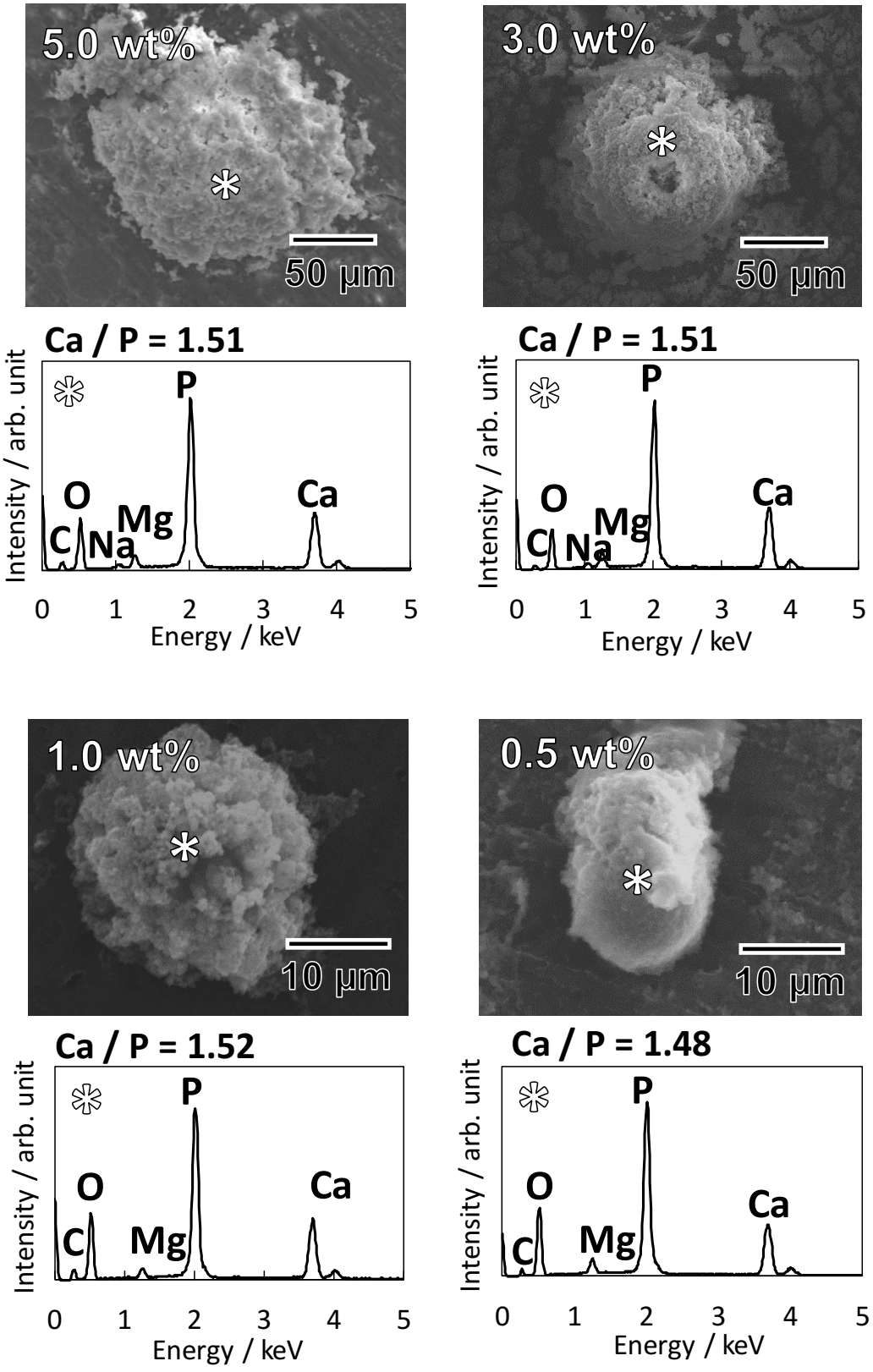

Figure 5 SEM images and EDX spectra of deposition on the surface of specimen after soaking in SBF for 7days.

Figure 6 shows TF-XRD patterns of the specimens after soaking in SBF for 7 days. No peaks characteristic to the apatite (JCPDS #09-0432) and other calcium phosphates were observed for all the specimens.

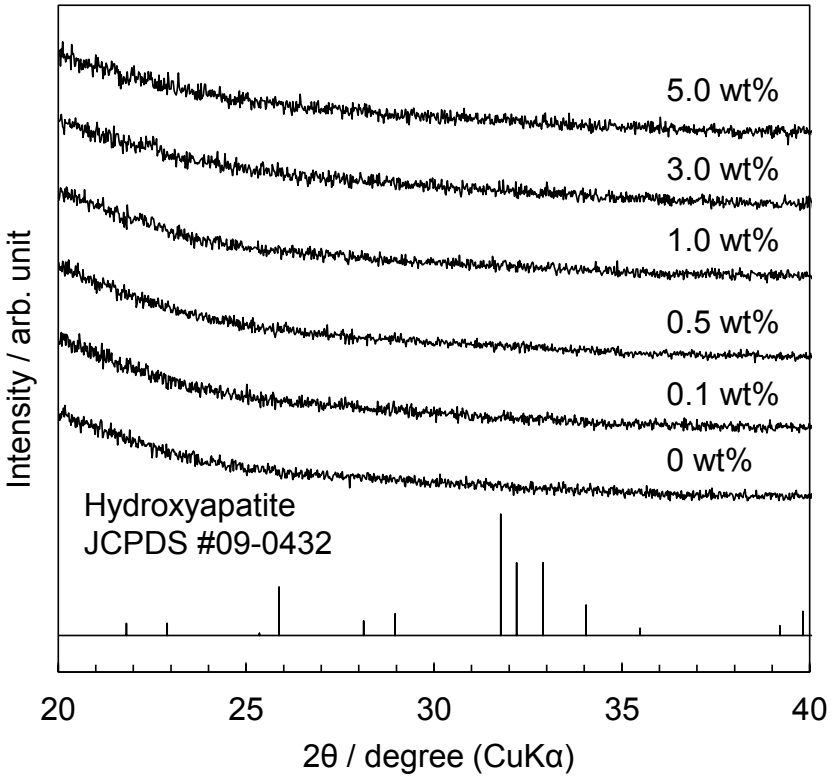

Figure 6 TF-XRD patterns of the surfaces of the different specimens added with *p*-TSS before soaking SBF for 7 days.

Figure 7 shows FT-IR spectra of surface of specimen after soaking in SBF for 7 days. The spectra of specimens added with less than 1.0 wt% of p-TSS remained about the same as before soaking in SBF. On the other hand, the intensity of the C=O peaks derived from TEGDMA became weak and new peaks assigned to P-O bond in $–PO_3^{2-}\cdots Ca^{2+}$ complex appeared at 889 cm^{-1} [16] for the specimens added with *p*-TSS at 3.0 and 5.0 wt%.

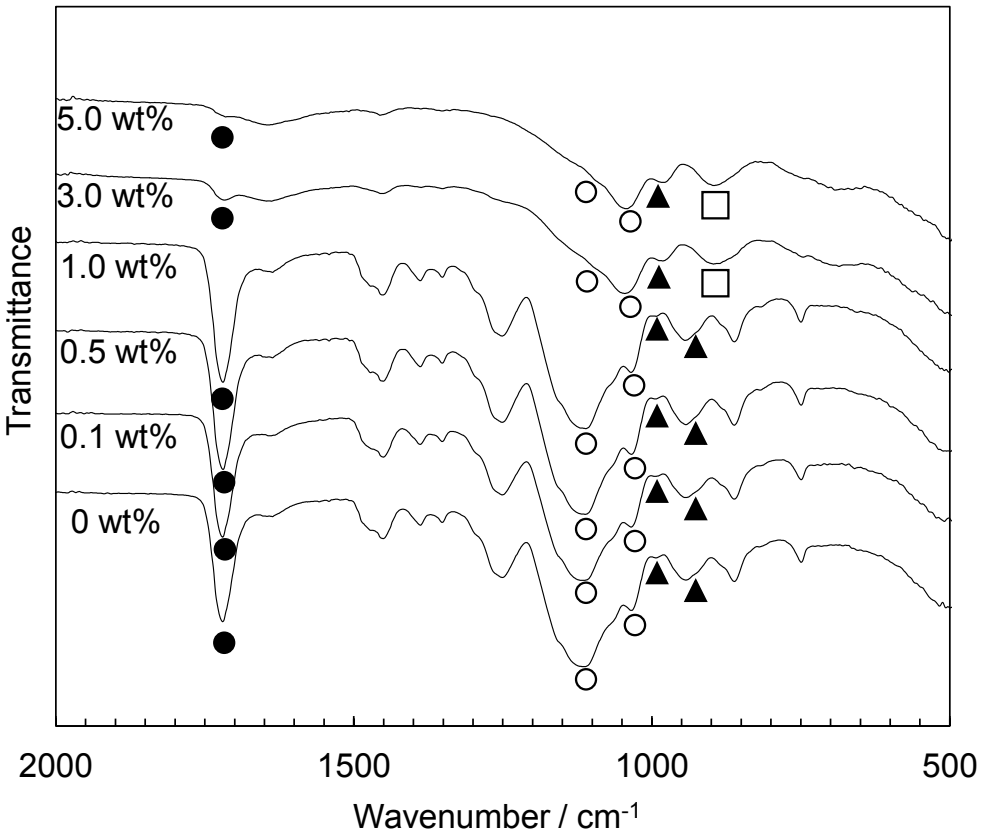

Figure 7 FT-IR spectra of the specimens added with *p*-TSS after soaking in SBF for 7 days (▲: P-O bond of VPA, △: P=O bond of VPA, ○: C-O-C bond of TEGDMA, ●: C=O bond of TEGDMA, □ : salt of $-PO_3^{2-}Ca^{2+}$).

Figure 8 shows the change in P and Ca concentration, and in SBF with soaking of the specimens for various periods. Increase in P concentration was inhibited when the specimen containing 0.1, 0.5 and 1.0 wt% of *p*-TSS. However, P concentration was increased for the specimens added with *p*-TSS at 0, 3.0 and 5.0wt%. On the other hand, Ca concentration in SBF was monotonically decreased after soaking of the specimens.

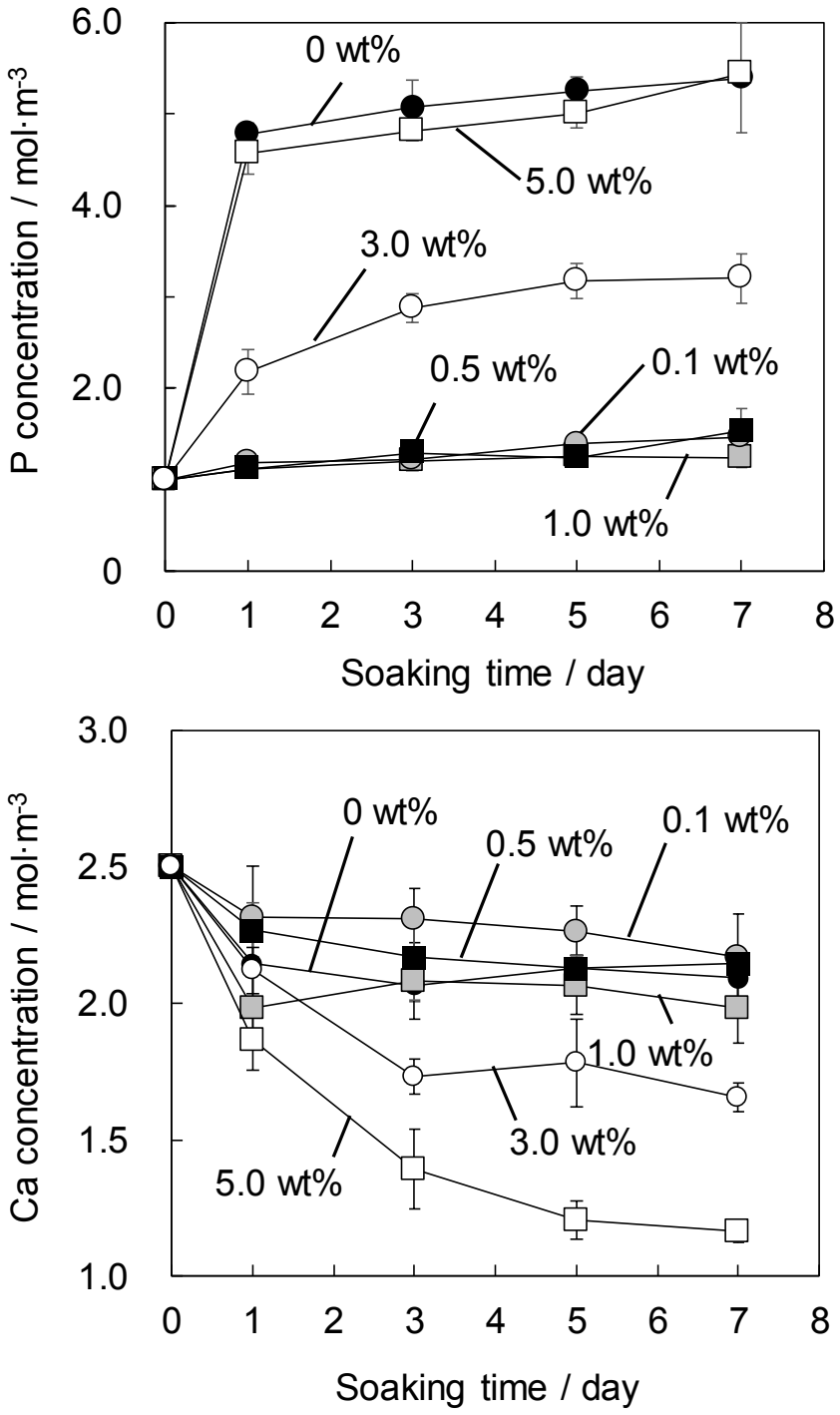

Figure 8 Change in P and Ca concentrations of SBF with soaking of the different specimens (n = 3).

Figure 9 shows the change in pH value in SBF with soaking of specimens. Significant decrease in pH was suppressed at 0.1, 0.5 and 1.0 wt% of *p*-TSS, but not at 0, 3.0 and 5.0 wt%.

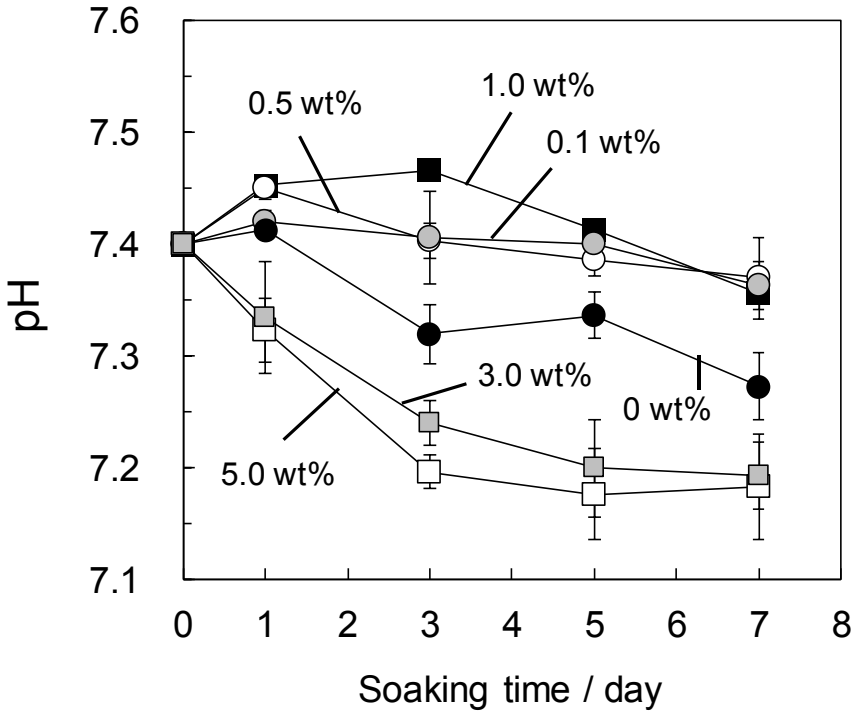

Figure 9 Change in pH of SBF with soaking of the different specimens (n = 3).

4. Discussion

Copolymerization of VPA and TEGDMA were completed regardless of amount of *p*-TSS addition in to the reaction, judging from the result that no peaks of C=C bond derived from uncured VPA and TEGDMA were detected (see Figure 1). Despite that initial VPA content was constant irrespective of the added *p*-TSS, amount of the phosphorus incorporated into the copolymers was different (see Figure 2). Furthermore, higher molecular weight and high crosslink density lead to an increase in the T_g [17]. The

molecular weight and/or crosslink density of obtained copolymers would increase with increase in additive *p*-TSS, as evidenced by the T_g shifting to higher temperature (see Figure 3). These results indicate that *p*-TSS accelerates polymerization reaction of VPA and TEGDMA. The *p*-TSS reacted with VPA shown equation (1) would inhibit the formation of the salt consisting NDT and VPA to start and promote the polymerization.

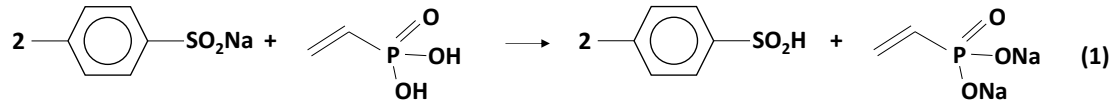

(1)

This result indicated that it was becoming increasingly difficult to wash any phosphorus-containing compounds from the polymerized VPA after it had been treated with *p*-TSS and soaked in ultrapure water.

The dissolution of phosphorus-containing molecules from the copolymer and decrease in pH in SBF were suppressed significantly by addition of 0.1-1.0 wt% of *p*-TSS, but not addition of large amount of *p*-TSS at 3.0 wt% or more (see Figures 8 and 9). Generally, solubility of polymer decreases with increase in molecular weight and/or crosslink density. However, the copolymer treated with 3.0 and 5.0 wt% of *p*-TSS released compound consisting phosphorus into SBF, in spite that they would have higher crosslink density.

In this case, not only molecular weight and/or crosslink density but also hydrophilicity of polymer would affect dissolution of the copolymer in SBF. Yui *et al.* prepared the dental resin from bisphenol A diglycidyl ether dimethacrylate and 2-hydroxylethyl methacrylate and reported that highly hydrophilic resin was dissolved easily in pure water due to enhanced diffusion of water molecule to the resin and subsequent cleavage of the hydrogen bond between the polymer chains [18]. Moreover, decrease in pH of inner resin led to the acid hydrolysis reaction of ester bond [19, 20]. This research found that increase in addition of *p*-TSS enhanced hydrophilicity of the copolymer, because it led to increase in the content of phosphate groups (see Figures 2). Therefore, dissolution of the copolymer could be enhanced because ester bond of TEGDMA is hydrolyzed by the proton dissociated from the phosphate as a catalysis.

The depositions composed of Ca and P were formed on the copolymers added with 1.0-5.0 wt% of *p*-TSS after soaking in SBF for 7 days (see Figure 4, 5). However, their morphology was different from that of the apatite formed on the organic polymer in simulated body environment [15]. Although the $PO_3^{2-}\cdots Ca^{2+}$ complex formation was confirmed by FT-IR (see Figure 7), P-O bond in orthophosphate ion (PO_4^{3-}) characteristic to the apatite and amorphous calcium phosphate was not observed [21]. Furthermore, the no peaks corresponding to calcium phosphate were observed (see Figure 6). Consequently, it is assumed that a kind of amorphous calcium polyvinylphosphate is formed on their surfaces.

The results of this study therefore revealed that lower additive amount of *p*-TSS was able to be enhance the chemical durability of the copolymer. Although it suppressed the decrease in pH in SBF, the phosphate groups in the copolymer hardly contributed to form apatite. Ohtsuki *et al.* reported that apatite formation was promoted by not only the functional groups inducing heterogeneous nucleation, but also release of chemical species such as Ca^{2+} increasing supersaturation degree respect with apatite in SBF [22]. In the terms of this points, only incorporation of phosphate groups would be insufficiently of crystal growth of apatite after nucleation. To enhance the apatite formation on the present copolymers, incorporation of calcium salt and selection of content amount of phosphate groups able to release sufficient amount of Ca^{2+} are necessary. These points should be further examined in the future study.

5. Conclusion

Effects of *p*-TSS as polymerization accelerator on chemical durability and calcification of copolymer containing phosphate groups prepared from VPA and TEGDMA were investigated in SBF. Addition of *p*-TSS at 1.0 wt% or less suppressed dissolution of VPA-TEGDMA copolymer in SBF, but not addition of large amount of *p*-TSS. The copolymers precipitated the calcium polyvinylphophate in SBF because of the tight ionic interaction of $-PO_3^{2-}\cdots Ca^{2+}$.

Reference

[1] L. L. Hench, *J. Am. Ceram. Soc.,* "Bioceramics," **81**, 1705-1728 (1998).

[2] T. Kokubo, H.M. Kim, M. Kawashita, "Novel bioactive materials with different mechanical properties," *Biomaterials*, **24**, 2161-2175 (2003).

[3] M. Jarcho, C.H. Bolen, M.B. Thomas, J. Bobick, J.F. Kay, R.H. Doremus, "Hydroxylapatite synthesis and characterization in dense polycrystalline form," *J. Mater. Sci.*, **11**, 2027–2035 (1976).

[4] S.B Cho, K. Nakanishi, T. Kokubo, N. Soga, T. Kamamura, T. Kitsugi, T. Yamamuro, "Dependence of apatite formation on silica gel on its structure: effect of heat treatment," *J. Am. Ceram. Soc.*, **78**, 1769-1774 (1995).

[5] M. Uchida, H.M. Kim, T. Fujibayashi, T. Nakamura, "Structural dependence of apatite formation on titania gels in a simulated body fluid," *J. Biomed. Mater. Res. A.*, **64A**, 164-170 (2003).

[6] M. Tanahashi, T. Matsuda, "Surface functional group dependence on apatite formation on self-assembled monolayers in a simulated body fluid," *J. Biomed. Mater. Res.*, **34**, 305-315 (1997).

[7] J. Tan, R.A. Gemeinhart, M. Ma, W.M. Saltzman, "Improved cell adhesion and proliferation on synthetic phosphonic acid-containing hydrogels," *Biomaterials*, **26**, 3663-3671 (2005).

[8] I.C. Stancu, R. Filmon, C. Cincu, B. Marculescu, C. Zaharia, Y. Tourmen, M.F. Basle, D. Chappard, "Synthesis of methacryloyloxyethyl phosphate copolymers and in vitro calcification capacity," *Biomaterials*, **25**, 205-213 (2004).

[9] F.R Tay, N.M King, B.I. Suh, D.H. Pashley, "Effect of delayed light-cured activation on bond-strengths between composites and adhesives" *Arch. Orofac. Sci.,*, **1**, 36-41 (2006).

[10] R.L Bowen, E.N, Cobb, J.E Rapson, "Adhesive bonding of various materials to hard tooth tissues: improvement in bond strength to dentin," *J. Dent. Res.*, **61**, 1070-1076

(1982).

[11] J. Yamauchi, “Study of dental adhesive resin containing phosphoric acid methacrylate monomer,” *The Journal of The Japanese Society for Dental Materials and Devices*, **5**, 144-154 (1986).

[12] A. Göpferich, “Mechanisms of polymer degradation and erosion,” *Biomaterials*, **17**, 103-114 (1996).

[13] J. Malacarne, R.M. Carvalho, M.F. Goes, N. Svizero, D.H. Pashley, F.R. Tay, C.K. Yiu, M.R. Carrilho, “Water sorption/solubility of dental adhesive resins,” *Dent. Mater.,* **22**, 973-980 (2006).

[14] T. Kokubo, H. Takadama, “How useful is SBF in predicting in vitro bone bioactivity?,” *Biomaterials*, **27**, 2907-2915 (2006).

[15] T. Kawai, C. Ohtsuki, M. Kamitakahara, T. Miyazaki, M. Tanihara, Y. Sakaguchi, S. Konagaya, “Coating of an apatite layer on polyamide films containing sulfonic groups by a biomimetic process,” *Biomaterials*, **25**, 4529-4534 (2004).

[16] S. Jin, E. Gonsalves, “Functionalized copolymers and their composites with polylactide and hydroxyapatite,” *J. Mater. Sci.: Mater. Med.*, **10**, 363-368 (1999).

[17] S.L. Gibson, F.A. Landis, P.L. Drzal, “Combinatorial investigation of the structure-properties characterization of photopolymerized dimethacrylate networks,” *Biomaterials*, **27**, 1711-1717 (2006).

[18] C.K. Yui, N.M. King, M.R.O. Carrilho, S. Sauro, F.A. Rueggeberg, C. Prati, R.M. Carvalho, D.H. Pashley, F.R. Tay, “Effect of resin hydrophilicity and temperature on water sorption of dental adhesive resins,” *Biomaterials*, **27**, 1695-1703, (2006).

[19] T.N. Rahima, D. Mohamada, H. M. Akilb, I.A. Rahmana, *Dental. Materials*, **28**, 63-70 (2012).

[20] Y. Nishitani, K. Takahashi, Y. Hayashi, T. Hoshika, G. Horikawa, T. Nakata, K. Tanaka, H. Sano, M. Yoshiyama, *Adhesive. Dentistry,* **26**, 92-98 (2008) (in Japanese).

[21] P. Layrolle, A, Ito, T. Tateish, “Sol-gel synthesis of amorphous calcium phosphate and sintering into microporous hydroxyapatite bioceramics,” *J. Am. Ceram. Soc.*, **81**,

1421-1428 (1998).

[22] C. Ohtsuki, T. Kokubo, T. Yamamuro, “Mechanism of apatite formation on CaO-SiO_2-P_2O_5 glass in a simulated body fluid,” *J. Non-Cryst. Solids*, **143**, 84-92 (1992).

Chapter 2

Effects of Phosphate Group Content on Apatite-forming Ability of Polymer-$CaCl_2$ Composites in Simulated Body Fluid

1. Introduction

The organic-inorganic composites applied as bone substitute have been researched to improve the mechanical properties of bioactive ceramics leading to bone adsorption. Surface of bioactive ceramics can form low crystallinity apatite layer in the part of bone defect for bonding to bone tissue. Some researchers have been revealed the specific molecular structures, such as Si-OH [1], Ti-OH [2], and carboxyl [3] groups, induce heterogeneous nucleation of apatite in simulated body fluid (SBF) due to the interaction with Ca^{2+}. Thus, these phenomena suggest that modification of these groups into the copolymer contributes to the fabrication of bioactive composites.

The abilities of phosphate ($-PO_3H$) groups have been reported to be not only form bone-like apatite rapidly in SBF [3], but also enhance the activities of osteoblasts [4,5] to prepare the composites with high biological compatibility. In Chapter 1, the copolymers containing phosphate groups were prepared from vinylphosphonic acid (VPA) and triethylene glycol dimethacrylate (TEGDMA) through the radical polymerization. Although lower additive amount of sodium *p*-toluene sulfonate (*p*-TSS) as a polymerization accelerator inhibited degradation of the copolymer, the apatite was not formed in SBF. These results suggest that the presence of phosphate groups only is not sufficient to form the apatite on the surface of substrate in SBF.

However, the release of Ca^{2+} from substrate also promotes apatite formation because of increase in supersaturation degree respect with apatite [6]. In order to incorporate Ca^{2+} into polymer, the treatment with calcium salts solution such as $CaCl_2$ has been performed [7, 8]. Thus, the chemical modification with Ca^{2+} as an inorganic specie into the VPA-based copolymer would be improve the apatite-forming ability of the composites.

Phosphate group content is also expected to be a key factor for apatite formation on the composites. Phosphate can bind with Ca^{2+} through ion-ion interaction [3,9]. It would affect the behavior of heterogeneous nucleation of apatite in SBF. Increase in carboxyl content in the polymer promotes apatite formation, when Ca^{2+} content was fixed [10]. Several researchers examined apatite-forming ability of the synthetic polymer [11] or natural polymer [12] containing phosphonic acid through the phosphorylation process. However, these reports had no discussion regarding the effects of phosphate group content on surface condition and its apatite formation behavior in SBF.

In this Chapter, the composites consisting of $CaCl_2$ and VPA-based copolymers with different phosphate content were prepared by addition of 2-hydroxyethyl methacrylate (HEMA) and TEGDMA. Apatite formation on the copolymers in SBF was investigated and discussed in terms of Ca^{2+} release, ionic interaction between the phosphate and Ca^{2+}, and variation in surface ζ potential.

2. Materials and methods

2.1. Preparation of VPA-HEMA-TEGDMA copolymer

Table 1 shows the molar ratio of additive monomer in total amount of 10 g for preparation of the copolymers. The monomer of VPA (95%, Tokyo Chemical Industry Co., Ltd, Tokyo, Japan), HEMA (95%, Wako Pure Chemical Industries, Ltd, Osaka, Japan), and TEGDMA (90%, Wako Pure Chemical Industries, Ltd) were mixed. Then 0.5 wt% of *p*-TSS (98%, Tokyo Chemical Industry Co., Ltd), and 2 wt% of *N*,*N*'-dimethyl-*p*-toluidine (97%, Wako Pure Chemical Industries, Ltd) were added to total amount of monomers. After (±)-camphorquinone (97%, Wako Pure Chemical Industries, Ltd) was added at concentration of 1 mol% to total molar number of monomers, the mixture was stirred with protection from light for 1 hour.

Then, 1.1 g of mixture was poured into the polypropylene cup and the monomers were copolymerized by irradiation of blue light (λ= 460 nm) for 1hour. After obtained copolymer specimens were dried at 60°C for 1 day, they were cut and polished with

waterproof abrasive paper (SiC, #1000) into the square size of 10 mm ×10 mm × 1 mm. The square specimens were soaked in ultra-pure water for 1 day at room temperature to remove unreacted regents. In addition, the copolymer specimen was soaked in 30 cm^3 of 1 $kmol \cdot m^{-3}$ calcium chloride solution at 36.5ºC for 1 day after the drying of the specimen picked up from ultra-water for 1 day at room temperature.

Table 1 The molar ratio of additive monomers for preparation of specimens.

Specimen	VPA / mol%	HEMA / mol%	TEGDMA / mol%
40V55H05T	40	55	5
10V85H05T	10	85	5
01V94H05T	1	94	5

2.2. Preparation of SBF and Tris-NaCl buffer and soaking specimen in each solution

The copolymer specimens were soaked in 30 mL of SBF at 36.5°C for various time periods within 5 days. SBF (Na^+ 142.0, K^+ 5.0, Mg^{2+} 1.5, Ca^{2+} 2.5, Cl^- 147.8, HCO_3^- 4.2, HPO_4^{2-} 1.0, SO_4^{2-} 0.5 $mol \cdot m^{-3}$) was prepared by adding NaCl, $NaHCO_3$, KCl, $K_2HPO_4 \cdot 3H_2O$, $MgCl_2 \cdot 6H_2O$, $CaCl_2$, and Na_2SO_4 (Nacalai Tesque, Inc., Kyoto, Japan) to ultra-pure water [13]. The pH of the resulting solution was adjusted to 7.40 by the addition of tris(hydroxymethyl) aminomethane (Nacalai Tesque, Inc.) and the appropriate volume of 1 $kmol \cdot m^{-3}$ HCl solution.

Moreover, the specimens were soaked in 30 mL of Tris-NaCl buffer at 36.5°C for 1 day to measure the release amount of Ca^{2+} from the copolymers. Tris-NaCl buffer (50 $mol \cdot m^{-3}$ tris(hydroxymethyl) aminomethane and 142 $mol \cdot m^{-3}$ NaCl) was prepared by adding NaCl and then tris(hydroxymethyl) aminomethane (Nacalai Tesque, Inc.) into ultra-pure water, and then 1 $kmol \cdot m^{-3}$ of HCl solution ware added to the pH of buffer

adjust to 7.40.

2.3 Characterization

The copolymer specimens after soaked in the $CaCl_2$ solution were analyzed by wavelength-dispersive X-ray fluorescence analysis (ZSX101e, Rigaku Co., Tokyo Japan) to determine the Ca content. The surface of the copolymer specimens ware also analyzed with thin-film X-ray diffraction (TF-XRD; MXP3V, Mac Science, Co., Yokohama, Japan), scanning electron microscopy (SEM; S-3500N, Hitachi Co., Tokyo, Japan), energy dispersive X-ray (EDX) analysis system (EMAX Energy, Horiba Ltd, Kyoto, Japan) equipped with SEM and Fourier-transform infrared spectroscopy (FT-IR; FT/IR-6100, JASCO Co., Tokyo, Japan) before and after soaking in SBF. In the TF-XRD analysis, the angle of the X-ray (CuKα) was fixed at 1° relative to the surface of the sample. For the SEM-EDX analysis, the surfaces of the samples were coated with carbon using a carbon coater (CADE, Meiwafosis Co., Ltd., Osaka, Japan). For the FT-IR analysis, an attenuated total reflectance method was used to obtain FT-IR spectra for the surface of specimens at a resolution of 1 or 4 cm^{-1}.

The concentration of Ca in the Tris-NaCl buffer and P, Ca concentration of the SBF after soaking the copolymer specimens were measured with inductively coupled plasma optical emission spectrometry (ICP-OES; Optima 4300DV CYCLON, Perkin-Elmer Inc., London, UK). In addition, the value of pH in the SBF with soaking of the difference specimens was determined by a pH electrode (6261-10C, Horiba Ltd., Kyoto, Japan).

The surface ζ potential of the copolymer specimens in SBF was measured using ζ-potential analyzer (Otsuka Erectronic Co., Osaka, Japan) with connected box-like quartz cell. After the copolymer specimens were soaked in SBF for various periods, the surface of specimen was washed with ultra-pure water. The washed specimen was put on the quartz cell, and then flesh SBF and monitor particles of polyethylene latex (Otsuka Electronic Co.) were injected into the cell. In order to measure the surface ζ potential, the

electrophoretic mobility of the monitor particles was measured with laser Doppler method.

3. Results

Figure 1 shows FT-IR spectra of the different specimens before soaking in $CaCl_2$ solution. For the all spectra, the peaks attributed to stretch vibration of O-C bond for alcohol and torsion of the -OH groups were observed at 1075 and 1151 cm^{-1}, respectively, which were delivered from HEMA. In addition, the two peaks delivered from both HEMA and TEGDMA were detected at 1715 and 1022 cm^{-1}, which were corresponded to stretching vibration of C=O bond and O-C of ester, respectively. The 40V55H05T and 10V85H05T displayed the peak at 989 cm^{-1}, which was attributed to P-O bond of VPA. However, the peak of VPA was not conformed 01V94H05T.

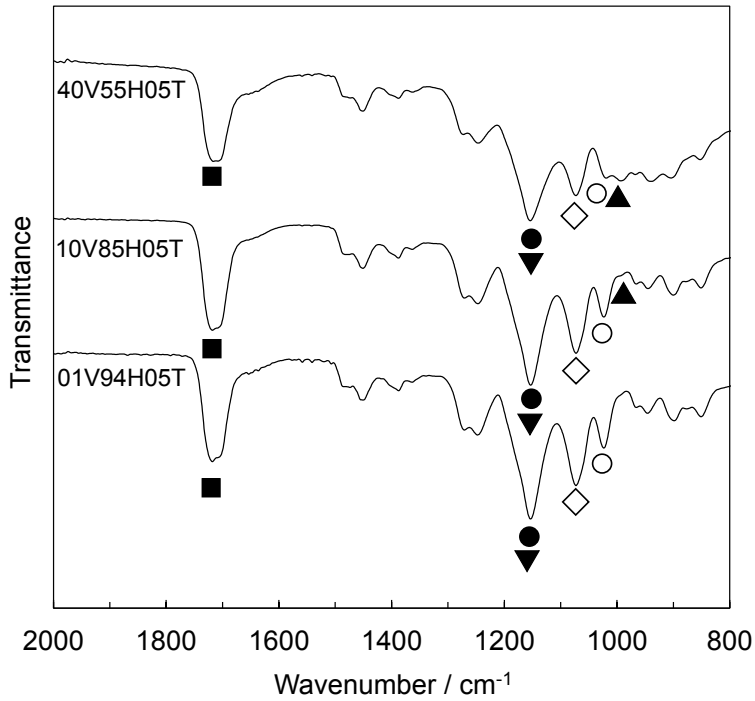

Figure 1 FT-IR spectra (resolution of 4 cm^{-1}) of the different specimens before soaking in $CaCl_2$ solution (■: ν(C=O) of HEMA; ●: τ(OH) of HEMA; ▼γ(CH_3) of HEMA and TEGDMA; ◇: ν(O-C) alcohol of HEMA; ○: ν(C-O) ester of HEMA and TEGDMA; ▲:P-O bond of VPA; ν is the stretching; γ, the rocking; τ, the torsion).

Figure 2 (A) shows the content of Ca in specimen added with various amount of VPA after soaked in $CaCl_2$ solution. The content was increased as VPA/HEMA ratio increased. Ca concentration in Tris-NaCl buffer after soaking the specimens for 1 day was shown Figure 2 (B). The concentration was increased with increase in VPA content.

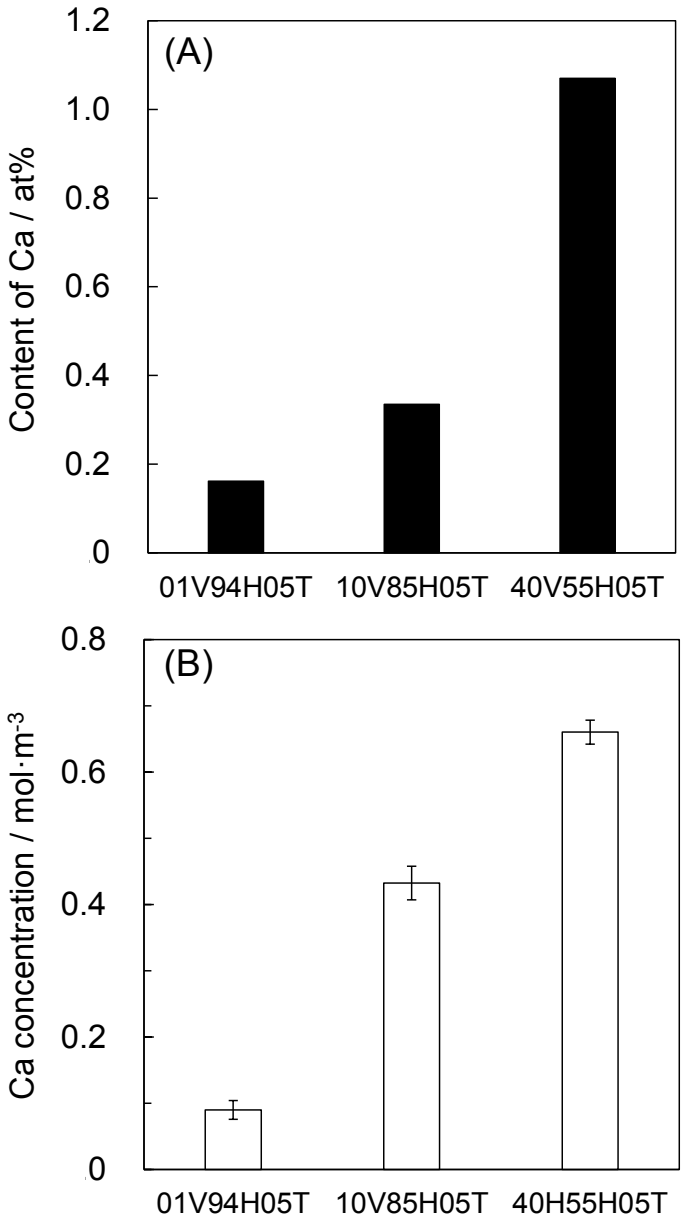

Figure 2 Ca content in the specimens after soaking in $CaCl_2$ solution (A) and Ca concentration in Tris-NaCl buffer with soaking of specimens for 1 day (B).

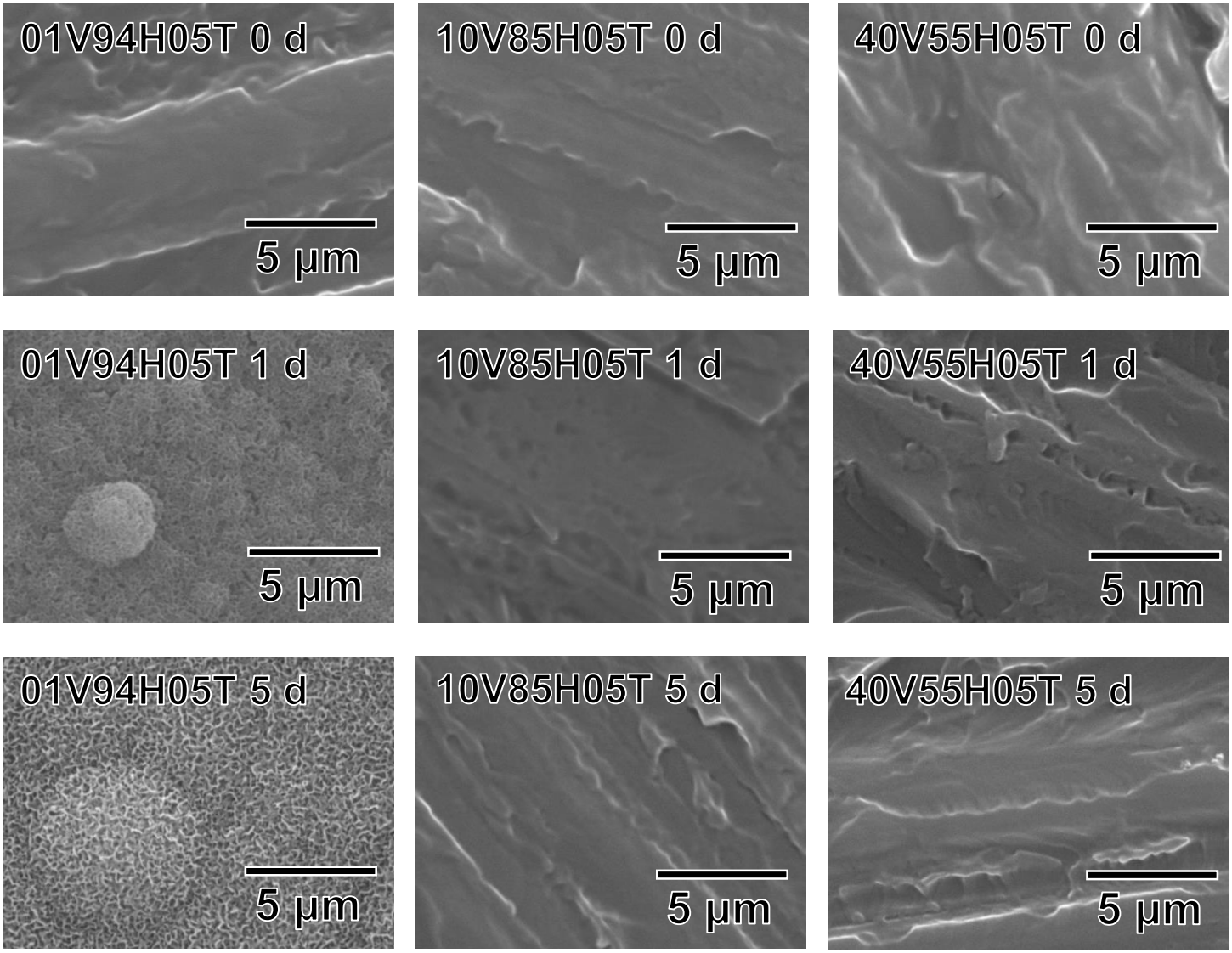

Figure 3 SEM images of surface of specimens after soaking in SBF for various periods.

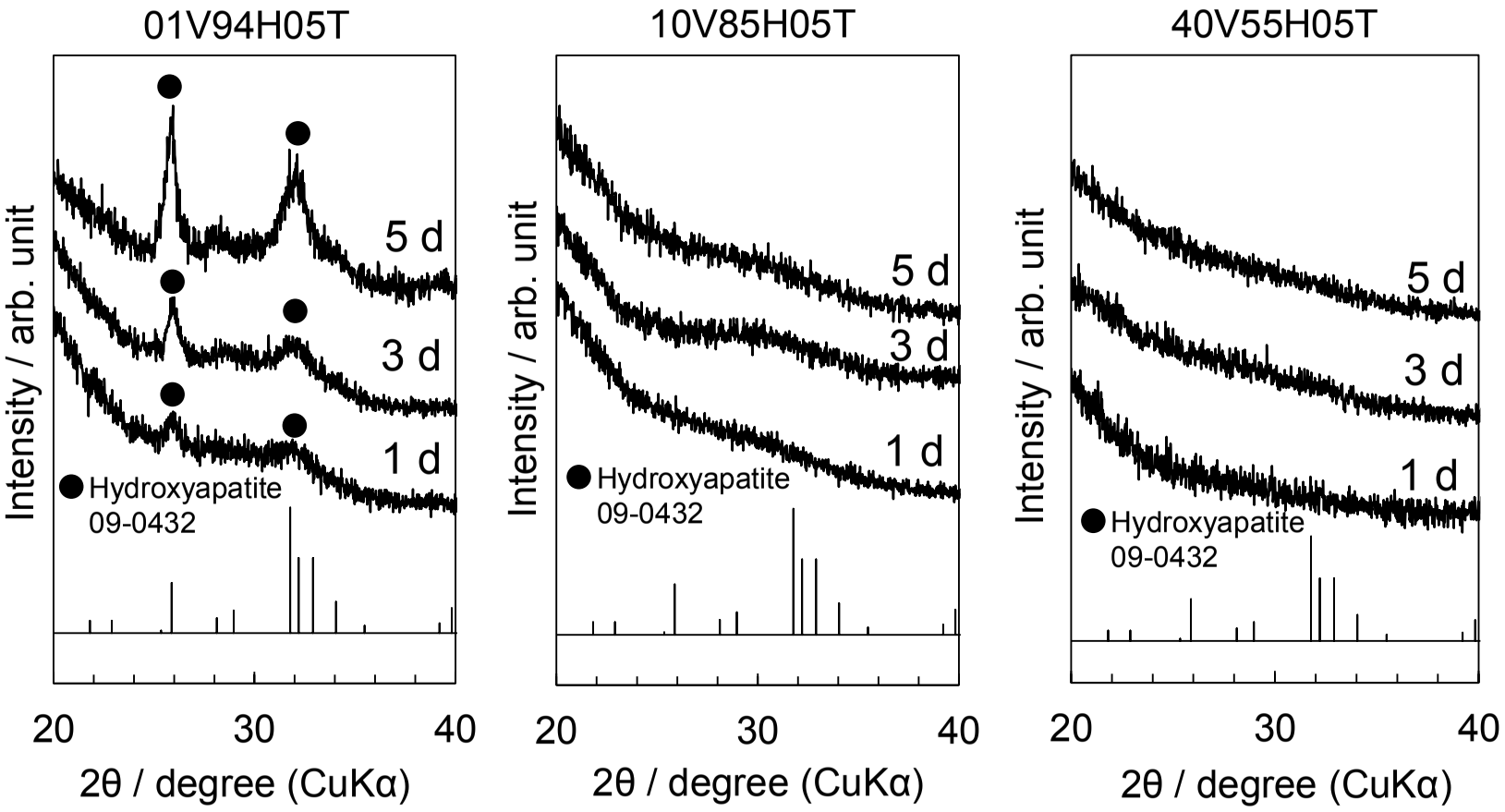

Figure 4 TF-XRD patterns of specimens solution after soaking in SBF for various periods.

Figure 3 shows SEM images of the surface of specimens after soaking in SBF for various periods. The depositions were observed on the 01V94H05T within 1 day, but not 10V85H05T and 40V55H05T within 5 days. The morphology of deposition was flake-like shape similar to bone-like apatite formed in simulated body environment [14].

Figure 4 shows TF-XRD patterns of the specimen after soaked in SBF for various periods. The two broad peaks were observed at in $2\theta = 26^{o}$ and 32^{o} corresponding to apatite (JCPDS#09-0432) for 01V94H05T within 1 day. On the other hand, the peaks were not observed in 10V85H05T and 40V55H05T within 5 days.

Figure 5 shows change in P, Ca concentration and pH in SBF after soaking the specimen for various periods. The P concentration was decreased with soaking time for the specimen of 01V94H05T. On the other hand, the P concentration was almost constant after soaking 10V85H05T or 40V55H05T. The Ca concentration was increased for all the specimens the early stage of soaking time, and subsequently slightly decreased. The degree of increase in Ca concentration increased in the order: 01V94H05T < 10V85H05T < 40V55H05T. The pH value was monotonically decreased only for 40V55H05T, while the pH slightly increased and became constant for the other specimens.

Figure 6 shows the change in molar ratio of Ca/P and P content on the surfaces of 01V94H05T and 10V85H05T after soaking in SBF for various periods. The Ca/P ratio of both specimens was decreased after 3 hours and then increased. Ca/P ratio of 01V94H05T was higher than 10V85H05T irrespective of soaking time. The P content of 01V94H05T was increased form 6 hours, while that of 10V85H05T was constant with soaking time in SBF.

Figure 7 shows the change in ζ potential of the specimen of 01V94H05T and 10V85H05T. The potential of 01V94H05T was changed from negative to positive after soaking in SBF after 9 hours. On the other hand, the potential of 10V85H05T was slightly increased from the negative value, but the potential became near the zero after 6 hours.

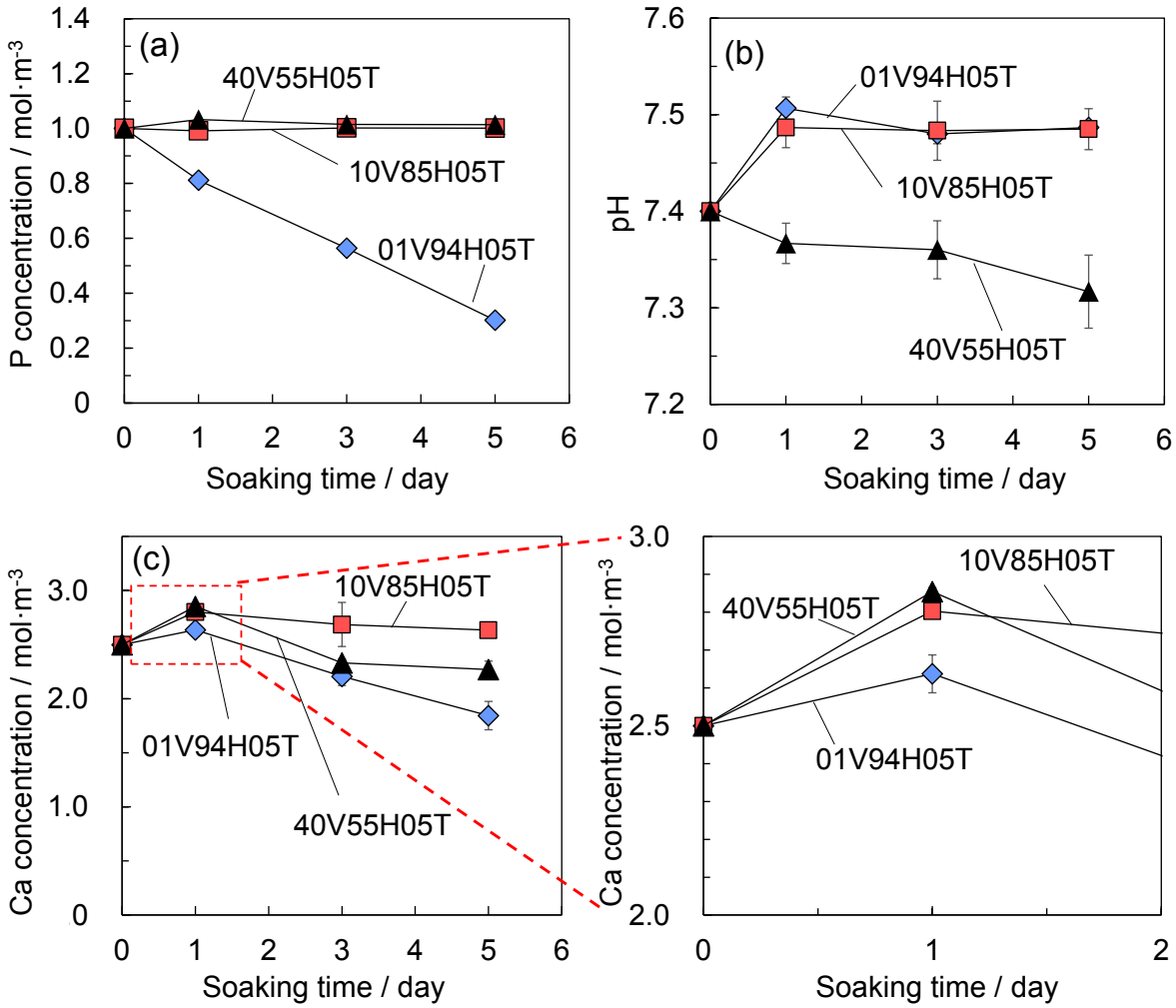

Figure 5 Change in P concentration (A), pH (B), and Ca concentration (C) in SBF with soaking of specimens for various periods.

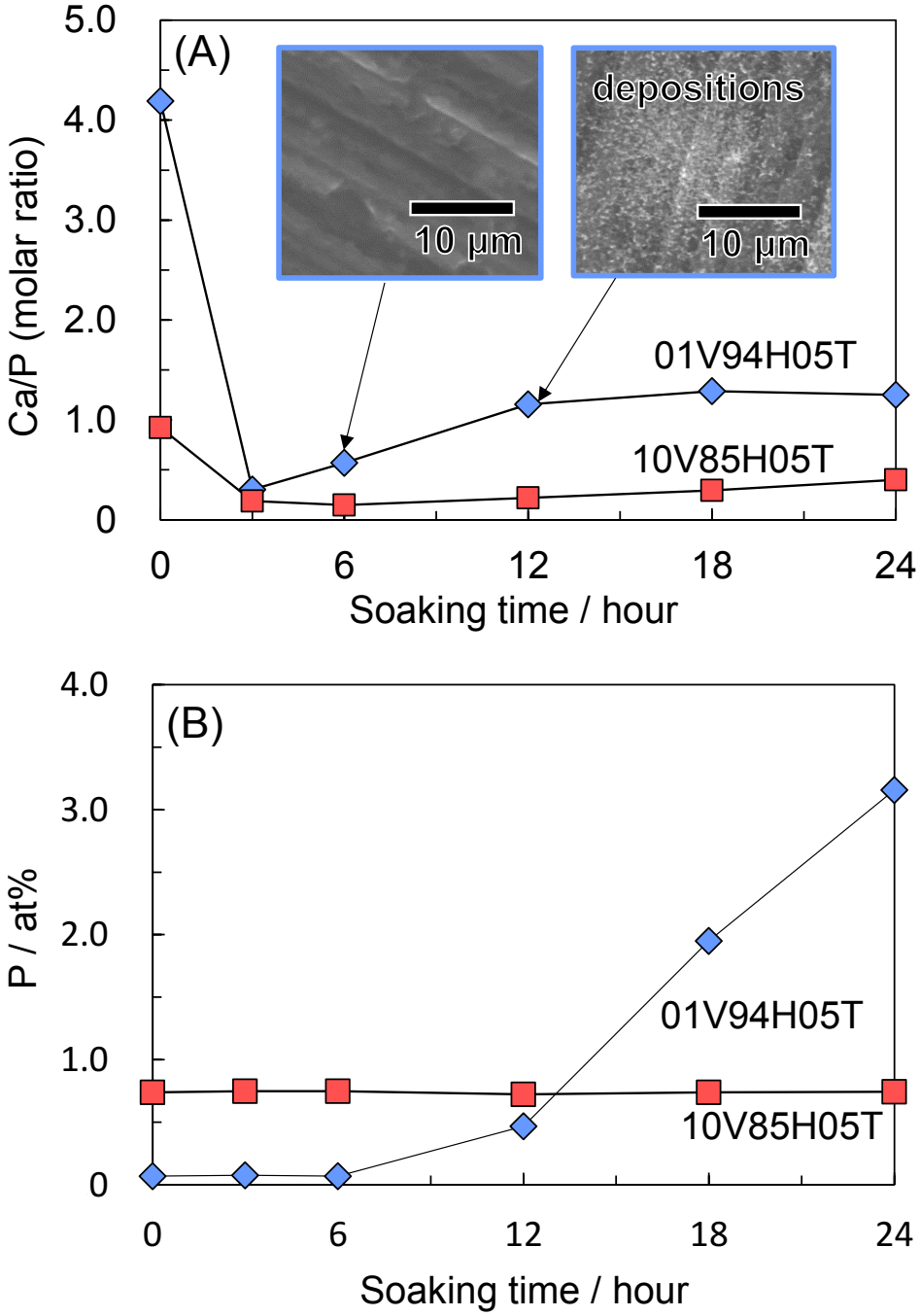

Figure 6 Change in molar ratio of Ca/P (A) and abundance of P (B) on the surface of 01V94H05T ad. 10V85H05T after soaking in SBF.

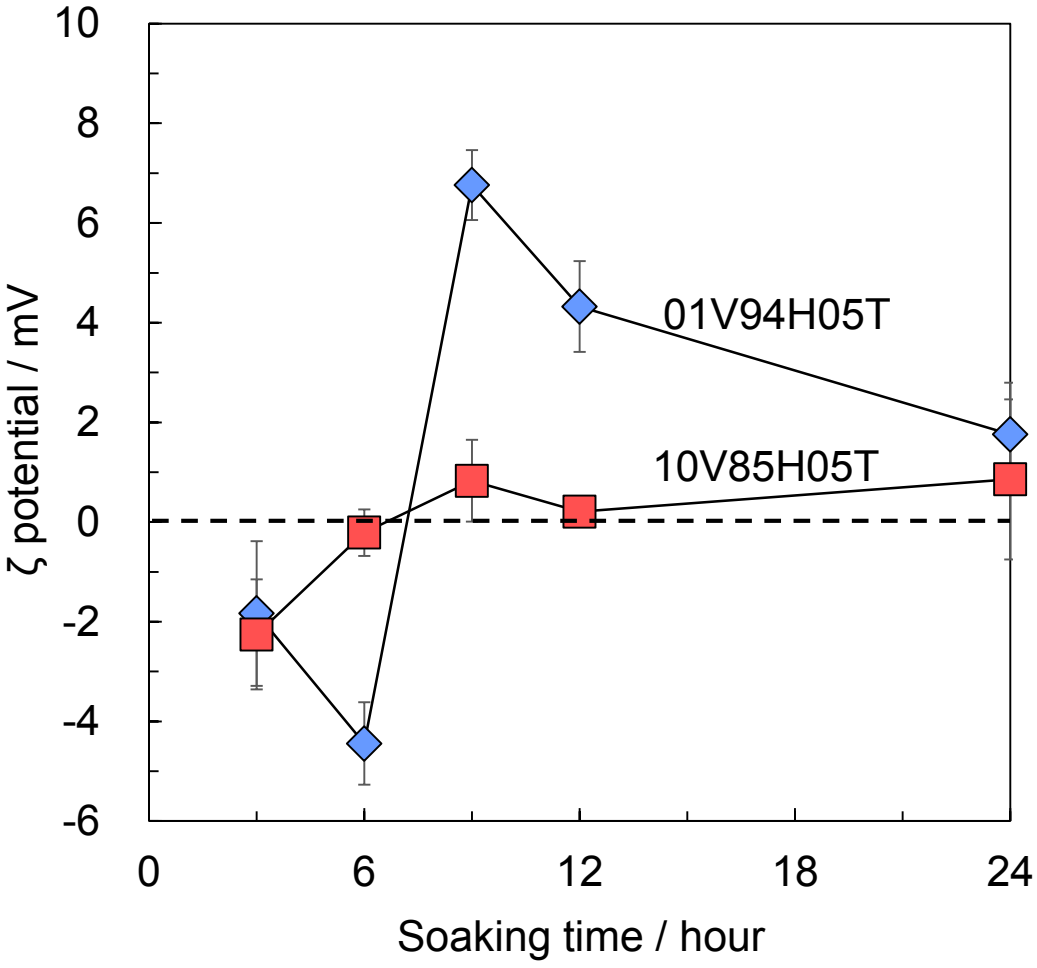

Figure 7 Change in surface ζ potential of 01V94H05T and 10V85H05T after soaking in SBF for various periods (n = 3).

Figure 8 shows FT-IR spectra of specimen after soaked in SBF for various periods. The peak at 900 cm^{-1} attributed to C-C stretching vibrations of HEMA was observed for 01V94H05T after soaked in SBF for 0-9 hour [15,16]. The peak disappeared after 12 hours due to formation of deposition on the specimen. In contrast, 10V85H05T displayed peak at 889 cm^{-1} attributed to P–O bond in the $–P–O^{-}\cdots Ca^{2+}$ complex [17] as well as the above peak of C-C stretching for all soaking time.

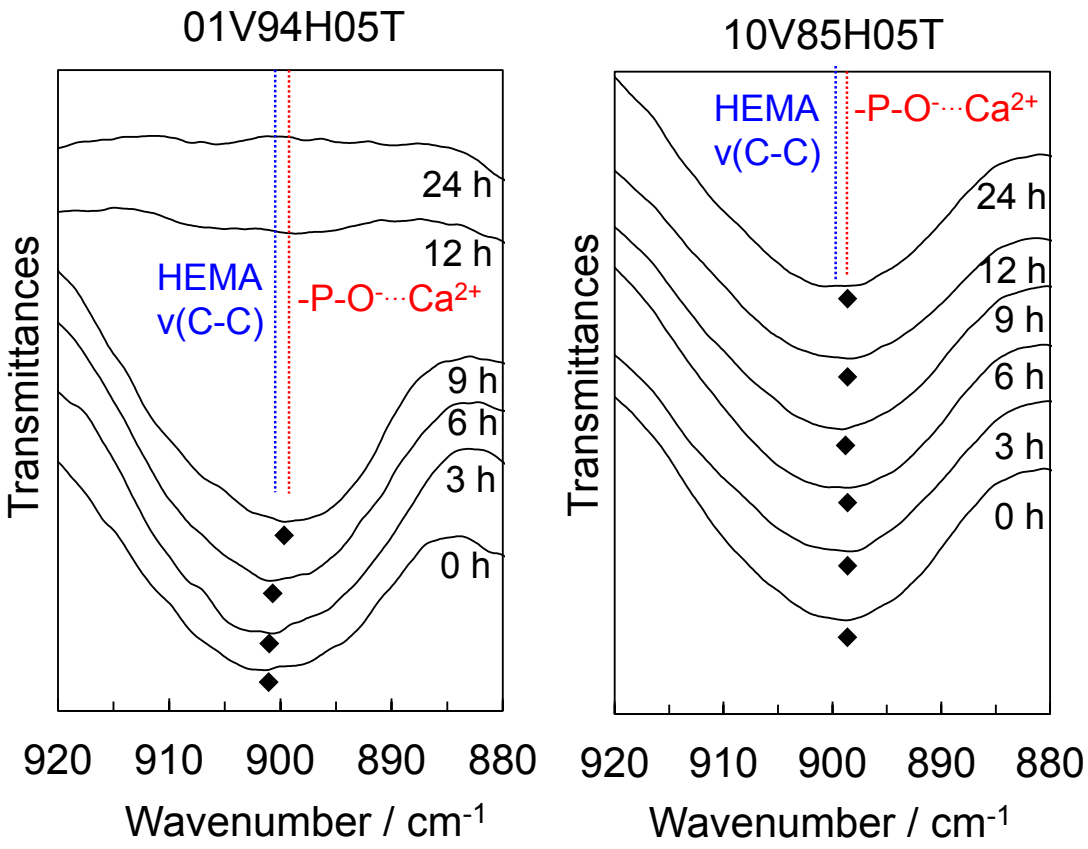

Figure 8 FT-IR spectra (resolution of 1 cm^{-1}) of the 01V94H05T and 10V85H05T after soaking in SBF for various periods.

4. Discussion

The FT-IR analysis for 40V55H05T and 10V85H05T revealed the polymerization of the VPA, HEMA and TEGDMA monomers, as evidenced by the observation of the vibration caused by the chemical bonds in the structure of these monomers (see Figure 1). But, the peaks delivered from phosphate groups of VPA was not detected. On the other hand, low amount of phosphorus in the 01V94H05T was also measured by EDX (see Figure 2 (A)). Thus, these results found that all specimens contained phosphate groups of VPA.

The amount of Ca incorporated into the prepared copolymer and release into Tris-NaCl increased with increase in content of phosphate group (see Figure 2). The swelling property is affected by not only cross-link density but also the charge of functional groups [5, 18]. The repulsion induced by the ionic groups with the same charge plays a role as driving force of the swelling. The increase in phosphate group content enhances the swelling, therefore lager content of the phosphate would promote the Ca^{2+} adsorption onto the copolymer by $CaCl_2$ treatment and Ca^{2+} release into the solution.

The apatite formation on the copolymer was rather suppressed with increase in phosphate content, in spite that Ca^{2+} release from the copolymer was enhanced. In order to discuss on that phenomenon, supersaturation degree with respect to apatite in SBF was calculated using the results of change in Ca and P concentration and pH value in SBF (see Figure 5). The relative supersaturation degree of σ is calculated according to equation (1) [19].

$$\sigma = \frac{IP_{HAp}^{\ 1/\nu} - Ksp_{HAp}^{\ 1/\nu}}{Ksp_{HAp}^{\ 1/\nu}} \tag{1}$$

IP_{HAp}, Ksp_{HAp}, and ν were ionic activity products of hydroxyapatite (HAp), solubility products of HAp (= 5.5×10^{-118}) and the number of ions in the molecule of HAp (=18), respectively. The IP_{HAp} was estimated according to equation (2) and using Ca^{2+} and PO_4^{3-} concentrations, and pH of SBF.

$$IP_{HAp} = (\gamma_{Ca^{2+}})^{10}(\gamma_{PO_4^{3-}})^{6}(\gamma_{OH^-})^{2}[Ca^{2+}]^{10}[PO_4^{3-}]^{6}[OH^-]^{2} \quad (2)$$

The value of $\gamma_{Ca^{2+}}$, $\gamma_{PO_4^{3-}}$ and γ_{OH^-} are supposed to be 0.36, 0.06 and 0.72 at physiological ionic strength (μ=0.16) [20]. Figure 9 shows change in relative supersaturation degree in SBF with soaking of copolymers for various periods. For all the specimens, the degree of supersaturation was slightly increased and subsequently decreased. The degree of the increase in supersaturation increased in the order: 40V55H05T ≈ 01V94H05T < 10V85H05T. However, the apatite was only formed 01V94H05T (see Figure 3 and 4). These results suggest that apatite formation of the copolymer was governed by surface chemical state rather than increase in supersaturation degree due to Ca^{2+} release.

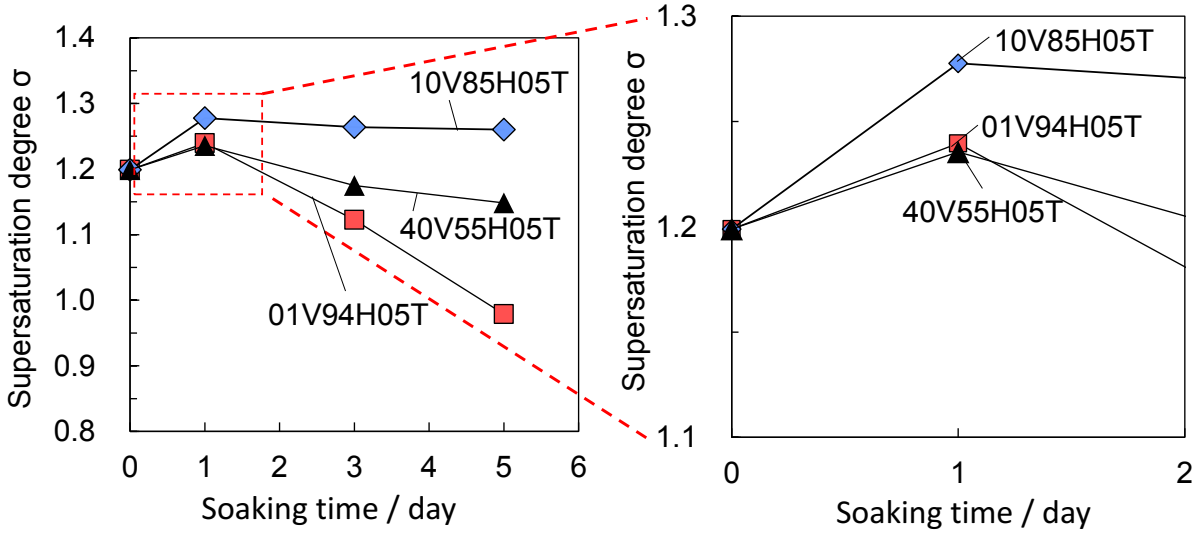

Figure 9 Change in supersaturation degree respect with apatite in SBF with soaking of specimens for various periods.

The difference in surface state of the specimens having various content of phosphate group in SBF can be interpreted as follows. ζ potential of 01V94H05T increased more significantly than 10V85H05T after 6 hours in SBF (see Figure 7). It is reported that the potential of soft solid like a gel or polymer is governed by not only the

charge on the outermost surface but also that inside of the solid in contrast to hard solid such as metal oxide [21, 22]. Therefore Ca^{2+} would be accumulated near the surface of the soft specimens after soaking in SBF. In addition, the complex of -P-O^{-} $\cdots$ Ca^{2+} was formed only in 10V85H05T in SBF (see Figure 8). Judging from the result, it is assumed that amount of free Ca^{2+} is larger than that of Ca^{2+} tightly bound to phosphate group on the surface and/or inside of 01V94H05T, and that negative charge on 10V85H05T is neutralized in SBF by tight binding with Ca^{2+}. The free Ca^{2+} would readily bond with phosphate ions in SBF to convert into the apatite. Subsequent decrease in ζ potential of 01V94H05T after 9 hours supports this assumption. On the other hand, further ion adsorption to induce the apatite nucleation did not occur on 10V85H05T.

The surface potential is previously reported as the factor that contributes to the apatite formation on various substrates in SBF [23]. For example, ζ potential of high molecular weight polyethylene incorporated with -SO_3H groups and Ca^{2+} convert into positive in SBF and subsequently adsorb phosphate ion to induce the apatite nucleation [24]. However, the polymer modified with only -SO_3H did not form the apatite in SBF. According to the principle of the apatite formation in the research, the surface potential of 10V85H05T did not convert to positive enough to adsorb HPO_4^{2-} and PO_4^{3-}, and therefore it did not form the apatite. The no change in P abundance on 10V85H05T in SBF also suggests the insufficient phosphate ion adsorption (see Figure 6).

The results in this study showed that materials with larger amount of phosphate group rather inhibit the apatite formation in SBF. However, phosphate groups in the self-assemble monolayer on the gold can interact with PO_4^{3-} after binding with Ca^{2+} in SBF, and then apatite formation was induced [3]. This suggests that the binding state of the phosphate groups with Ca^{2+} is different from the present results. On the other hand, acidity of phosphate-containing compounds is different by their chemical structure [25]. The effects of chemical structure on the binding state and apatite deposition on phosphate-containing composites should be investigation in future works.

5. Conclusion

The effects of the amount phosphate groups on apatite-forming ability of poly(VPA-HEMA-TEGDMA)-$CaCl_2$ composites were examined in SBF. The increase in additive amount of VPA enhanced Ca^{2+} release from copolymer. However, apatite formation was only induced on the copolymer added with 1 mol% of VPA. Higher VPA content rather inhibited the apatite formation, because phosphate ion could not react with Ca^{2+} adsorbed on the surface *via* the increase in amount of Ca^{2+} tightly binding with phosphate group. It was found that materials with high phosphate content were not always favorable for the rapid apatite formation in simulated body environment.

Reference

[1] S.B. Cho, K. Nakanishi, T. Kokubo, N. Soga, T. Kamamura, T. Kitsugi, T. Yamamuro, "Dependence of apatite formation on silica gel on its Structure: effect of heat treatment", *J. Am. Ceram. Soc.*, **78**, 1769-1774 (1995).

[2] M. Uchida, H-M. Kim, S. Fujibayashi, T. Nakamura, "Structural dependence of apatite formation on titania gels in a simulated body fluid", *J. Biomed. Mater. Res. part A*, **64A**, 164-170 (2003).

[3] M. Tanahashi, T. Matsuda, "Surface functional group dependence on apatite formation on self-assembled monolayers in a simulated body fluid", *J. Biomed. Mater. Res.*, **34**, 305-315 (1997).

[4] R.A. Gemeinhart, C.M. Bare, R.T. Haasch, E.J. Gemeinhart, "Osteoblast-like cell attachment to and calcification of novel phosphate-containing polymeric substrate", *J. Biomed. Mater. Res. part A*, **78A**, 433-440 (2006).

[5] J. Tan, R.A. Gemeinhart, M. Ma, W.M. Saltzman, "Improved cell adhesion and proliferation on synthetic acid-containing hydrogel", *Biomaterials*, **26**, 3663-3671 (2005).

[6] C. Ohtsuki, T. Kokubo, T. Yamamuro, "Mechanism of apatite formation on CaO-SiO_2-P_2O_5 glass in a simulated body fluid", *J. Non-Cryst. Solids*. **143**, 84-92 (1992).

[7] R. Nakamura, T. Miyazaki, Y. Morita, E. Ishida, R. Iwamatsu, C. Ohtsuki, "Apatite

formation abilities of various carrageenan gels in simulated body environment", *J. Ceram Soc. Jpn.*, **118**, 487-490 (2010).

[8] A. Takeuch, C. Ohtsuki, T. Miyazaki, H. Tanaka, M. Yamazaki, M. Yamazaki, M. Tanihara, "Deposition of bone-like apatite on silk fiber in a solution that mimics extracellular fluid", *J. Biomed. Mater. Res. part A*, **65A**, 283-289 (2003).

[9] J. Ellis, M. Anstice, A.D. Wilso, "The glass polyphosphonate cement: A novel glass-ionomer cement based on poly(vinyl phosphonic acid)", *Clin. Mater.*, **7**, 341-346 (1991).

[10] T. Miyazaki, C. Ohtsuki, Y. Akioka, M Tanikara, J. Nakao, Y. Sakaguchi, S. Konagaya, "Apatite Deposition on Polyamide Films Containing Carboxyl Group in a Biomimetic Solution", *J. Mater. Sci.: Mater. Med.*, **14**, 569-574 (2003).

[11] S. Jin, E. Gonsalves, "Functionalized copolymers and their composites with polylactide and hydroxyapatite", *J. Mater. Sci.: Mater. Med.*, **10**, 363-368 (1999).

[12] Y.J. Yin, X.Y. Luo, J.F. Cui, C.Y. Wang, X.M. Cuo, K.D. Yao, "A study on biomineralization behavior of N-methylene phosphochitosan scaffolds", *Macromol. Biosci.*, 4, 971-977 (2004).

[13] T. Kokubo, H. Takadama, "How useful is SBF in predicting in vitro bone activity ?", *Biomaterials*, **27**, 2907-2915 (2006).

[14] T. Kawai, C. Ohtsuki, M. Kamitakahara, T. Miyazaki, M. Tanihara, Y. Sakaguchi, S. Konagawa, "Coating of an appetite layer on polyamide films containing sulfonic groups by a biomimetic process", *Biomaterials*, **25**, 4529-4534 (2004).

[15] L. Ferreira, M.M. Vidal, M.H. Gil, "Evaluation of poly(2-hydroxyethyl methacrylate) gels as drug delivery systems at different pH values", *Int. J. Pharm*, **1**, 169-180 (2000).

[16] M.D.G. Faria, J.J.C.T. Dias, R. Fausto, "Conformation stability for methyl acrylate: a vibrational spectroscopic ab initio MO study", *Vib. Spectr.*, **2**, 43-60 (1991).

[17] J. Ellis, M. Anstice, A.D. Wilson, "The glass polyphosphonate cement: a novel glass-ionomer cement based on poly(vinylphosphonic acid)", *Clin. Mater.*, **7**, 341-346 (1991).

[18] Q. Garrett, B. Laycock, R.W. Garrett, "Hydrogel lens monomer constituents

modulate protein sorption", *Invest. Ophthalmol Sci.*, 41, 1687-1695 (2000).

[19] K. Hata, T. Kokubo, T. Nakamura, T. Yamamuro, "Growth of a bonelike apatite layer on a substrate by a biomimetic process", *J. Am. Ceram. Soc.*, **78**, 1049-1053 (1995).

[20] W. Neuman, M. Neuman, "The chemical dynamics of bone mineral", *Chicago, University of Chicago Press*, (1958).

[21] H. Ohshima, K. Makino, T. Kondo, "Interfacial electric phenomena and Donnan potential in membrance", *Membrane*, **12**, 425-430 (1987).

[22] K. Makino, H. Ohshima, T. Kondo, "Surface potential an ion-penetrable charged membrane", *J. Theor. Biol.*, **125**, 367-368 (1987).

[23] H-M. Kim, T. Himeno, M. Kawashita, J.H. Lee, T. Kokubo, T. Namamura, "Surface potential change in bioactive titanium metal during the process of apatite formation in simulated body fluid", *J. Biomed. Mater. Res. part A*, **67A**, 1305-1309 (2003).

[24] I.B. Leonor, H-M. Kim, F. Balas, M. Kawashita, R.L, Reis, T. Kokubo, T. Nakamura, "Surface potential change in bioactive polymer during the process of biomimetic apatite formation in a simulated body fluid", *J. Mater. Chem.*, **17**, 4057-4063 (2007).

[25] M. Moszern, U. Salz, J. Zimmermann, "Chemical aspects of self-etching enamel-dentin adhesives: a systematic review", *Dent. Mater.*, 21, 895-910 (2005).

Chapter 3

Structural Effects of Phosphate Groups on Apatite Formation on Polymer-$CaCl_2$ Composites in Simulated Body Environment

1. Introduction

Bone-bonding bioactivity is one of essential properties to implant the bone substitute in bone defects for a long time. It has been discovered that existence of Si-OH groups on the bioactive ceramics allows bonding to bone tissue *via* formation of low-crystalline apatite layer [1-4]. However, bioactive ceramics would cause adsorption of bone tissue surrounding the implantation part due to their higher Young's moduli of them than that of bone tissue (i.e. stress shielding).

Tanahashi *et al*. revealed that phosphate groups ($-PO_3H$) immobilized in the self-assembly monolayer exhibited inducing heterogeneous nucleation of apatite in simulated body fluid (SBF) [4]. This fundamental research indicates that chemical modification with phosphate groups provide the bone-bonding bioactive polymer or organic-inorganic composites showing mechanical properties similar to living bone. Datta *et al.* found that the poly(vinyl alcohol) modified with the phosphate groups using phosphoric acid treatment formed calcium phosphate in SBF [5]. In addition, López-Pérez *et al.* also reported that surface modification using poly(vinylphosphonic acid) enhanced the osteoblast-like cell adhesion and growth on the poly(ε-polycaprolactone) scaffold [6].

In Chapter 2, the effects of phosphate group content on the apatite-forming behavior of composites consisting of vinylphosphonic acid-based copolymer and $CaCl_2$ were investigated. As a result, the increase in phosphate group content rather inhibited the apatite formation in SBF, in spite that the composites released Ca^{2+} into SBF. These results suggest that modification with the phosphate groups using vinylphosphonic acid has adverse the effect on the apatite formation in SBF.

The reason why such different phenomena occurred is considered to be the molecular structure of phosphate groups. They have two types of structure: phosphonic

acid (-C-PO_3H_2) and phosphoric acid (-O-PO_3H_2). Tanahashi *et al*. and Datta *et al.* used -O-PO_3H_2. In contrast, -C-PO_3H_2 was used in Chapter 1 and 2. Such structural difference is expected to affect interaction with Ca^{2+} and the subsequent apatite formation, because stability of the ionized phosphate groups would be dependent on element substitution in them due to inductivity effect (I effect) [7]. However, this point has remained unclear.

In this Chapter, polymer-$CaCl_2$ composites containing either -C-PO_3H_2 or -O-PO_3H_2 were prepared under the same synthetic condition and examined the apatite-forming behavior on their surfaces in SBF. Furthermore, mechanism of the apatite formation on the composites was discussed by using chemical analytical and computational approach.

2. Materials and methods

2.1 Preparation of composite modified with different type of phosphate groups

Vinylphosphonic acid (VPA, 95 %, Tokyo Chemical Industry Co., Ltd., Tokyo, Japan) for -C-PO_3H_2, and methacryloyloxyethyl phosphate (MOEP, 90%, Phosmer^{TM} M, Yuni Chemical Co., Ltd., Nara, Japan) for -O-PO_3H_2 were used to incorporate the different phosphate into the copolymer. 2-hydroxyethyl methacrylate (HEMA, 95 %, Wako Pure Chemical Industries, Ltd., Osaka, Japan) and triethylene glycol dimethacrylate (TEGDMA, 90 %, Wako Pure Chemical Industries, Ltd.) were mixed with VPA or MOEP. The molar ratio of monomers was VPA:HEMA:TEGDMA = 10:85:5 or MOEP:HEMA:TEGDMA = 7:88:5, and total amount of monomers was 10 g. The sequence of the photo-induced copolymerization was same to the method of Chapter 2. Finally, the 10 g of copolymer in the size of 10 mm ×10 mm ×1 mm was obtained. The copolymers were soaked in 30 cm^3 of 0, 0.1 or 1 $kmol \cdot m^{-3}$ $CaCl_2$ solution at 36.5°C for 1 day. The specimen prepared from VPA and MOEP was denoted as VPA(C)XCa or MOEP(O)XCa, respectively, where X of 0, 01 and 1 corresponds to 0, 0.1 and 1 $kmol \cdot m^{-3}$ $CaCl_2$ solution, respectively.

2.2 Soaking of specimens in SBF, SBF1.5Ca or Tris-NaCl buffer

SBF (Na^+ 142.0, K^+ 5.0, Mg^{2+} 1.5, Ca^{2+} 2.5, Cl^- 147.8, HCO_3^- 4.2, HPO_4^{2-} 1.0, SO_4^{2-} 0.5 mol·m^{-3}) with pH 7.40 were prepared following method as described by literature [8]. In addition, the solution which has Ca^{2+} concentration 1.5 times of SBF (SBF1.5Ca) with pH 7.25 was also prepared by the same method of SBF [9]. The specimens were soaked in 30 cm^3 of SBF or SBF1.5Ca at 36.5°C for a maximum of 14 days.

Tris-NaCl buffer (NaCl 142, tris(hydroxymethyl) aminomethane 50 mol·m^{-3}) with pH 7.40 was prepared in the same method of Chapter 2. The specimens were soaked in 30 cm^3 of Tris-NaCl buffer at 36.5°C for various periods to measure the release amount of Ca^{2+} from them.

2.3 Characterization of the specimens

The neutralizing titration was performed to measure the the phosphate group content and acid dissociation constant (pK_a) of the specimens. 30 cm^3 of 0.16 kmol·m^{-3} NaCl solution with soaking of 0.1 g of VPA(C)0Ca or MOEP(O)0Ca was titrated using 0.01 kmol·m^{-3} of NaOH solution at 36.5°C. While the titration, pH value of the solution was measured by pH electrode (6261-10C, Horiba Ltd., Kyoto, Japan).

Ca content of the specimens before soaking in $CaCl_2$ solution were measured by energy-dispersive X-ray (EDX) analysis system (EMAX Energy, Horiba Ltd.). The surface of the specimens after soaking in SBF or SBF1.5Ca were analyzed by thin-film X-ray diffraction (TF-XRD; MXP3V, Mac Science, Co., Yokohama, Japan), X-ray photoelectron spectroscopy (XPS; KRATOS Nova, KRATOS Analytical Ltd., Manchester, UK) and scanning electron microscope (SEM; S-3500N, Hitachi Co., Tokyo, Japan). For the analysis using TF-XRD, the angle of incident X-ray (CuKα) was fixed at 1° against surface of specimen. In the XPS analysis, the spectra were measured with high resolution scan at 20 eV of pass energy, using AlKα ($h\nu$ = 1486.6 eV) as X-ray source.

The binding energy of these element spectra was calibrated by binding energy of methylene group (284.6 eV). The observed spectra were subjected to peak fitting for searching possible components using the blend function consisting of Gaussian (70%) and Lorentzian (30%).

Surface ζ potential of the VPA(C)1Ca and MOEP(O)01Ca in SBF was measured by ζ potential & particle size analyzer (ELS-Z, Otsuka Electronics Co., Osaka, Japan) connected to box-like quartz cell. The specimens after soaked in SBF for various periods were washed with ultra-pure water, and then they were placed in the quartz cell. The fresh SBF added with monitor particles of polyethylene latex (Otsuka Electronics Co.) was injected into the cell, and subsequently electrophoretic mobility of the particles was measured by laser Doppler method to fine the ζ potential. The initial ζ potential of MOEP(O)0Ca and VPA(C)0Ca also measured as follows. The powdered specimens were soaked in Tris-NaCl buffer and subsequently electrophoretic mobility of the powder was measured to obtain the value of the potential.

The Ca and P concentration, and pH of SBF or Tris-NaCl buffer after soaking the composite specimens were measured by inductively coupled plasma atomic emission spectrometer (ICP-AES; ICPE-9820, SHIMADZU Co., Kyoto, Japan) and the pH meter, respectively.

2.4 Evaluation of the formation constant for phosphate groups-containing polymer-Ca^{2+} complex.

The stability constant of the polymer-Ca^{2+} complex was determined by reference to the method reported by literature [10]. The Ca^{2+} was incorporated into 0.1 g of the VPA(C)0Ca and MOEP(O)0Ca in the 30 cm^3 of a 10 $mol \cdot m^{-3}$ $CaCl_2$ for 5 days at 36.5°C. Subsequently, they were soaked in 30 cm^3 of Tris-NaCl buffer similar to physiological condition (ion strength: $\mu = 0.16$, pH 7.40, 36.5°C) for 5 days. The common logarithm of the stability constant (log β) for the complex in the buffer was calculated using Eqn. (1):

$$\log\beta = \log\left(\frac{[-\mathrm{P_{ion}}\cdots\mathrm{Ca^{2+}}]}{[*\mathrm{Ca^{2+}}][*-\mathrm{P_{ion}}]}\right) \quad (1)$$

where [-$P_{ion}\cdots Ca^{2+}$], [*Ca^{2+}], [*-P_{ion}] are the molar concentration of the complex between ionized phosphate groups in the copolymer, free Ca^{2+} and ionized phosphate groups not interacted with Ca^{2+}, respectively, in the Tris-NaCl buffer. These values of the concentration were calculated by the content of phosphate groups in the copolymer, pKa of the groups at μ = 0.16, and concentration of Ca in the $CaCl_2$ solution and buffer measured by ICP-AES.

2.5 Simulation of the dipole moment and molecular orbital of the model

The highest occupied molecular orbital (HOMO), the lowest unoccupied molecular orbital (LUMO) and dipole moment for different type of the phosphate groups interacted with Ca were evaluated *via* computational approach. The model molecular of CH_3-CH_2-PO_3Ca and CH_3-O-PO_3Ca were developed. The models with the lowest energy were found using the restricted local density approximation and the Perdew-Wang correlational (LDA/PWC) method® with double-numerical basis sets, as implemented in the DMOl3 software package®[11-12]. The ground-state geometries were calculated with the phosphate groups bound to Ca as structural models to evaluate their electron density states. The dipole moments of the species were determined using the Hirshefeld approach.

3. Results

Table 1 shows content of phosphate groups in the copolymer prepared from different monomers, their pKa at 36.5°C, and ζ potential in Tris-NaCl buffer. VPA(C) and MOEP(O) copolymer contained nearly equivalent amount of the phosphate group. The constants of first and second proton dissociation of MOEP(O) were lower than those of VPA(C). The MOEP(O) had lower negatively charge than VPA(C) in the Tris-NaCl buffer. The phosphate content in the specimens indicates that 32.5 and 48.8% of the initial additive amount of VPA and MOEP monomers, respectively, were reacted to cnstruct the

polymer chains.

Table 1 Phosphate groups content (n = 4), acid dissociation constant and ζ potential (n = 3) of different copolymer under physiological condition.

	VPA(C)	MOEP(O)
Phosphate groups / mmol·g^{-1}	0.24±0.02	0.24±0.002
pKa_1	3.63	3.48
pKa_2	6.11	5.96
ζ potential / mV	-15.9±0.9	-27.0±0.4

Figure 1 show Ca/P molar ratio of the specimens after treated with different concentration of $CaCl_2$ solution (A) and Ca concentration in Tris-NaCl buffer following soaking of the specimens (B). The ratio for VPA(C) and MOEP(O) were almost similar at the same $CaCl_2$ concentration. The Ca concentration in the Tris-NaCl buffer increased and became almost constant after 7 days for all the specimens. The Ca concentration at 14 days was in the order: MOEP(O)1Ca > VPA(C)1Ca ≈ MOEP(O)01Ca > VPA(C)01Ca.

Figure 2 shows TF-XRD patterns of the composite specimens after soaking in SBF for various periods. MOEP(O)01Ca and MOEP(O)1Ca displayed two broad peaks at 2θ = 26° and 32° attributed to apatite (JCPDS #09-0432) after 7 days and 1 day, respectively. In contrast, VPA(C)01Ca and VPA(C)1Ca did not displayed these peaks within 14 days.

Figure 3 shows SEM images of the surfaces of different specimens after soaking in SBF for various periods. The deposition was observed on the MOEP(O)01Ca and MOEP(O)1Ca after 7 days and 1 day, respectively, but not VPA(C)01Ca and VPA(C)1Ca. The morphology of primary particles having plate scale-like shape in the deposition was similar to the apatite formed in SBF [13].

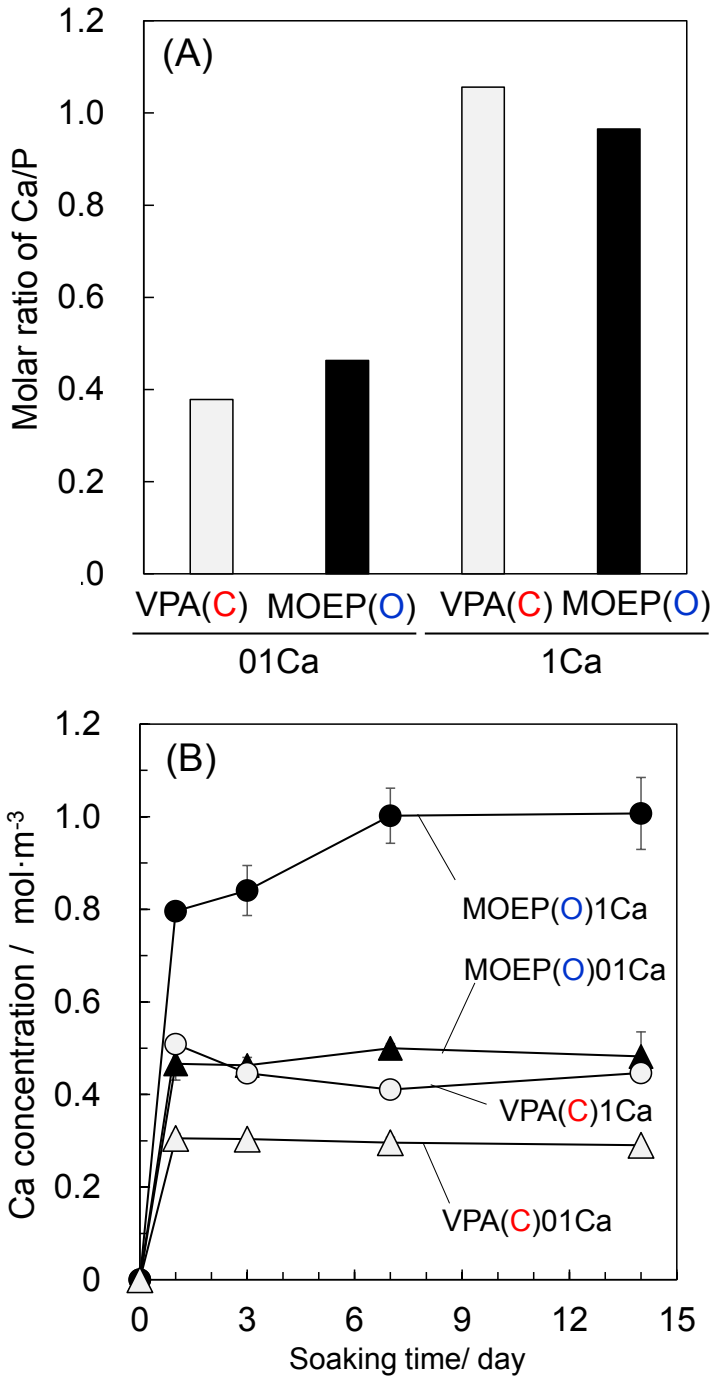

Figure 1 Ca/P molar ratio of the different composite after soaking in 0.1 or 1 kmol·m^{-3} of $CaCl_2$ solution (A) and Ca concentration in Tris-NaCl buffer following soaking of the composites for various periods (n =3) (B).

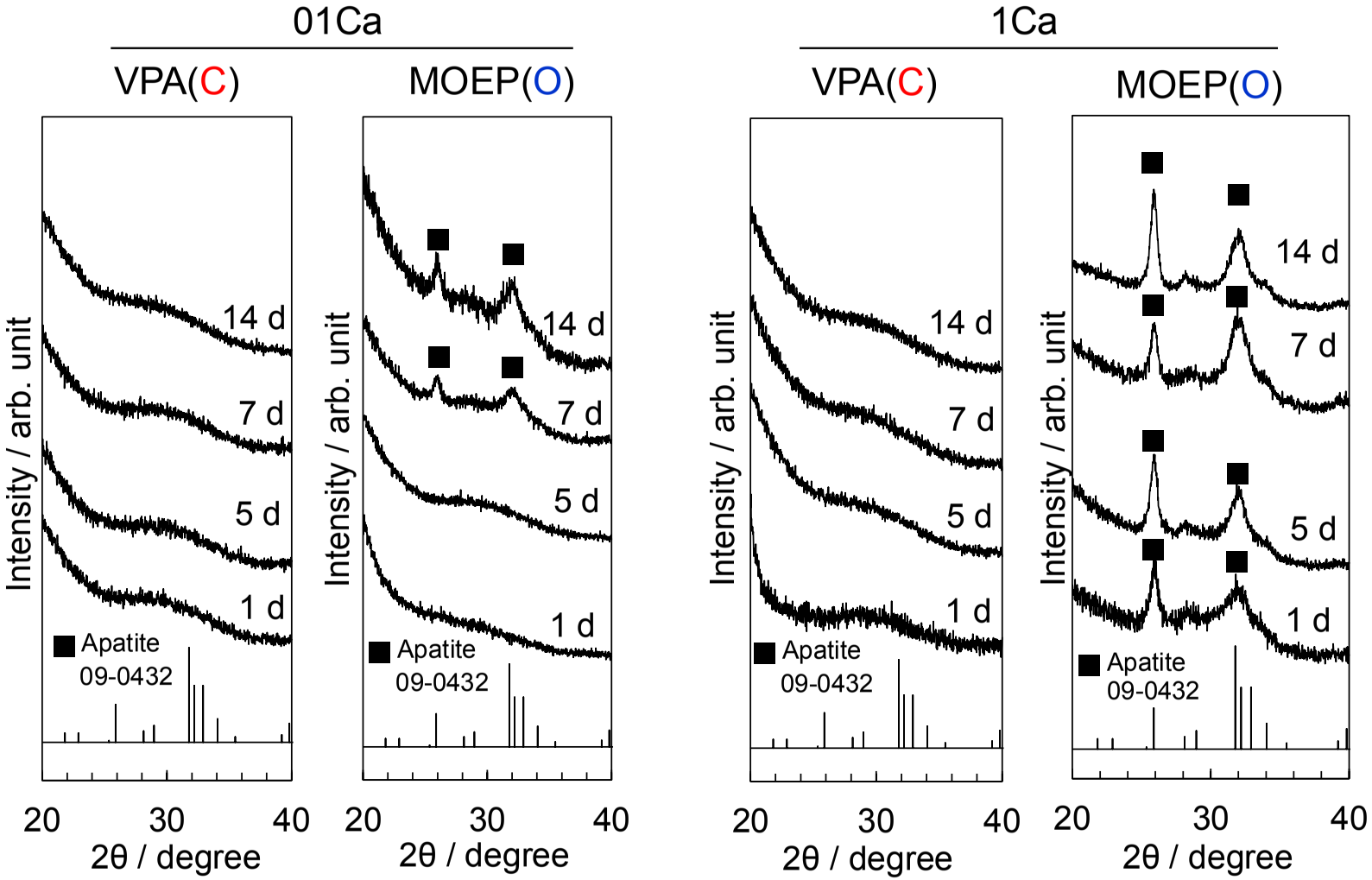

Figure 2 TF-XRD patterns of the composite specimens after soaking in SBF for various periods.

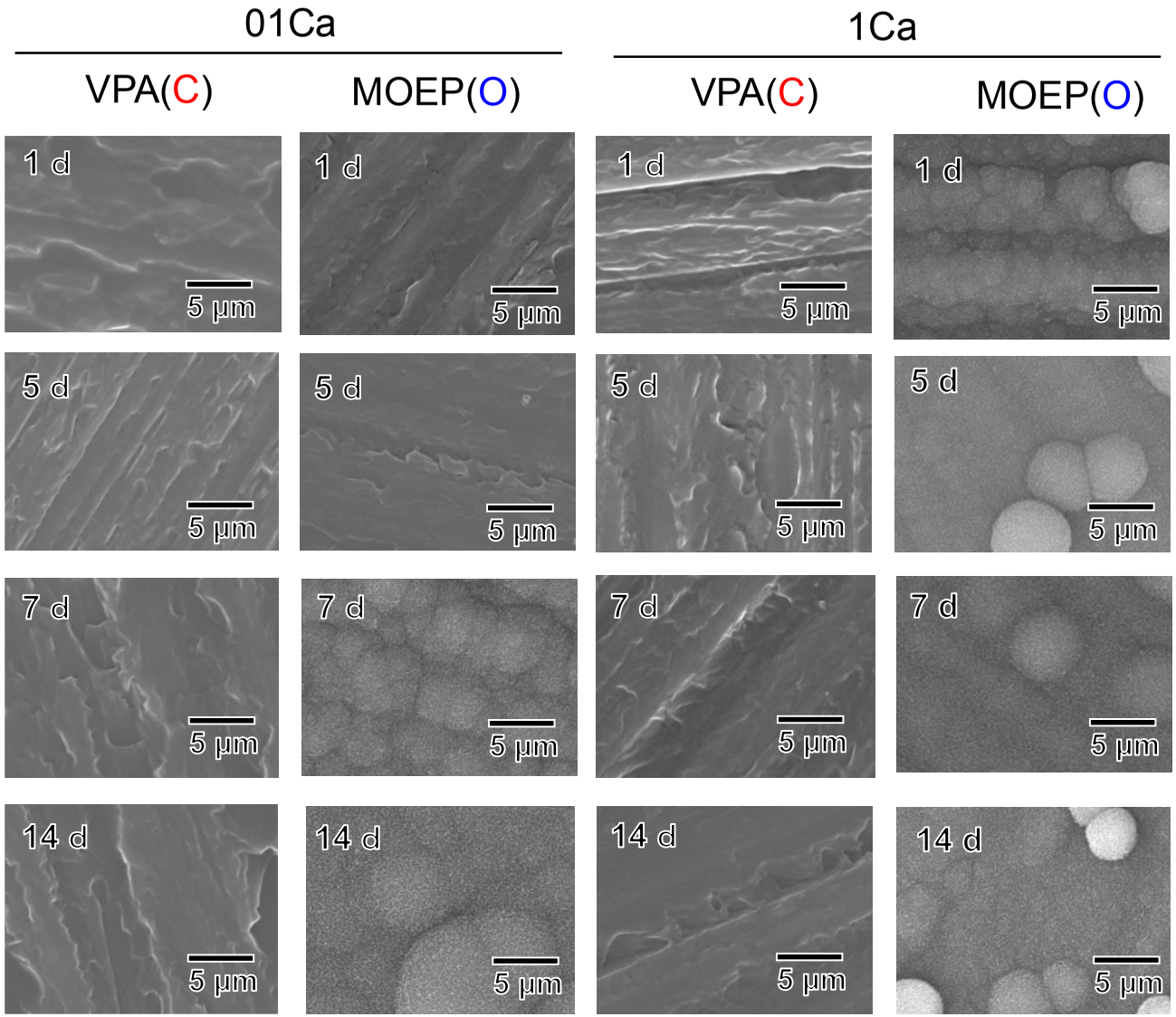

Figure 3 SEM images of the composite specimens after soaking in SBF for various periods.

Figure 4 (A) shows XPS spectra of the surfaces of VPA(C)1Ca and MOEP(O)01Ca after soaking in SBF for various periods. The VPA(C)1Ca displayed peaks assigned to -C-PO_3H_2 and -C-PO_3Ca at 133.2 and 132.7 eV, respectively [14]. The peak position did not shift regardless of soaking time. In contrast, MOEP(O)01Ca displayed peaks assigned to -O-PO_3H_2 and -O-PO_3Ca at 134.5 and 133.8 eV, respectively [15]. These peaks were decreased after 3 hours, while those corresponding to $CaHPO_4$ [16] and octacalcium phosphate (OCP) [17] were newly observed at 133.4 and 133.2 eV, respectively. Then, the peak corresponding to the apatite was observed at 133.0 eV after 1 day [18]. Figure 4 (B) shows change in rate of component for each calcium phosphate formed on the MOEP(O)01Ca calculated from the area of the fitting peaks in P_{2p} spectra. Proportion of $CaHPO_4$ and OCP initially increased up to 3 hours and then decreased with soaking time, while that of the apatite monotonically increased. Phase of the calcium phosphate was almost the apatite after 7 days.

Figure 5 shows change in the surface ζ potential of the VPA(C)1Ca and MOEP(O)01Ca following soaking in SBF. The potential of both specimens changed from negative to positive after 5 days. Afterwards the potential of VPA(C)1Ca was almost constant, while that of MOEP(O)01Ca decreased to negative after 7 days.

Figure 6 shows change in Ca and P concentration, and pH value following soaking of different specimens in SBF for various periods. Ca concentration after 1 day decreased according to: VPA(C)1Ca > MOEP(O)1Ca ≈ MOEP(O)01Ca > VPA(C)01Ca. Then, the Ca concentration gradually decreased for all the specimens. P concentration significantly decreased for MOEP(O)01Ca and MOEP(O)1Ca, while it was almost constant for VPA(C)01Ca and VPA(C)1Ca. The pH value of the SBF following the soaking of all the specimens were increased after 1 day, and then gradually decreased.

Figure 7 shows P_{2p} XPS spectra of VPA(C)0Ca and MOEP(O)0Ca after soaked in SBF1.5Ca for various interval. The peaks assigned to -C-PO_3H_2 and -C-PO_3Ca were observed for VPA(C)0Ca and they were almost constant regardless of the soaking time.

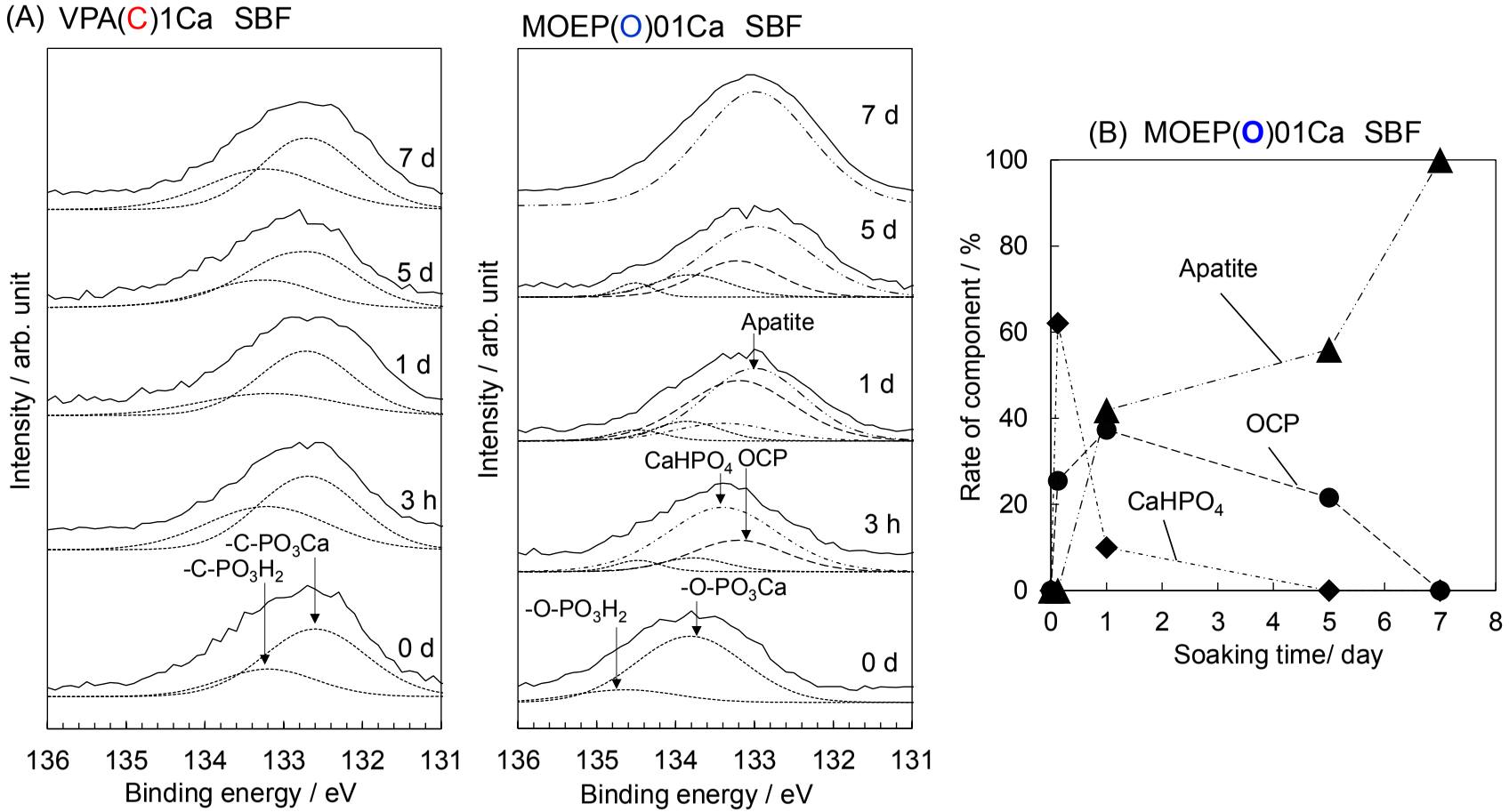

Figure 4 P_{2p} XPS spectra of VPA(C)1Ca and MOEP(O)01Ca (A) and change in rate of component of calcium phosphate formed on the MOEP(O)01Ca (B) after soaking in SBF for various periods.

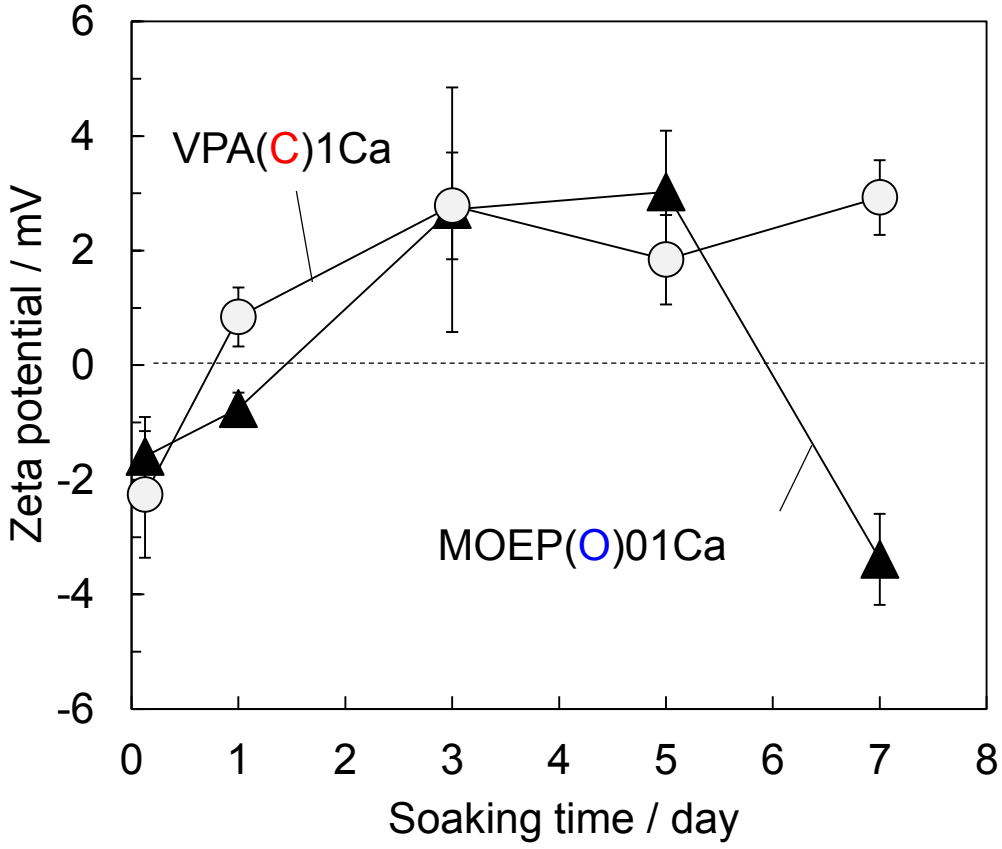

Figure 5 Change in surface ζ potential of VPA(C)1Ca and MOEP(O)01Ca after soaking in SBF for various periods (n = 3).

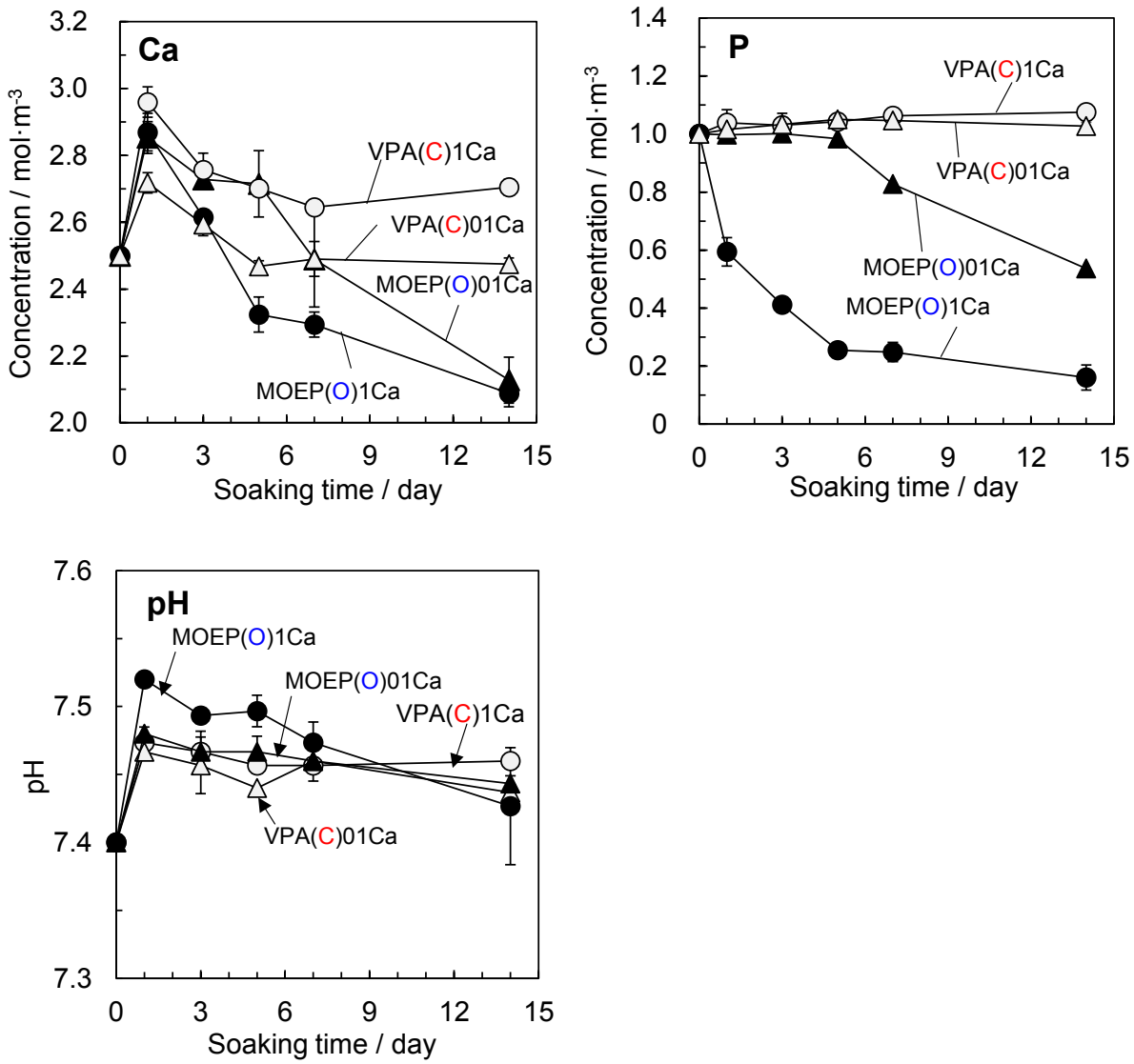

Figure 6 Change in Ca and P concentration and pH in SBF following soaking of different composite specimens for various periods (n = 3).

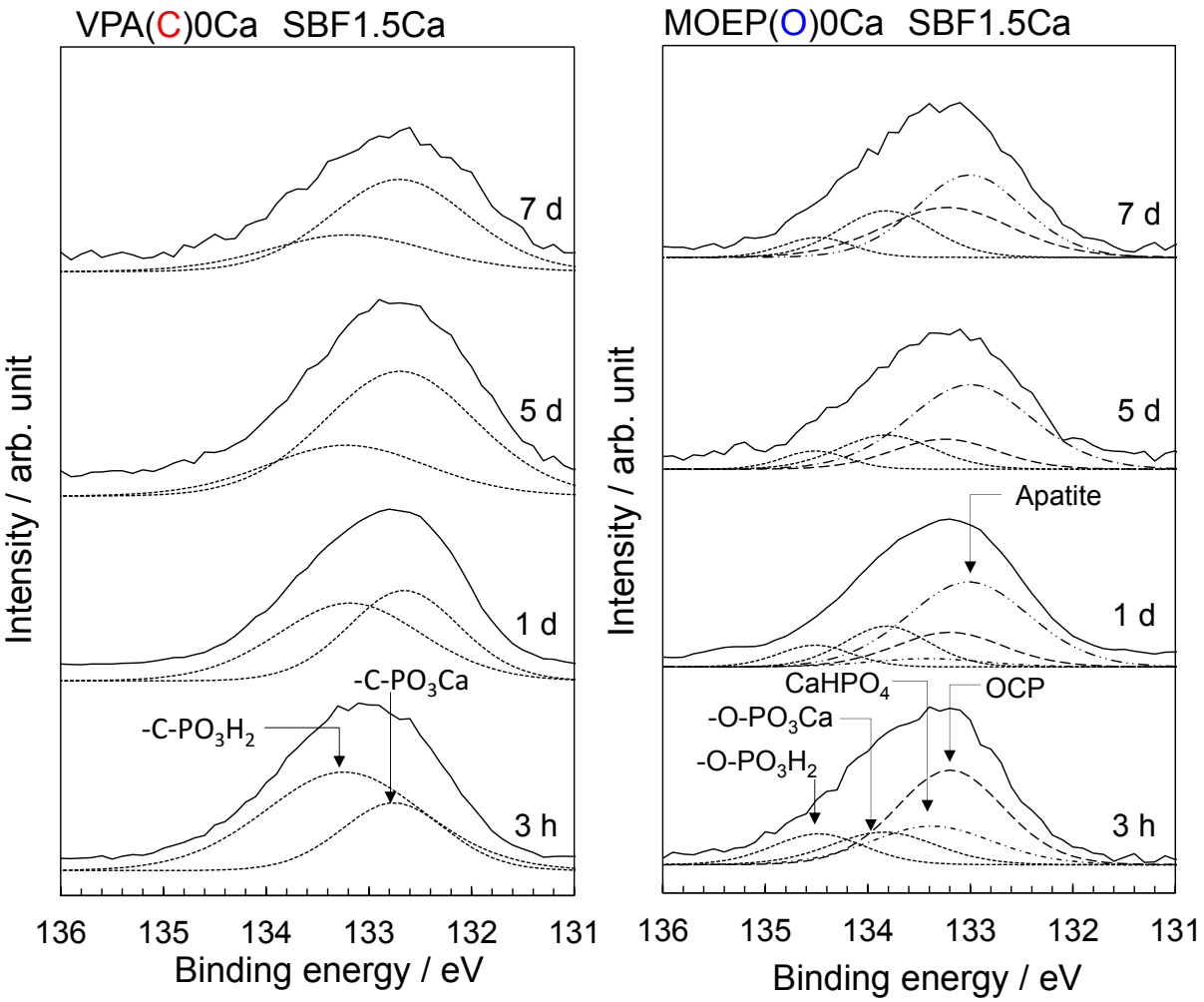

Figure 7 P_{2p} XPS spectra of VPA(C)0Ca and MOEP(O)0Ca after soaking in SBF1.5Ca for various periods.

On the other hand, the peaks assigned to $CaHPO_4$ and OCP as well as -O-PO_3H_2 and -O-PO_3Ca were observed for MOEP(O)0Ca after 3 hours. The peaks delivered from $CaHPO_4$ and OCP were almost replaced by those of the apatite after 1 day. This means that initial process of the calcium phosphate formation is almost similar irrespective of incorporation of Ca^{2+} in advance, in comparison with Figure 4.

Table 2 shows stability constants of polymer-Ca^{2+} and $CaHPO_4$ (aq.) complex under the physiological condition. The constant for the $CaHPO_4$ (aq.) complex under this condition was calculated by the constant under the ion strength $I = 0.02$ at 37°C reported by Chughtai e*t al* [19]. The constant increased in the order: MOEP(O) < HPO_4^{2-} < VPA(C).

Table 2 Stability constants of ionized phosphate group-Ca^{2+} complex on the different polymers (n = 4) in comparison with that of $CaHPO_4$ (aq.) under the physiological condition.

	VPA(C)	$CaHPO_4$(aq.)	MOEP(O)
log β	4.44±0.07	3.41	3.08±0.13

Figure 8 shows the structure with the lowest energy from the molecular models of CH_3-CH_2-PO_3Ca and CH_3-O-PO_3Ca, and their calculated distribution of highest occupied molecular orbital (HOMO) and lowest unoccupied molecular orbital (LUMO). The O atom bind with P *via* double bond close to the Ca atom in the CH_3-CH_2-PO_3Ca. On the other hand, this was located in the reverse direction from Ca in CH_3-O-PO_3Ca. The HOMO distributed around the O atoms, while the LUMO distributed widely around the Ca atom in for both the phosphates. The energy levels of the HOMO and LUMO for CH_3-CH_2-PO_3Ca were -0.156 and -0.188, and for CH_3-O-PO_3Ca were -0.186 and -0.146 eV, respectively. The value of the dipole moment of CH_3-CaH_2-PO_3Ca and CH_3-O-PO_3Ca were 9.35 and 15.7 Debye. This indicates that structural difference in phosphate groups bound with Ca was not at the molecular orbital level, but rather a result of the

most stable structure and polarization.

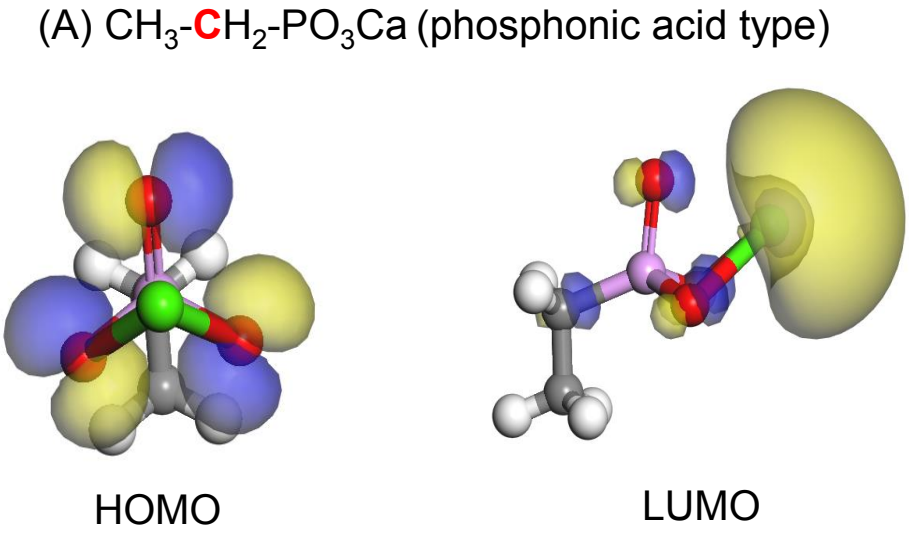

Figure 8 The model structure of CH_3-CH_2-PO_3Ca (A) and CH_3-O-PO_3Ca (B) with the lowest energy for each types of phosphate groups (white: H, gray: C, red: O, purple: P, green: Ca atom) and their HOMO-LUMO distribution.

4. Discussion

The composites containing equivalent amount of the phosphate group and Ca were prepared through the photo-induced radical polymerization (see Table 1 and Fig. 1(A)). It was revealed that the composite modified with -O-PO_3H_2 and had much higher apatite-forming ability in SBF than that modified with -C-PO_3H_2, when it was treated with $CaCl_2$ solution (See Figs. 2 and 3). This means that modification with -O-PO_3H_2 is more effective for the apatite formation on the composites rather than -C-PO_3H_2.

Heterogeneous nucleation is occurred by formation of pre-nucleation-cluster (embryo) which becomes larger than critical size r^* on substrate. The activation free energy (ΔG^*) for the heterogeneous nucleation is expressed in Eqn. (2) [20]:

$$\Delta G^* = \frac{16\gamma^3 f(\theta)}{3\left(\frac{kT}{V_\beta}\ln(\sigma)\right)^2} \tag{2}$$

where γ and $f(\theta)$ are interface energy between the nucleus and solution, and function of contact angle between nucleus and the substrate surface, respectively. On the other hand, V_β is molecular volume of crystalline phase and σ is supersaturation degree with respect to the crystalline. σ respect with apatite is calculated by Eqn. (3):

$$\sigma = \frac{IP_{HAp}}{Ksp_{HAp}} \tag{3}$$

where IP_{HAp} and Ksp_{HAp} are ion activity product and solubility product with respect to the apatite, respectively. Forthermore, IP_{HAp} can be calculated from pH and concentrations of Ca and P as Eqn. (4):

$$IP_{HAp} = (a_{Ca^{2+}})^{10} \cdot (a_{PO_4^{3-}})^6 \cdot (a_{OH^-})^2 \left[Ca^{2+}\right]^{10} \left[PO_4^{3-}\right]^6 \left[OH^-\right]^2 \tag{4}$$

where value of $a_{Ca^{2+}}$, $a_{PO_4^{3-}}$ and a_{OH^-} are supposed to be 0.36, 0.06 and 0.72 at physiological ionic strength (μ=0.16) [21] and Ksp_{HAp} is solubility product for hydroxyapatite (5.5×10^{-118}) [22]. Therefore, heterogeneous apatite nucleation in this

study would be governed by the supersaturation degree and the surface condition of the specimens.

Release of Ca^{2+} from substrate can increase in supersaturation degree respect with apatite in SBF [3]. Figure 9 shows change in logarithm of σ in SBF after soaking of different specimens for various periods. The supersaturation degree decreased according to VPA(C)1Ca ≈ MOEP(O)01Ca > VPA(C)01Ca > MOEP(O)1Ca. Although the largest amount of Ca^{2+} released from MOEP(O)1Ca in Tris-NaCl buffer (See Fig. 1(B)), the supersaturation degree was the lowest in all the specimens. It is considered that the formation of apatite on MOEP(O)1Ca rapidly occurred within 1 day (see Figs. 2 and 3), and that ion consumption degreased in the supersaturation in SBF after that time. Although the supersaturation degree of MOEP(O)01Ca and VPA(C)1Ca were almost

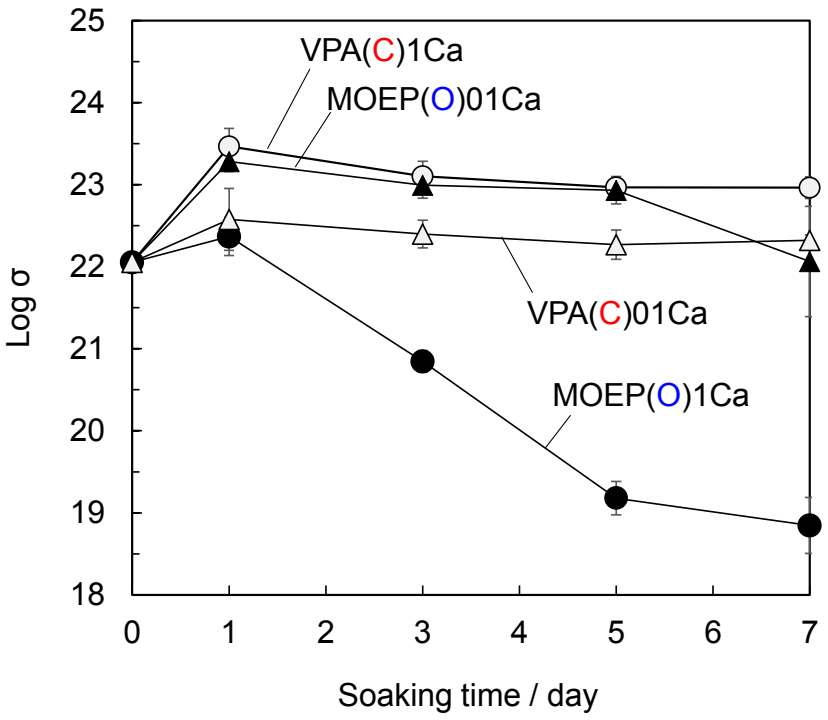

Figure 9 Change in common logarithm of supersaturation degree with respect to apatite in SBF following soaking of different composite specimens (n = 3).

similar, the former formed the apatite, but not the latter. These results indicate that surface condition for the heterogeneous nucleation of the apatite were governed by structural difference in the phosphate groups.

It was confirmed by XPS that surface reaction process was significantly different between -C-PO_3H_2 and -O-PO_3H_2 (see Figure 4(A)). VPA(C)1Ca only adsorbs Ca^{2+} to form the -C-$PO_3^{2-}\cdots Ca^{2+}$ complex, but not HPO_4^{2-} in SBF. This is supported by the fact that P concentration in SBF with soaking of VPA(C)1Ca was almost constant (see Figure 6). In contrast, MOEP(O)01Ca formed $CaHPO_4$ and OCP at initial stage, and subsequently that OCP were converted into apatite (see Figure 4(B)). Similar conversion from OCP to the apatite on the plasma-treated polymer in SBF was discussed by Oyane *et al.*[23]. These results indicate that only MOEP(O)01Ca adsorbs HPO_4^{2-} following Ca^{2+} adsorption to form the precursor of the apatite. In addition, MOEP(O)0Ca formed the calcium phosphate even without release of Ca^{2+} in SBF1.5Ca (see Figure 7). Thus, these results suggest that specific structure of the phosphate group provides the surface condition preferable for the apatite nucleation *via* adsorption of HPO_4^{2-} in SBF.

It is reported that the surface ζ potential is one of the factor governing the heterogeneous nucleation of apatite on bioactive materials in SBF [24-25]. In the case of bone-bonding bioactive Ti metal treated by alkaline solution [24] and sintered hydroxyapatite [26], negatively charged surface becomes positive by Ca^{2+} adsorption in SBF and again becomes negative by subsequent phosphate adsorption to finally form the apatite. In contrast, VPA(C)1Ca did not demonstrate such behavior, in spite that ζ potential of both the specimens converted from negative to positive (see Figure 5). Based on the results of XPS and ζ potential measurement, difference in apatite-forming behavior cannot be explained in terms of only the surface charge.

Concerning the initial reaction process of each phosphate group on the composites with Ca^{2+} with HPO_4^{2-} in SBF, the mechanism of apatite formation will be discussed in terms of the following viewpoints: (1) interaction energy between the reactive chemical species in the transition state, and (2) thermodynamic stability of the

products.

On the viewpoint (1), transition state -$PO_3Ca\cdots HPO_4^{2-}$ formed on the all specimens is assumed. The interaction energy is obtained as the sum of frontier orbital interaction and Coulomb interaction [27-28]. In the model shown Figure 8, the LUMO around the Ca atom was expected to accept the HOMO electron of HPO_4^{2-}. Comparing the energy level of each orbital, the significant gap was observed between the LUMO in both models (-0.146 and -0.118 eV) and the HOMO level of HPO_4^{2-} (-8.9 eV) estimated from the vertical ionization energy [29]. This means that the Coulomb interaction contributes more to formation of the transition state than the frontier orbital. Results of the computational simulation of the polarizability indicated that Coulomb interaction of -O-$PO_3^{2-}\cdots Ca^{2+}$ complex with HPO_4^{2-} was stronger than -C-$PO_3^{2-}\cdots Ca^{2+}$. Therefore, the transition state in MOEP(O) would be more stable than VPA(C), leading to decrease in activation energy for $CaHPO_4$ formation in the former.

On the viewpoint (2), thermodynamic stability between $CaHPO_4$ (aq.) and the complex composed of Ca^{2+} and one of the phosphate groups on the specimens was compared. The magnitude of the complex formation constant in Table 2 indicates that Ca^{2+} bound with MOEP(O) specimen has higher ability to further bond to HPO_4^{2-} *via* the ion-dipole interaction, and subsequently convert into $CaHPO_4$, because the stability of -O-$PO_3^{2-}\cdots Ca^{2+}$ complex was the lowest.

The $Ca^{2+}\cdots HPO_4^{2-}$ interaction on the surface of MOEP(O) specimen had an important role for the apatite formation. It was recently reported that the heterogeneous apatite nucleation on the Ti su treated with H_2O_2 in SBF progresses *via* formation of the pre-embryo consisting of Ca^{2+}, HPO_4^{2-}, and OH^- [30-31]. Furthermore, self-assembled monolayers containing carboxyl groups formed the cluster by aggregation of pre-nucleation complex of $[Ca(HPO_4)_3]^{4-}$ in the process of apatite deposition [32-33].

Summarizing the mechanism described above, apatite formation process on the surface of MOEP(O) is assumed as follows. An increase in $[Ca(HPO_4)_3]^{4-}$ concentration results in formation a lot of clusters with size larger than r^*. Subsequently, the formed

cluster would be converted into OCP as precursor of the apatite through ion adsorption in SBF. In fact, Habraken *et al.* demonstrated that the amorphous calcium phosphate with the formula $[Ca_2(HPO_4)_3]^{2-}$ grows into Ca-deficient OCP through the aggregation of the complex and ions in the supersaturated solution with respect to the apatite [33].

Finally, the results in this study found that differences in molecular structure of the phosphate groups govern the apatite formation on the composites, because low thermodynamic stability of $-PO_3^{2-}\cdots Ca^{2+}$ complex on the specimen enhances the formation of calcium phosphate cluster that is preferable for the heterogeneous nucleation of apatite. It is also expected that such structural difference affects the ability of the composites to bone to existing bone. In order to clarify this point in detail, adsorption behavior of protein and response of osteoblast cells should be investigated in further works.

5. Conclusion

The effects of structural difference in phosphate groups on apatite-forming behavior on the surface of polymer-$CaCl_2$ composite were examined in SBF. The composites modified with phosphoric acid ($-O-PO_3H_2$) induced heterogeneous nucleation of apatite. However, these consisting of phosphonic acid ($-C-PO_3H_2$) formed no apatite, because the amount of adsorbed HPO_4^{2-} in SBF was insufficient for the nucleation. The reason of this phenomena was assumed that thermodynamic stability of $-O-PO_3^{2-}\cdots Ca^{2+}$ interaction was lower than $-C-PO_3^{2-}\cdots Ca^{2+}$. Therefore, it was found that chemical structure of phosphate groups governed reactivity of Ca^{2+} on the composites with HPO_4^{2-} in SBF to give the calcium phosphate clusters as a precursor of the apatite.

Reference

[1] L.L Hench, “Bioceramics,” *J. Am. Ceram. Soc.*, **81**, 1707-1728 (1998).

[2] T. Kokubo, H.-M. Kim, M. Kawashita, “M. Novel bioactive materials with different mechanical properties” *Biomaterials*, **24**, 2161-2175 (2003).

[3] C. Ohtsuki, T. Kokubo, T. Yamamuro, "Mechanism of apatite formation on $CaO-SiO_2-P_2O_5$ glass in a simulated body fluid," *J. Non-Cryst. Solids*, **143**, 84-92 (1992).

[4] M. Tanahashi, T. Matsuda, "Surface functional group dependence on apatite formation on self-assembled monolayers in a simulated body fluid," *J. Biomed Mater. Res.*, **34**, 305-315 (1997).

[5] P. Datta, J. Chatterjee, S. Dhara, "Electrospun nanofibers of a phosphorylated polymer-A bioinspired approach for bone graft applications," *Collids Surf. B Biointerfaces*, **94**, 177-183 (2012).

[6] P.M. López-Pérez, R.M. Silva, R.A. Sousa, I. Pashkuleva, R.L. Reis, "Plasma-induced polymerization as a tool for surface functionalization of polymer scaffolds for bone tissue engineering: an in vitro study," *Acta Biomater.*, **6**, 3704-3712 (2010).

[7] O. Exner, "The inductive effect: theory and quantitative assessment," *J. Phys. Org. Chem.*, **12**, 265-274 (1999).

[8] T. Kokubo, H. Takadama, "How useful is SBF in predicting in vitro bone bioactivity?," *Biomaterials*, **27**, 2907-2915 (2006).

[9] S.B Cho, F. Miyaji, T. Kokubo, N. Nakanishi, N. Soga, T. Nakamura, "Apatite Formation on Various Silica Gels in a Simulated Body Fluid Containing Excessive Calcium Ion," *J. Cream. Soc. Jpn.*, **104**, 399-404 (1996).

[10] Ö Szabadka, E. Varga, L. Nagy, "Determination of protonation- and metal complex stability constants for a chelating monomer and its immobilized in polymer resin," *Talanta*, **59**, 1081-1088 (2003).

[11] J.P. Perdew, Y. Wang, "Accurate and simple analytic representation of the electron gad correlation energy," *Phys. Rev. B*, **45** 13244-13249 (1992).

[12] B. Delly, "From molecules to solids with the DMOl3 approach," *J. Chem. Phys.*, **113**, 7756-7764 (2000).

[13] T. Kawai, C. Ohtsuki, M. Kamitakahara, T. Miyazaki, M. Tanihara, Y. Sakaguchi, S. Konagaya, "Coating of an apatite layer on polyamide films containing sulfonic groups by

a biomimetic process," *Biomaterials*, **25**, 4529-4534 (2004).

[14] X. Zhou, S.H. Goh, S.Y. Lee, "Interpolymer complexation between poly(vinylphosphonic acid) and poly(vinylpyridine)s," *Polymer*, **38**, 5333-5338 (1997).

[15] I.F. Amaral, P.L. Granja, M.A. Barbosa, "Chemical modification of chitosan by phosphorylation: an XPS, FT-IR and SEM study," *J. Biomater. Sci. Polym. Ed.*, **16**, 1575-1593 (2005).

[16] T. Hanawa, M. Ota, "Calcium phosphate naturally formed on titanium in electrolyte solution," *Biomaterials*, **12,** 767-774 (1991).

[17] C.C. Chusuie, D.W. Goodman, M.J. Stiodonk, D.R. Justes, E.A. Schweikert, "Calcium phosphate phase identified using XPS and time-of-flight cluster SIMS," *Anal. Chem*., **71**, 149-153 (1999).

[18] L. Radev, M.H. Fernades, I.M. Salvado, D. Kovacheva, "Organic/Inorganic bioactive materials part III: in vitro bioactivity of gelatin / silicocarnotite hybrids," *Cent. Eur. J. Chem.*, **7**, 721-730 (2009).

[19] A. Chughtai, R. Marshall, G. H. Nancollas, "Complexes in calcium phosphate," *J. Phys. Chem.*, **72**, 208-211 (1968).

[20] T. Kawai, C. Ohtsuki, M. Kamitakahara, M. Tanihara, T. Miyazaki, Y. Sakaguchi, S. Konagaya, "A comparative study of apatite deposition on polyamide films containing different functional groups under a biomimetic condition," *J. Ceram. Soc. Jpn.*, **113**, 588-592 (2005).

[21] W. Neuman, M. Neuman, "The chemical dynamics of bone mineral," *University of Chicago, Chicago,* 1958, 3-3.

[22] H. McDowell, T.M. Gregory, W.E. Brown, "Solubility of $Ca_{10}(PO_4)_6(OH)_2$ in the system $Ca(OH)_2$-H_3PO_4-H_2O at 5, 15, 25, and 37°C," *J. Res. Nat. Bur. Stand. A. Phys. Chem.*, **81**, 273-281 (1977).

[23] A. Oyane, M. Uchida, Y. Yokogawa, C. Choong, J. Triffitt, A. Ito, "Simple surface modification of poly(ϵ-caprolactone) to induce its apatite-forming ability," *J. Biomed. Mater Res. A*., **75A**, 138-145 (2005).

[24] H.-M. Kim, T. Himeno, M. Kawashita, J.-H. Lee, T. Kokubo, T. Nakamura, "Surface potential charge in bioactive titanium metal during the process of apatite formation in simulated body fluid," *J. Biomed. Mater. Res. A*., **67A**, 1305-1309 (2003).

[25] M. Hashimoto, K. Hayashi, S. Kitaoka, Enhanced apatite formation on Ti metal heated in P_{O2}-contorolled nitrogen atmosphere," *Mater Sci. Eng. C*, **33**, 4155-4159 (2013).

[26] H.-M. Kim, T. Himeno, T. Kokubo, T. Nakamura, "Process and kinetics of bonelike apatite formation on sintered hydroxyapatite in a simulated body fluid," *Biomaterials*, **21**, 4366-4373 (2005).

[27] *Chemical Reactivity and Reaction Path*s ed. G. Klopman, Wiley-Interscience New York, 1974.

[28] G. Klopman, "Chamical reactivity and the concept of charge- and frontier-contolled reactions," *J. Am. Chem. Soc.*, **90**, 223-234 (1968).

[29] E. Pluhařová, M. Ončák, R. Seidel, C. Schroeder, W. Schroeder, B. Winter, S.E. Bradforth, P. Jungwirth, P. Slavíček, "Transforming anion instability into stability: contrasting photoionization of three protonation forms of the phosphate ion upon moving into water," *J. Phys. Chem. B*, 2012, **116**, 13254-13264.

[30] S. Hayakawa, K. Tsuru, K. Uetsuki, K. Akasaka, Y. Shirosaki, A. Osaka, "Calcium phosphate crystallization on titania in a flowing Kokubo solution," *J. Mater. Sci: Mater. Med.*, **26**, 222 (2005).

[31] K. Uetsuki, S. Nakai, Y. Shirosaki, S. Hayakawa, A. Osaka, "Nucleation and growth of apatite on an anatase layer irradiated with UV light under different environmental conditions," *J. Biomed. Mater. Res. A*, **101A**, 712-719 (2013).

[32] A. Dey P.H. Bomans, F.A. Müller, J. Will, P. M. Frederik, G. With, N.A. Sommerdijk, "The role of prenucleation clusters in surface-induced calcium phosphate crystallization," *Nat. Mater.*, **9**, 1010-1014 (2010).

[33] W.J. Habraken, J. Tao, L.J. Brylka, H. Friedrich, L. Bertinetti, A. S. Schenk, A. Verch, V. Dmitrovic, P.H. Bomans, P.M. Frederik, J. Laven, P. Schoot, B. Aichmayer, G. With, J.J. DeYoreo, N.A. Sommerdijk, "Ion-association complexes unite classical and non-

classical theories for the biomimetic nucleation of calcium phosphate," *Nat. Commun.*, **4**, 1507 (2013).

Chapter 4

Evaluation of Apatite-forming Ability of Sulfinic Acid Groups on Polymer-$CaCl_2$ Composites in Simulated Body Fluid

1. Introduction

Fundamental research has been found that specific functional groups lead to the low-crystalline apatite layer formation on the artificial materials which bond to bone tissue. Bioactive ceramics such as Bioglass® [1] and glass-ceramic A-W [2] exhibit bone-bonding ability, because Si-OH groups [3] contained in them induced heterogeneous nucleation of apatite. Moreover, Ti-OH [4], Ta-OH [5], phosphate ($-PO_3H_2$) [6] are also able to induce formation of bone-like apatite in simulated body fluid (SBF) *via* interaction between the functional group and Ca^{2+}. These discoveries applied to the fabrication of the bioactive metals [7] and organic-inorganic composites [8-9] using the chemical modification with these groups. Especially, bioactive composites and polymers have been attracted attention as bone substitutes which are possible to show Young's moduli similar to bone tissue and form into the defect shape.

In order to improve the bone-bonging ability of the composites and polymer, the effects of modification with sulfonic acid ($-SO_3H$) groups on apatite formation in SBF and activity of osteoblast cells *in vitro* have been examined. Miyazaki *et al*. prepared the nanocomposites consisting of poly(vinylsulfonic acid-2-hydoxyethyl methacrylate (HEMA)) and Ca^{2+} [10]. These nanocomposites formed apatite in SBF within 7 days and showed plastic deformation. Chaterji *et al.* demonstrated that increase in content of sulfate groups in the poly(sulfopropyl acrylate -acrylamide) hydrogel improved the adhesion and proliferation of MG-63 osteoblast-like cells, because of increase in serum protein uptake [11]. Therefore, incorporation of sulfonic acid groups has the potential to be one of the way for preparation of bioactive flexible materials.

Sulfinic acid ($-SO_2H$) is classified as sulfur-containing functional group and it has similar chemical structure of sulfonic acid groups. In medical field, sodium *p*-

toluenesulfinate has been applied as the polymerization accelerator for setting of adhesive dental resin [12] as well as sodium benzenesulfonate [13]. In Chapter 1, addition of *p*-TSS inhibited the dissolution of the copolymers consisting of phosphate groups in SBF. However, bone-bonding ability of sulfinic acid groups has never been investigated.

Structural difference in acidic functional groups composed of the same elements is expected to affect the apatite-forming ability on the composites in SBF. In Chapter 3, it was found that behavior of the apatite nucleation on the composites was dramatically changed by structural difference in phosphate groups in SBF. It is also therefore expected that a comparative study of sulfinic acid and sulfonic acid will provide fundamental insights into the relationship between the chemical structure and apatite formation behavior. Thus, the potential of sulfinic acid groups for inducing heterogeneous nucleation of apatite should be clarified in the first place.

In this Chapter, the polymer-$CaCl_2$ composites modified with sulfinic acid groups were prepared through the radical polymerization of sodium 4-vynilbenzene sulfinate ($VBSO_2$) and HEMA. The apatite-forming behavior on the surface of composites containing various amount of sulfinic acid groups was examined to reveal the ability of them to induce the nucleation of apatite in SBF.

2. Materials and methods

2.1 preparation of composite specimens

$VBSO_2$ (90%, Tokyo Chemical Industry Co., Ltd, Tokyo, Japan) and HEMA (95%, Wako Pure Chemical Industries, Ltd, Osaka, Japan) were used as vinyl monomers with a total amount of 0.01 mol. Two different polymerizations were conducted with $VBSO_2$ ratios of 0 and 10 mol% relative to the total amount of monomer. These monomers were dissolved in ultra-pure water with *N*,*N*'-methylenebisacrylamide (99%, Wako Pure Chemical Industries) and *N*,*N*,*N*',*N*'-tetramethylethylenediamine (98%, Wako Pure Chemical Industries) at 1 and 0.15 mol%, respectively, relative to the total monomers. The mixture solution was then

stirred for 5 min and adjusted to a total volume of 10 cm^3 in a volumetric flask. Subsequently, 2,2'-Azobis(2-methylpropionamidine) dihydrochloride (95%, Wako Pure Chemical Industries) was added at 1 mol% relative to the total amount of monomer, and 1 cm^3 of the resulting mixture was poured into the polypropylene cup and polymerized at 60 °C for 1 day.

The copolymers prepared in this way were dried at room temperature for 1 day, before being cut into squares of 10 × 10 mm^2 in size. The copolymers were then soaked in 30 cm^3 of a 10 or 50 $mol \cdot m^{-3}$ $CaCl_2$ solution at 36.5 °C for 1 day. Then the copolymers were washed in ultra-pure water and dried at room temperature for 1 day. The specimens prepared from 0 and 10 mol% of $VBSO_2$ were referred as $0VBSO_2$ XCa and $10VBSO_2$ XCa, respectively, and X gives the molar concentration of the $CaCl_2$ solution used.

2.2 Soaking of specimens in SBF and Tris-NaCl buffer

SBF (Na^+ 142.0, K^+ 5.0, Mg^{2+} 1.5, Ca^{2+} 2.5, Cl^- 147.8, HCO_3^- 4.2, HPO_4^{2-} 1.0, SO_4^{2-} 0.5 $mol \cdot m^{-3}$) with pH7.40 was prepared by following method as described by reference [14]. The composite specimens were soaked in 30 cm^3 of SBF at 36.5 °C for 5 days.

Tiris-NaCl buffer was used for measurement of Ca^{2+} release form specimens under the condition similar to SBF. Tris-NaCl buffer (NaCl 142, tris(hydroxymethyl) aminomethane 50 $mol \cdot m^{-3}$) with pH7.0 was prepared by following method as described above in Chapter 2. The composites were soaked in 30 cm^3 of Tris-NaCl buffer at 36.5 °C for 12 h.

2.3 Characterization

The chemical structures of the specimens before soaking in $CaCl_2$ solution were analyzed by Fourier transform infrared spectroscopy (FT-IR; FT/IR-6100, JASCO Co., Tokyo, Japan) using an attenuated total reflectance method. The scan

range for the FT-IR analysis was set from 950 to 1800 cm^{-1} at a resolution of 4 cm^{-1}. The Ca contents of the composites after soaking in $CaCl_2$ solution were mesured by energy dispersive X-ray (EDX) analysis (EMAX Energy, Horiba Ltd, Kyoto, Japan) equipped with a scanning electron microscope (SEM; S-3500N, Hitachi Co., Tokyo, Japan). The surface of the specimen was coated with carbon using a carbon coater (CADE, Meiwafosis Co., Ltd, Osaka, Japan) immediately prior to the EDX analysis.

The structural changes in the surfaces of the composites after soaking in SBF were characterized by thin-film X-ray diffraction (TF-XRD; MXP3V, Mac Science, Co., Yokohama, Japan) and SEM. The TF-XRD analysis was performed using monochromatic Cu-Kα radiation which was fixed at 1° against the surface of each composite specimen with a scan rate of 0.02° sec^{-1}. Furthermore, cross-section of the composite specimen with apatite after soaking in SBF was observed by SEM.

The adhesion strength of the apatite formed on the specimen was evaluated by peel-off test. Chukoh Flo® adhesive tape (ASF-110 FR, Chukoh Chemical Industries, Ltd, Tokyo, Japan) was attached to the surface of apatite on each composite specimen and then peeled off. The surface of each specimen was observed using SEM after the test.

The Ca and P concentration in the Tis-NaCl buffer and SBF after soaking of composite specimens were measured by inductively coupled plasma optical emission spectrometry (ICP-OES; Optima 4300DV CYCLON, Perkin-Elmer Inc., London, UK).

3. Results

Figure 1 shows the FT-IR spectra of the copolymers prepared using different additive amount of $VBSO_2$ before soaking in $CaCl_2$ solution. In the spectra of all specimens, peaks attributed to stretching vibrations of the C=O, O–C (alcohol) and C–O (ester) bonds derived from HEMA were observed at 1706, 1074 and 1023 cm^{-1},

respectively [15]. A peak was also observed at 1165 cm^{-1} for all of the copolymer, which was attributed to the vibration of the CH_3 and torsion of OH groups of HEMA. Furthermore, all of the copolymers displayed a peak assigned to amide I at 1635 cm^{-1} [16]. Peaks also appeared at 1030 and 1008 cm^{-1}, which were attributed to in-plane deformation vibration of C-H and stretching vibration of S=O bonds [17], respectively, but these were only observed in the spectra of $10VBSO_2$.

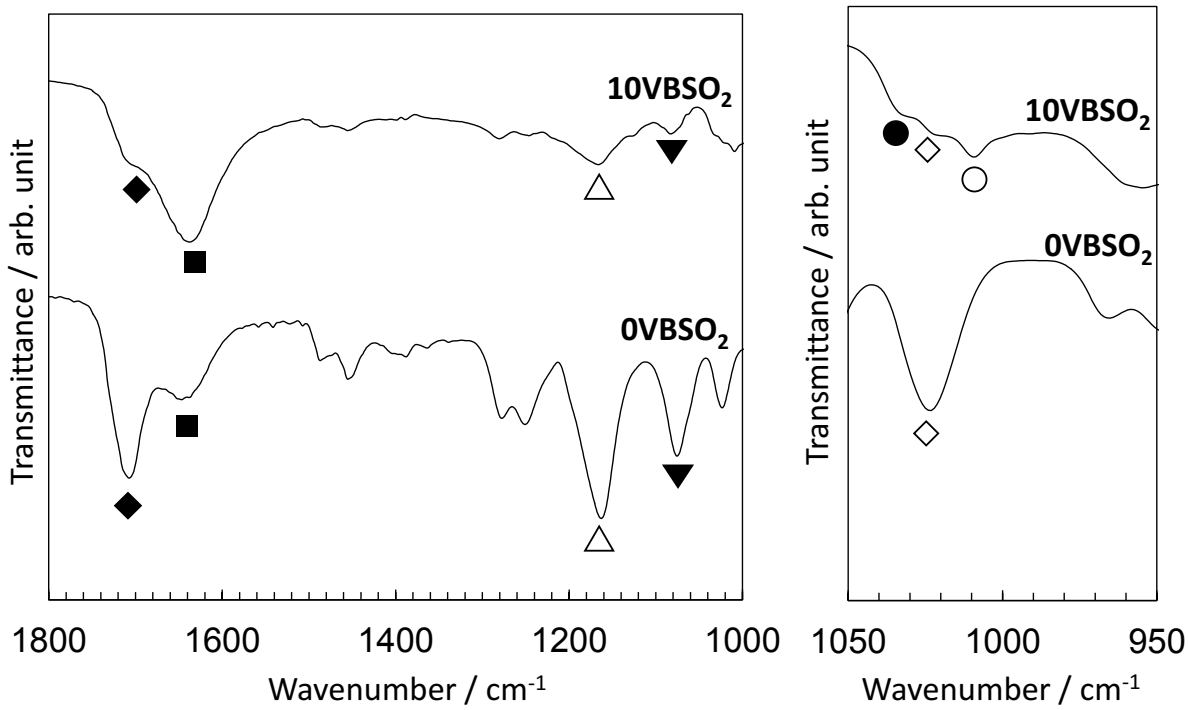

Figure 1 FT-IR spectra of different copolymer specimens before soaking in $CaCl_2$ solution (◆: ν(C=O) of HEMA; ■: Amid I; △: γ(CH_3) or τ(OH) of HEMA; ▼: ν(O-C) alcohol of HEMA; ●: S=O bond of $VBSO_2$; ◇: ν(C-O) ester of HEMA; ○: C-H bond of in-plane deformation vibration for $VBSO_2$; ν is the stretching; γ, the rocking; τ, the torsion).

Figure 2 (A) shows the Ca contents of the different composite specimens after soaking in various concentrations of $CaCl_2$ solution for 1 day. The Ca content of $10VBSO_2$ was found to be larger than that of $0VBSO_2$ regardless of the $CaCl_2$ concentration. Figure 2 (B) shows the Ca concentration in Tris-NaCl buffer following the

soaking of each composite for 12 h. The higher concentration of Ca in Tris-NaCl buffer following soaking of $10VBSO_2$ was observed as compared with $0VBSO_2$ regardless of the $CaCl_2$ concentration.

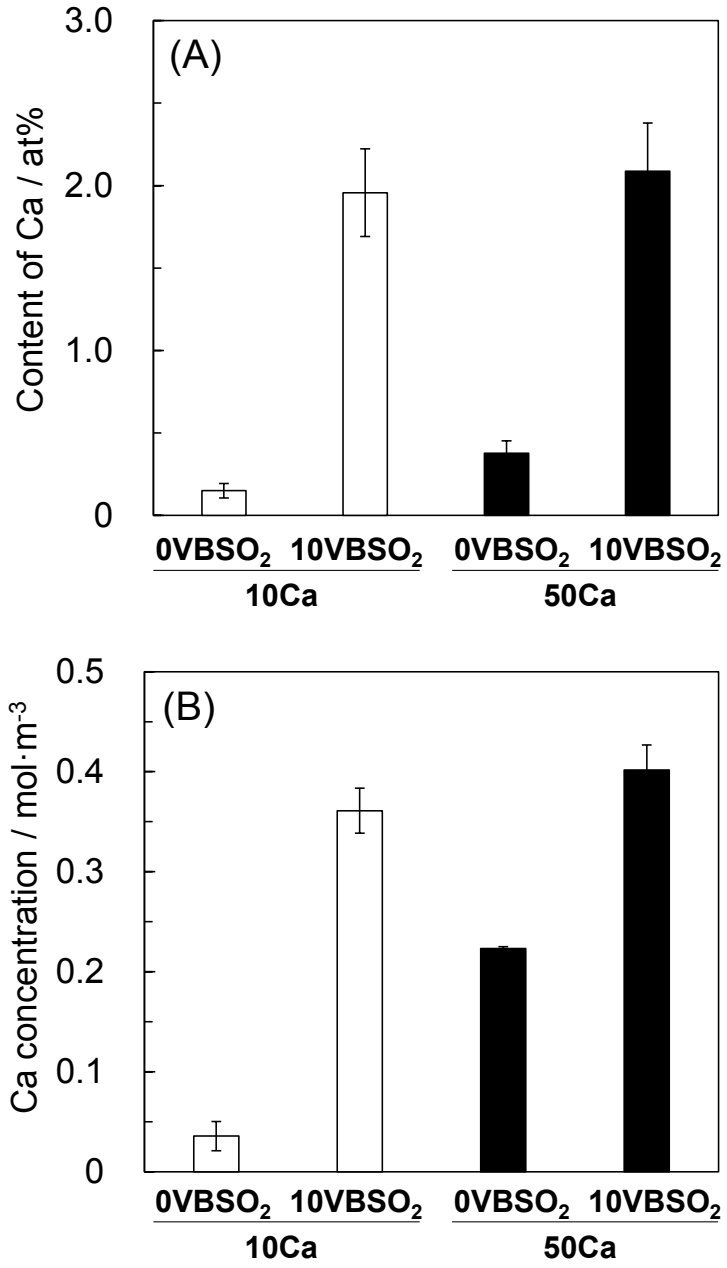

Figure 2 Ca contents of the different copolymer after soaking in various concentrations of $CaCl_2$ solution (A) and the Ca concentrations in Tris-NaCl buffer after soaking of composite spevimens for 12 h (B) (n = 3).

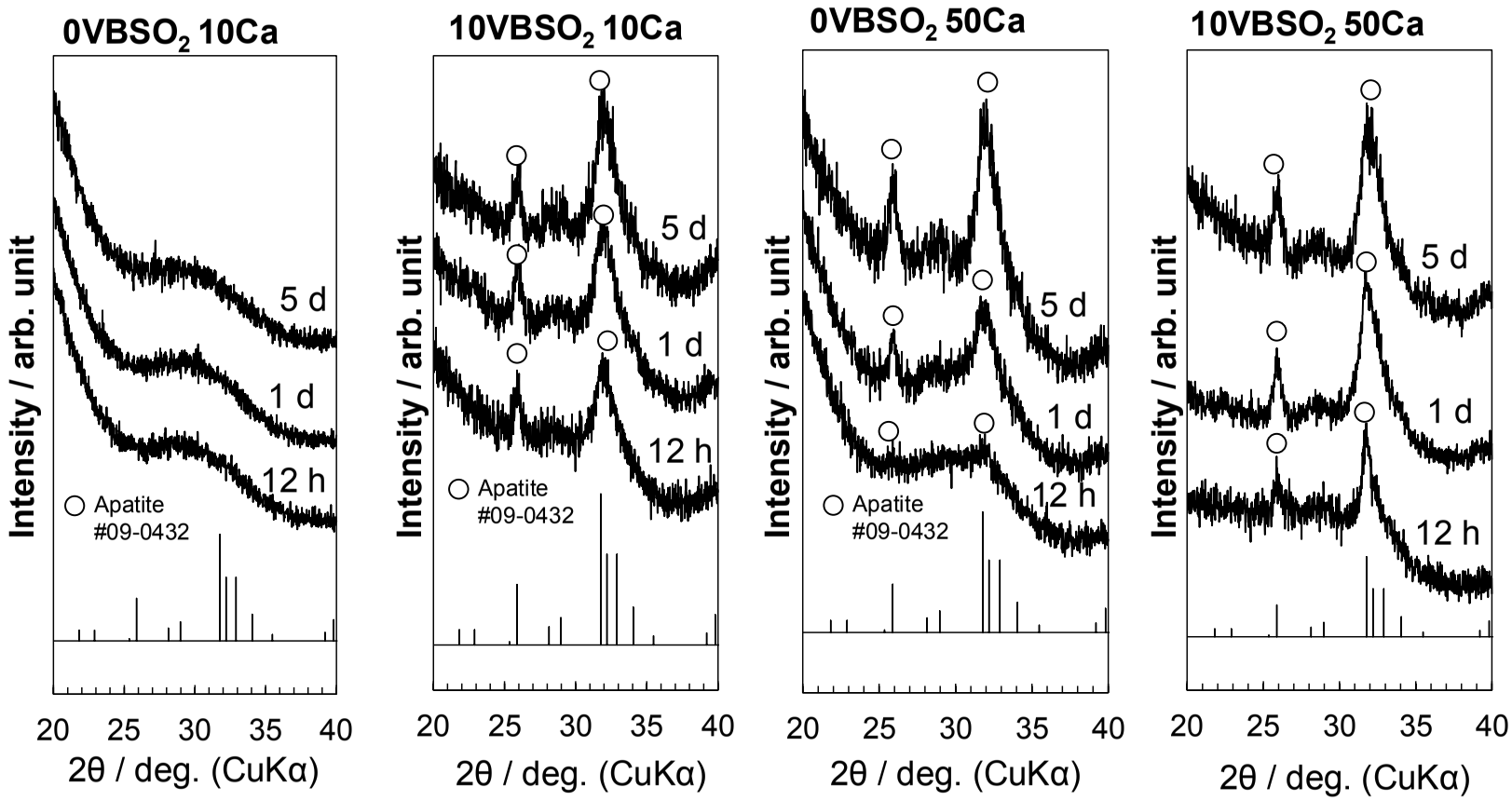

Figure 3 TF-XRD patterns of surface of composite specimens after soaking in SBF for various periods.

Figure 3 shows TF-XRD patterns of the different composite specimens after soaking in SBF for various time interval. The 10VBSO$_2$ 10Ca and 50Ca displayed broad peaks at $2\theta = 26°$ and 32° corresponding to apatite (JCPDS #09-0432) after they were soaked for 12 hours. The apatite peaks also observed in 0VBSO$_2$ 50Ca after 12 hours. However, the 0VBSO$_2$ 10Ca hydrogel did not show any peaks corresponding to apatite, even after 5 days.

Figure 4 shows SEM images of the cross-section of different composites after soaking in SBF for 5 days. The image of the 0VBSO$_2$ 10Ca revealed that the material adopted a spherical morphology following the deposition of apatite, with a gap forming between the surface and the depositions. In contrast, the images of the 10VBSO$_2$ 10Ca

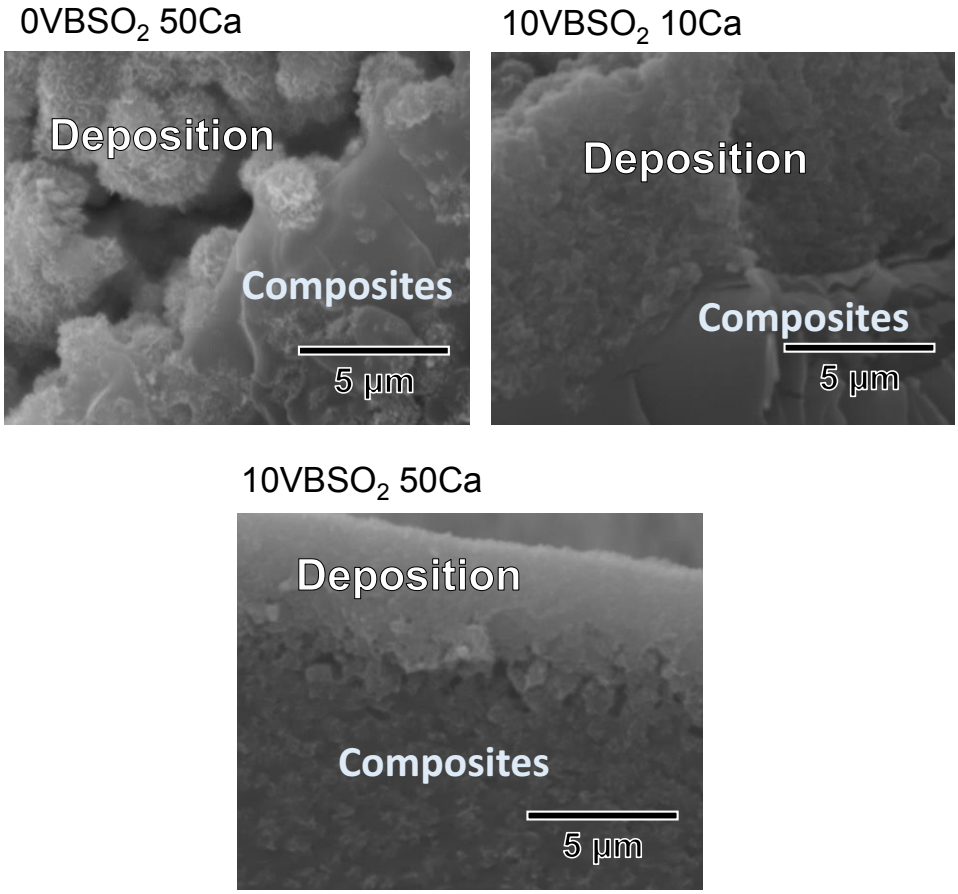

Figure 4 SEM images of cross-section of composite specimens after soaking in SBF for 5 days.

and 50Ca revealed the formation of a continuous layer of deposited materials, which sat in close contact with the surface.

Figure 5 shows the SEM images of the $0VBSO_2$ 50Ca and $10VBSO_2$ 50Ca, before being soaked in SBF for 1 day and subjected to a peeling-off test using tape. Almost all of the depositions formed on the surface of the $0VBSO_2$ 50Ca were removed after the test, whereas the depositions on the $10VBSO_2$ 50Ca remained intact.

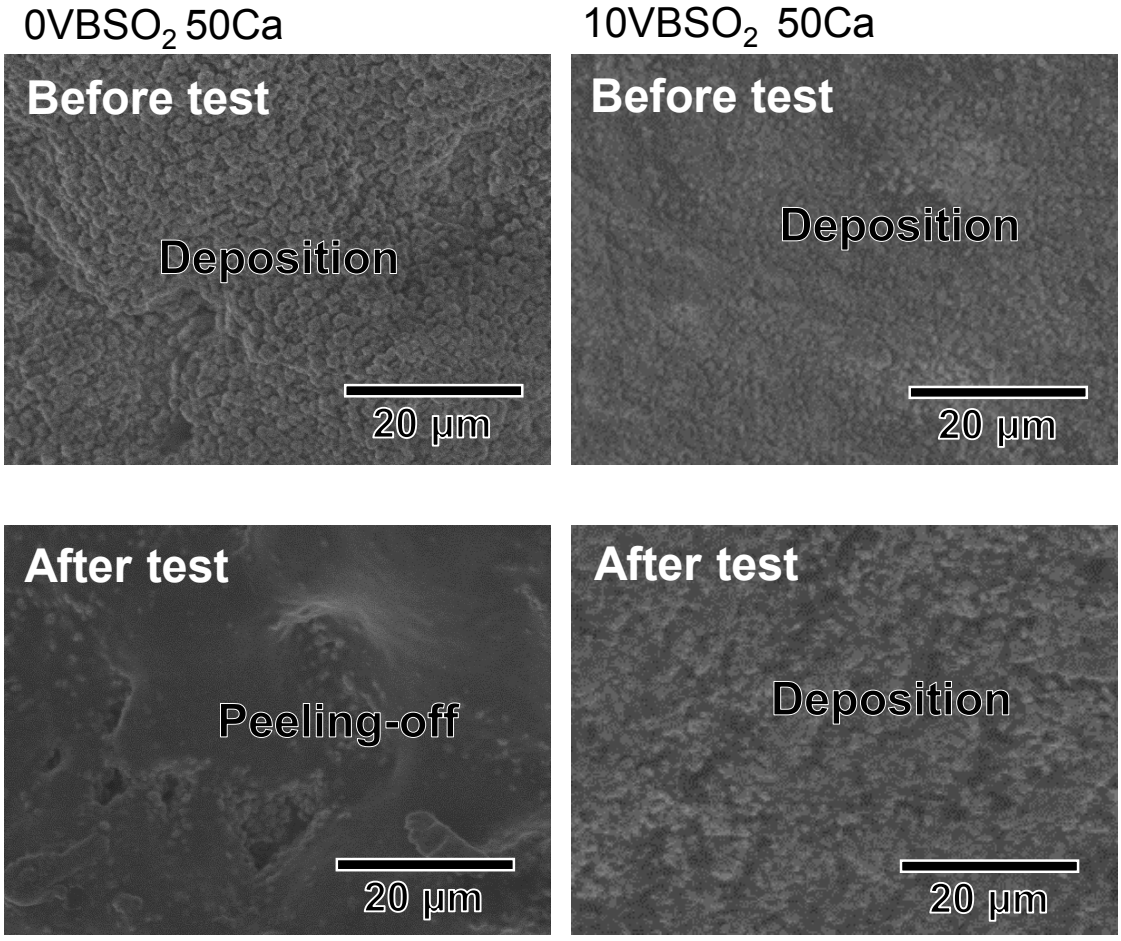

Figure 5 SEM images of the surfaces of the $0VBSO_2$ 50Ca and $10VBSO_2$ 50Ca after being soaked in SBF for 1 day, which were all subjected to the peeling-off test.

Figure 6 shows the change in P concentrations in SBF after soaking of the different specimens for various times interval. The P concentration remained almost constant for the 0VBSO$_2$ 10Ca regardless of the soaking time. The reduction in the P concentration was of the order 0VBSO$_2$ 50Ca < 10VBSO$_2$ 50Ca < 10VBSO$_2$ 10Ca.

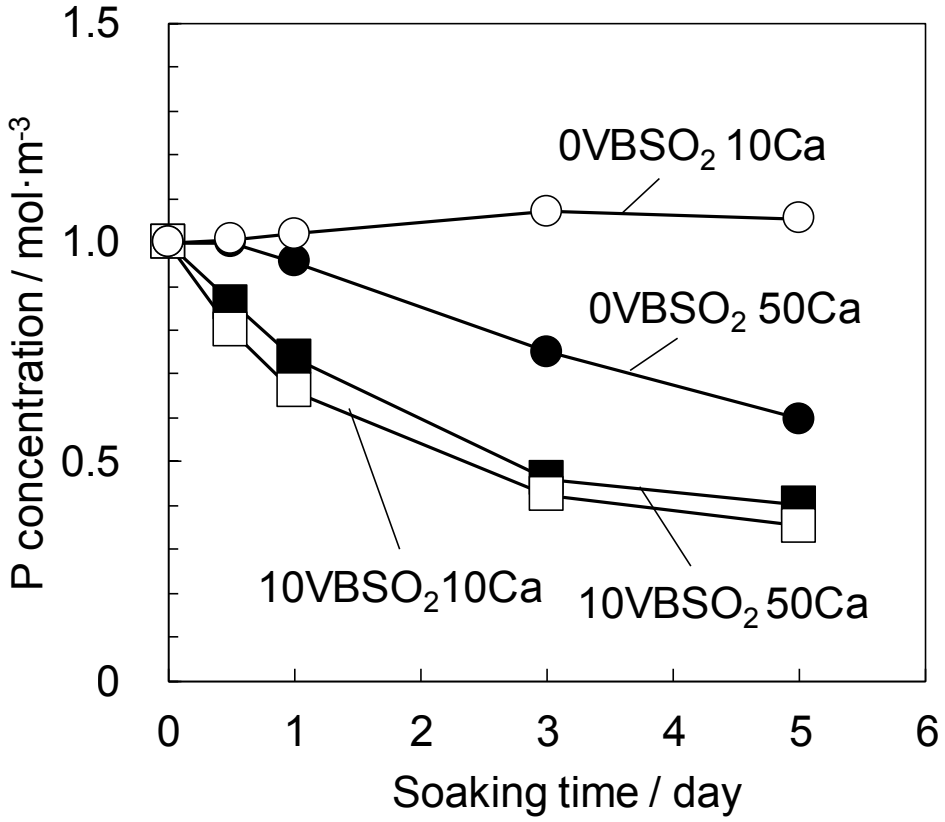

Figure 6 Change in P concentration in SBF with soaking of different composite specimens for various periods.

4. Discussion

FT-IR analysis revealed that the S=O bond in sulfinate and C–OH bonds in alcohol were consisted in the 10VBSO$_2$ copolymer prepared from the monomer of VBSO$_2$ and HEMA, respectively (see Figure 1). This result therefore confirmed

that the sulfinic acid groups had achieved to incorporate into the copolymer as organic matrix of composites by the radical polymerization.

All of the composite specimens modified with sulfinic acid groups formed apatite irrespective of the $CaCl_2$ concentration, whereas those without sulfinic acid groups formed apatite only after being treated with 50 $mol \cdot m^{-3}$ $CaCl_2$ (see Figure 3). The higher level of P consumption in SBF after the soaking of the $10VBSO_2$ 10Ca and 50Ca in SBF were observed than that of $0VBSO_2$ 50Ca (see Figure 6). These results therefore indicate that a much larger amount of apatite was formed on the surface of the $10VBSO_2$ composites as compared with the $0VBSO_2$. Taken together, these results revealed that the incorporation of sulfinic acid groups enhanced the apatite-forming ability of the composites.

More Ca^{2+} ions were released from into the Tris-HCl buffer from the $10VBSO_2$ composites than the corresponding $0VBSO_2$ material, regardless of the $CaCl_2$ concentration (See Figure 2(A) and (B)). This result therefore suggested that the modification with sulfinic acid groups were playing a critical role in the binding of the Ca^{2+} ions in $CaCl_2$ solution. On the other hand, it has been reported that Ca^{2+} adsorption increases as the degree of swelling for a polymer hydrogel increases in $CaCl_2$ solution [18]. Electrostatic repulsion between ionic functional groups is one of the major factors involved in swelling of the polymer hydrogels [19]. Therefore, presence of sulfinic acid groups on the specimens would make a considerable contribution to the incorporation and subsequent release of Ca^{2+} to accelerate apatite formation.

The sulfinic acid groups on the composites also affected the morphology of apatite deposited on the composites in SBF (see Figure 4). This change in the morphology was attributed to differences in the apatite nucleation process. The apatite deposited on the $10VBSO_2$ composites adopted a continuous layered structure, which was similar morphology of apatite observed on titanium metal treated with NaOH in SBF [7] and polyamide film modified with carboxylic acid

groups [20]. The sulfinic acid groups on the surface of the composites would become almost completely anion in SBF, because acid dissociation constant (pK_a) of benzenesulfinic acid is 1.29 [21]. Also, it was reported that ion-ion interactions between anionic functional groups and Ca^{2+} can provide to the heterogeneous nucleation of apatite in SBF [6]. Thus, these results suggest that the $10VBSO_2$ composites formed apatite layer on their surface through the heterogeneous nucleation.

In contrast, the $0VBSO_2$ 50Ca formed an assembly of spherical apatite particles in SBF. For homogeneous nucleation, particulate apatite tends to be precipitated by an increase in the degree of supersaturation with respect to apatite in SBF [8]. The main hydrophilic groups on the surface of $0VBSO_2$ 50Ca were the hydroxyl groups derived from HEMA, which would lead to the formation of ion-polar interactions with the Ca^{2+} [6]. However, these interactions are much less capable of inducing heterogeneous nucleation of apatite than ion-ion interactions, and it was therefore assumed that Ca^{2+} released from composites without sulfinic acid preferentially induced homogeneous nucleation and subsequently caused the growth of spherical particles.

Moreover, the apatite adhered to the surface of the $10VBSO_2$ 50Ca much more strongly than it did to the $0VBSO_2$ 50Ca (see Figure 5). According to the apatite formation on the polyamide films modified with carboxylic acid groups, ion-ion interaction of $-COO^{-}\cdots Ca^{2+}$ made a tight adhesion of apatite layer [20]. Taken together, it was assumed that the composites formed interaction such as $-SO_2^{-}\cdots Ca^{2+}$ and $(-SO_2^{-})_2\cdots Ca^{2+}$ on their surface and then not only affected the heterogeneous nucleation but also resulted in the tight adhesion of the apatite layer.

Finally, the results of this Chapter revealed that sulfinic acid groups are one of the functional groups for inducing heterogeneous nucleation of apatite in SBF. Therefore, it envisaged that the incorporation of this group into a polymer could be used as a general strategy for the fabrication of composite-type bone

substitute showing bone-bonding ability. Furthermore, it is expected that sulfinic acid groups could be used to be a model for comparison of apatite forming ability of them with sulfonic acid to examine the effects of structural change on apatite-formation behavior and further bone-bonding ability. To carry out this comparative study, the preparation of materials consisting sulfinic acid and sulfonic acid under the same condition should be required in future works.

5. Conclusion

The apatite formation behavior of polymer-$CaCl_2$ composites prepared from $VBSO_2$ and HEMA has been examined in SBF. The results revealed that the sulfinic acid groups on the surface of the composites formed apatite *via* heterogeneous nucleation of apatite under simulated body environment. It is expected that sulfinic acid contribute to fabrication of bioactive bone-bonding composites and understanding the structural effect on apatite formation as model structure.

Reference

[1] L.L Hench, "Bioceramics", *J. Am. Ceram. Soc.*, **81**, 1707-1728 (1998).

[2] T. Kokubo, H.-M. Kim, M. Kawashita, "Novel bioactive materials with different mechanical properties" *Biomaterials*, **24**, 2161-2175 (2003).

[3] C. Ohtsuki, T. Kokubo, T. Yamamuro, "Mechanism of apatite formation on CaO-SiO_2-P_2O_5 glass in a simulated body fluid", *J. Non-Cryst. Solids*, **143**, 84-92 (1992).

[4] M. Uchida, H.-M. Kim, T. Fujibayashi, T. Nakamura, "Structural dependence of apatite formation on titania gels in a simulated body fluid", *J. Biomed. Mater. Res. A.*, **64A**, 164-170 (2003).

[5] T. Miyazaki, H.-M. Kim, T. Kokubo, H. Kato, T Nakamura, “Induction and acceleration of bonelike apatite formation on tantalum oxide gel in simulated body fluid”, *J. Sol-gel. Tech.*, **21**, 83-88 (2001).

[6] M. Tanahashi, T. Matsuda, “Surface functional group dependence on apatite formation on self-assembled monolayers in a simulated body fluid”, *J. Biomed Mater. Res.*, **34**, 305-315 (1997).

[7] H.-M Kim, F. Miyaji, T. Kokubo, T. Kitsuki, T. Nalamura, “Preparation of bioactive Ti and its alloys via simple chemical surface treatment”, J. Biomed. Mater. Res., 32, 409-417 (1996).

[8] M.Y. Koh, C. Ohtsuki, T. Miyazaki, “Modification of polyglutamic acid with silanol groups and calcium salts to induce calcification in a simulated body fluid”, *J. Biomater. Appl.*, 25, 581-594 (2011).

[9] Y. Shirosaki, T. Okayama, K. Thuru, S. Hayakawa, A. Osaka, “In vitro bioactivity and MG63 cytocompatibility of chitosan-silicate hybrids”, *Int. J. Mater. Chem.*, **3**, 1-7 (2013).

[10] T. Miyazaki, M. Imamura, E. Ishida, M. Ashizuka and C. Ohtsuki, “Apatite formation abilities and mechanical poperties of hydroxyethylmethacrylate-based organic-inorganic hybrids incorporated with sulfonic groups and calcium ions,*” J. Mater. Sci. Mater. Med .*, **20**, 157-161 (2009) .

[11] S. Chaterji, R.A. Gemeinhart, “Enhanced osteoblast-like cell adhesion and proliferation using sulfonate-bearing polymeric scaffold”, *J. Biomed. Mater. Res. A.*, **83A**, 990-998 (2007).

[12] J. Yamauchi, “study of dental adhesive resin containing phosphoric acid methacrylate monomer”, *J. Jpn. Soc. Dent. Mater. Devices.*, **5**, 144-154 (1986).

[13]K.L. Van Landuyt, J. Snauwaert, J. De Munck, M. Peumans, Y. Yoshida, A. Poitevin, E. Coutinho, K. Suzuki, P. Lambrechts, B. Van Meerbeek, “Systematic review of the chemical composition of contemporary dental adhesives”, *Biomaterials*, **28**, 3757-3785 (2007).

[14] T. Kokubo, H. Takadama, “How useful is SBF in predicting in vitro bone bioactivity?”, *Biomaterials*, **27**, 2907-2915 (2006).

[15] L. Ferreira, M.M. Vidal, M.H. Gil, “Evaluation of poly(2-hydroxyethyl methacrylate) gels as drug delivery system at different pH value”, *Int. J. Pharm.*, **194**, 169-180 (2000).

[16] M. Liu, H. Liu, Y. Liu, L. Bai, G. Yang, C. Yang, J. Cheng, “Preparation and characterization of temperature-responsive poly (N-isopropylacrylamide-co-N, N’-methylenebisacrylamaide) monolith for HPLC”, *J. Chromatogr*, **1218**, 286-292 (2011).

[17] C. Halm, J. Evarts, M.J. Kurth, “A new attachment / cleavage strategy: polymer-bound allylic sulfones in a solid-phase route to trisubstituted olefins”, *Tetrahedron. Lett.*, **38**, 7709-7712 (1997).

[18] R. Nakata, T. Miyazaki, Y. Morita, E. Ishida, R. Iwatsuki, C. Ohtsuki, “Apatite formation abilities of various carrageenan gels in simulated body environment”, *J. Ceram. Soc. Jpn.*, **118**, 487-490 (2010).

[19] C.M. Hassan, F.J. III Doyle, N.A. Peppas, Dynamic behavior of glucose-responsive poly(methacrylic acid-γ-ethylene glycol) hydrogels”, *Macromolecules*, 30, 487-490 (1997).

[20] T. Miyazaki, C. Ohtsuki, Y. Akioka, M. Tanihara, J. Nakao, Y. Sakaguchi, . Konagaya, “Apatite deposition on polyamide films containing carboxyl group in a biomimetic solution”, *J. Mater. Sci.: Mater. Med.*, **14**, 569–574 (2003).

[21] D. Veltwish, E. Janata, K.D. Asmus, “Primary processes in the reaction if OH·-radicals with sulphoxides”, *J. Chem. Soc. Perkin. Trans*., **2**, 146–153 (1980).

Chapter 5

Structural Effects of Sulfur-containing Acidic Functional Groups on Apatite Formation on Polymer-$CaCl_2$ Composites in Simulated Body Environment

1. Introduction

Bioactive ceramics such as Bioglass® [1] and glass-ceramic A-W [2] had been discovered to allow bonding to bone tissue directly, because Si-OH groups and release of Ca^{2+} induce formation of the low crystalline apatite layer on their surface [3]. Although bioactive ceramics had been clinically used as bone substitute, their high Young's moduli would cause bone adsorption surrounding the implantation part.

Modification with sulfonic acid (-SO_3H) groups has been also attracted attention for the improvement of bone-bonding ability of implants. Previously, it has been reported that the organic-inorganic nanocomposites and thermoreversible hydrogel consisting Ca^{2+} and -SO_3H delivered from carrageenan formed bone-like apatite in simulated body fluid (SBF) [4-5]. Furthermore, the polymer scaffold modified with poly (vinylsulfonic acid) enhanced the attachment and proliferation of osteoblasts *in vitro* [6]. These reports revealed that incorporation of -SO_3H groups contributes to fabrication of flexible bone substitutes showing bone-bonding ability and solution of the problem caused by the mismatch of Young's moduli.

In Chapter 4, apatite-forming ability of polymer-$CaCl_2$ composites modified with sulfinic acid (-SO_2H) groups was investigated in SBF. The composites containing -SO_2H treated with 50 $mol \cdot m^{-3}$ of $CaCl_2$ solution formed apatite with layered structure, which exhibited strong adhesion strength and contacted closely with the surface of composites. In contrast, particulate apatite deposited on the composites without -SO_2H. These results revealed that -SO_2H also induces heterogeneous nucleation of apatite in SBF.

The chemical structures of -SO_3H and -SO_2H consist same elements, but the

number of oxygen atoms binging to sulfur atom was different. It is assumed that difference in these structure changes the stability of interaction with Ca^{2+}, because the different number of oxygen atoms leads to negatively charge delocalization to stabilize the ionized acidic functional groups due to the inductive and mesomeric effects [7]. In Chapter 3, high stable interaction between Ca^{2+} and phosphate groups inhibited the apatite formation on the polymer-$CaCl_2$ composites in SBF. Thus, structural difference in the sulfur-containing acidic functional groups would also influence the apatite-forming ability of the composites. It is also expected that clarification of such points provides the fundamental supports for the design of bone-bonding bioactive composites.

In this Chapter, composites consisting of $CaCl_2$ and copolymer modified with either -SO_3H or -SO_2H were prepared using sodium 4-vinylbenzene sulfonate or sodium 4-vinylbenzen sulfinate and HEMA. The behavior of mineralization on the surface of composites was examined to discuss the structural effects of these acidic functional groups on apatite-forming ability in terms of the stability of interaction with Ca^{2+}.

2. Materials and methods

2.1 Preparation of composites modified with sufinate or sulfonate groups

Sodium 4-vinylbenzene sulfinate ($NaVBSO_2$, 90%, Tokyo Chemical Industry Co. Ltd., Tokyo, Japan) and sodium 4-vinylbenzen sulfonate ($NaVBSO_3$, 90%, Sigma-Aldrich Co., Saint Louis, USA) were used to incorporate the -SO_2H and -SO_3H, respectively, in the copolymer. 1.0 mmol of $NaVBSO_2$ or $NaVBSO_3$, and 9.0 mmol of 2-hydrohyetyl methacrylate (HEMA, 95%, Wako Pure Chemical Industrial Ltd., Osaka, Japan) were dissolved in the ultra-pure water. Furthermore, 5.0×10^{-4} mol of *N N*'-methylenebisacrylamide (99%, Wako Pure Chemical Industrial Ltd.), 1.5×10^{-5} mol of *N*, *N*, *N*'-tetrametyletylenediamide (98%, Wako Pure Chemical Industrial Ltd.) and 2, 2'-azobis(2-methylpropionamidine)dihydrochloride (95%, Wako Pure Chemical Industrial Ltd.) were added. The mixture of these regents was adjusted to a total volume of 10 cm^3 in a volumetric flask with addition of ultra-pure water. In order to copolymerize

these monomers, 1 cm^3 of resulting solution put in the polyethylene cup at 60°C for 1 day.

The copolymers after polymerization were cut into cylinder of Φ5 mm × 1 mm in size, and then soaked in 1 $kmol \cdot m^{-3}$ HCl solution for 1 day to remove the unreacted regents and sodium. The copolymers were soaked in ultra-pure water for 1 day and died in vacuum. The obtained specimens were soaked in 0 or 2.5 $mol \cdot m^{-3}$ $CaCl_2$ solution at 36.5°C for 1 day. The different copolymers prepared from $NaVBSO_2$ and $NaVBSO_3$ were abbreviated as $VBSO_2$ xCa and $VBSO_3$ xCa, respectively, and x gives the concentration of the $CaCl_2$ solution used.

2.2 Soaking specimens in SBF and SBF1.5Ca for evaluation of apatite-forming ability

The cylinder-type composite specimens of $VBSO_2$ 2.5Ca and $VBSO_3$ 2.5Ca were soaked in 30 cm^3 of SBF (Na^+ 142.0, K^+ 5.0, Mg^{2+} 1.5, Ca^{2+} 2.5, Cl^- 147.8, HCO_3^- 4.2, HPO_4^{2-} 1.0, SO_4^{2-} 0.5 $mol \cdot m^{-3}$, pH7.40) for various interval.

In addition, 9 mg of powdered copolymer specimens prepared by clashing the cylinder specimens of $VBSO_2$ 0Ca and $VBSO_3$ 0Ca were soaked in SBF1.5Ca which has Ca^{2+} concentration 1.5 times of normal SBF (SBF1.5Ca) [24] with a pH 7.25 at 36.5°C for various periods.

SBF and SBF1.5Ca were prepared by following methods in the literature [8] and [9], respectively.

2.3 Soaking of specimens in Tris-NaCl buffer for measurement of Ca^{2+} release

The specimens were soaked in 30 cm^3 of Tris-NaCl buffer (NaCl 142, tris(hydroxymethyl)aminomethane 50 $mol \cdot m^{-3}$, pH7.40) at 36.5°C for various periods. The buffer was prepared through the method as described above in Chapter 2.

2.4 Characterization of the specimens

The chemical structure of different copolymers was analyzed by Fourier

transform infrared spectroscopy (FT-IR; FT/IR-6100, JASCO Co., Tokyo, Japan) using an attenuated total reflectance method. The content of acidic functional groups in the specimens were measured by neutralizing titration. The 30 cm^3 of 0.1 $kmol \cdot m^{-3}$ NaCl solution with soaking of specimens without Ca^{2+} was titrated with 10.0 $mol \cdot m^{-3}$ of NaOH solution. The point of neutralization was determined by change in pH of the solution measured using a pH meter (F-23IIC, Horiba Ltd., Kyoto, Japan). In order to determine the Ca content in the specimens, decrease in Ca concentration in the $CaCl_2$ solution after soaking of specimens were measured using inductively coupled plasma atomic emission spectrometry (ICP-AES; ICPE-9820, SHIMADZU Co., Kyoto, Japan).

The surface of the specimens after soaking in SBF or SBF1.5Ca were analyzed by thin-film X-ray diffraction (TF-XRD; MXP3V, Mac Science Co., Yokohama, Japan), energy dispersive X-ray analysis (EDX; EMAX Energy, Horiba Ltd) equipped with scanning electron microscope (SEM; S-3500N, Hitachi Co., Tokyo, Japan). In the TF-XRD analysis, incident X-ray (monochromatic CuKα radiation) was fixed at 1° relative to the surface of the specimen with a scan rate of $0.02° \cdot s^{-1}$. The surface of specimens after soaking in SBF1.5Ca were observed by SEM.

The concentration of Ca in the Tris-NaCl buffer, and Ca and P in SBF1.5Ca after soaking of specimens for various periods were measured using ICP-AES.

The ζ potential of powdered copolymer specimens without $CaCl_2$ treatment was measured by ζ-potential and particle size analyzer (Otsuka Electronic Co., Osaka, Japan). The Tris-NaCl buffer with soaking of specimens was injected into the quartz cell, and then the electrophilic mobility was measured by the laser Doppler method to calculate the ζ potential.

2.5 Determining the stability constant of the complex consisting Ca^{2+} and different acidic functional groups

The stability constant of complex, which consists Ca^{2+} and ligand of ionized *p*-toluenesulfinic acid or *p*-toluenesulfonic acid, was determined to compare the

thermodynamic stability of interaction between Ca^{2+} and each acid groups. 3.0 - 4.2 mmol of sodium *p*-toluenedulfinate (98%, Tokyo Chemical Industry Co., Ltd.) or p-toluenesulfonic acid monohydrate (99%, Wako Pure Chemical Industrial Ltd.) was dissolved in 30 cm^3 of 1.0 $mol \cdot m^{-3}$ $CaCl_2$ solution. The ion strength and pH were adjusted to μ=0.16 and 6.4-6.7, respectively, by addition of NaCl and tris(hydroxymethyl)aminomethane. The free Ca^{2+} concentration in the solution was measured using Ca^{2+}-selective electrode (6583-10C, Horiba Ltd.). The stability constant β of the Ca^{2+} complex was calculated by Enq. (1):

$$\beta = \frac{[L_2 \cdots Ca^{2+}]}{[L]^2[Ca^{2+}]} = \frac{[Ca^{2+}]_{total} - [Ca^{2+}]}{([L]_{total} - 2\{[Ca^{2+}]_{total} - [Ca^{2+}]_{free}\})^2[Ca^{2+}]}, \quad (1)$$

where the $[L_2 \cdots Ca^{2+}]$, [L], and $[Ca^{2+}]$ are molar concentration of complex, free ligand, and free Ca^{2+}, respectively. In addition, $[L]_{total}$, and $[Ca^{2+}]_{total}$ in the eqn.(1) also mean total concentration of ligand and Ca^{2+} in the solution, respectively.

3. Results

Figure 1 shows FT-IR spectra of different dried copolymer specimens before soaking in $CaCl_2$ solution. The peak of HEMA in the both spectra was observed at 1072 cm^{-1}, which was attributed to stretching vibration of O-C bond for alcohol [10]. In addition, the peaks corresponding to the vibration of CH_3 and torsion of the OH groups of HEMA were also observed at 1146-1148 cm^{-1}. For both specimens, in-plane deformation vibrations of C-H and stretching vibration of S=O bonds were also observed at 1030 and 1008 cm^{-1} [11], respectively. They were derived from both type of monomer containing sulfur. However, $VBSO_3$ displayed the peak corresponding to antisymmetric stretching vibration of O=S=O [12] at 1122 cm^{-1}, but not $VBSO_2$.

Figure 2 shows the content of sulfur-containing acidic functional groups and calcium in the different specimens. The measurement of acidic functional groups content

revealed that $VBSO_2$ and $VBSO_3$ contented the nearly equivalent level of each group. The results of the measurement indicate that 74 and 79% of additive amount of acidic functional groups were introduced into the copolymer structure of $VBSO_2$ and $VBSO_3$, respectively. On the other hand, the content of Ca in the $VBSO_3$ was slightly lower than that in $VBSO_2$.

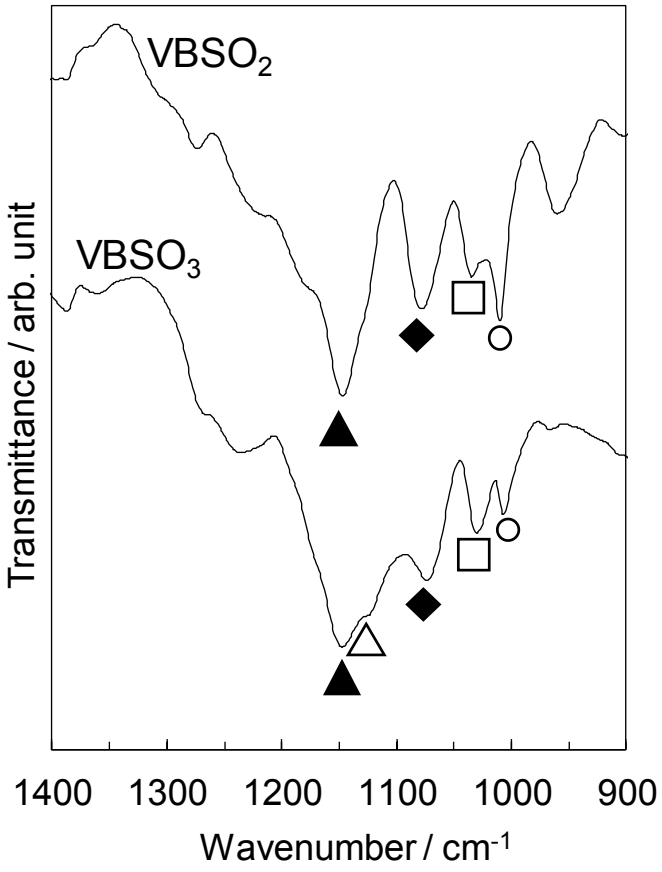

Figure 1 FT-IR spectra of different copolymer specimens before soaking in $CaCl_2$ solution (▲: γ(CH_3) or τ(OH) of HEMA; △:asymmetric stretching of O=S=O; ◆: ν(O-C) alcohol of HEMA; □: S=O bond of $VBSO_2$; ○: C-H bond of in-plane of $VBSO_3$ and $VBSO_2$ deformation; ν is the stretching; γ, the rocking; τ, the torsion).

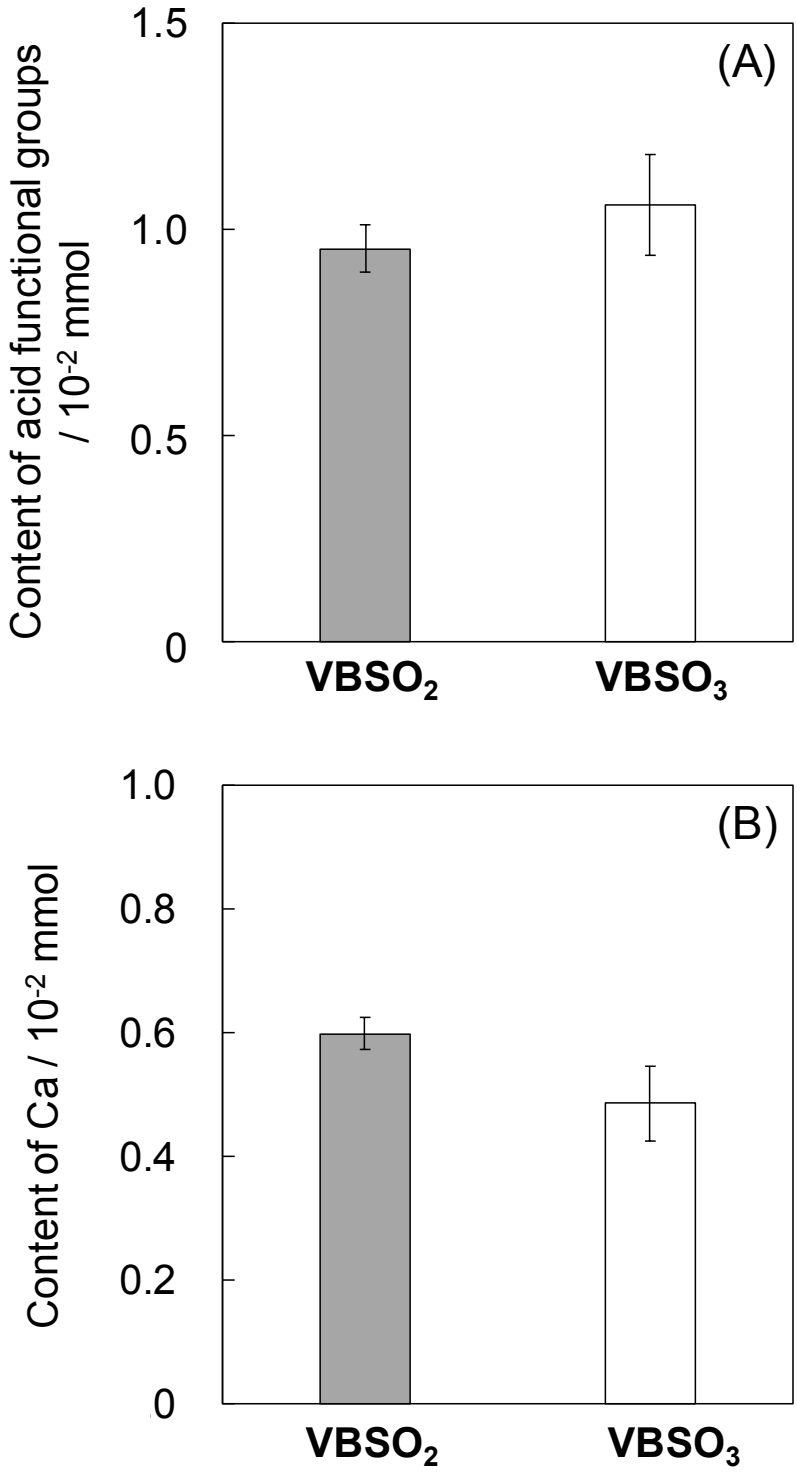

Figure 2 Content of sulfur-containing acidic functional groups (A) and Ca (B) in the different specimens.

Figure 3 shows the change in concentration of Ca in the Tris-NaCl buffer after soaking of the different composite specimens treated with $CaCl_2$ solution. The concentration of Ca was increased up to the 1 day after soaking both specimens. The Ca concentration after soaking of $VBSO_3$ 2.5Ca was higher than $VBSO_2$ 2.5Ca regardless of soaking time.

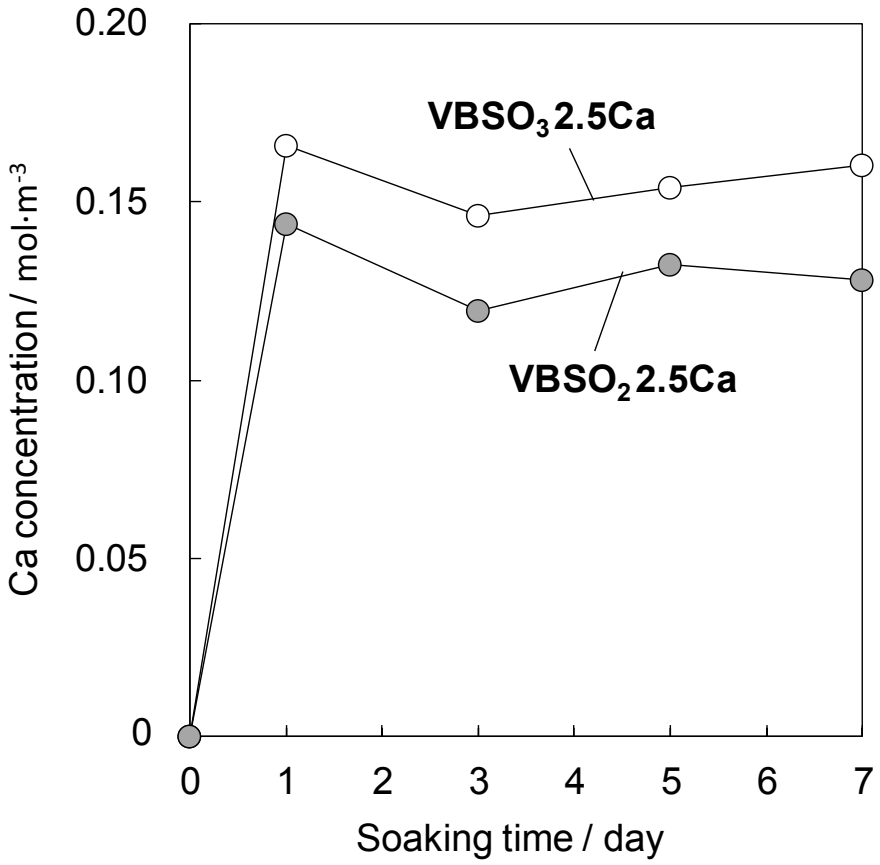

Figure 3 Change in concentration of Ca in Tris-NaCl buffer following soaking of the different composite specimens for various periods.

Figure 4 shows TF-XRD patterns of the composite specimens after soaking in SBF for various interval. The Peaks attributed to apatite (JCPDS #09-0432) were appeared in $VBSO_2$ 2.5Ca after 14 days. In contrast, the peaks corresponding to apatite were observed at $2\theta = 26$ and 32° in $VBSO_3$ 2.5Ca after 1 day.

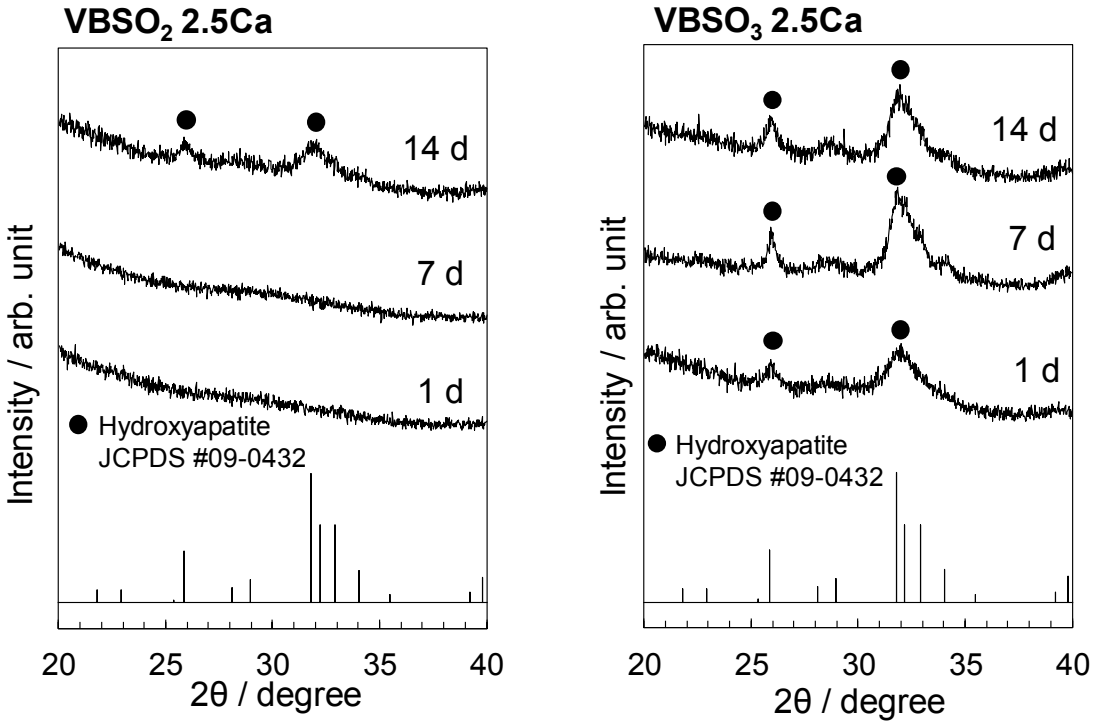

Figure 4 TF-XRD patterns of the different composite specimens after soaking in SBF for various periods.

Figure 5(A) shows the SEM images of powdered copolymer specimen without preliminary Ca^{2+} incorporation after soaking in SBF1.5Ca for various periods. The smooth surface was observed on the both $VBSO_2$ 0Ca and $VBSO_3$ 0Ca after 5 days. The deposition was observed on the only $VBSO_2$ 0Ca surface after 7 days. Figure 5(B) shows the high magnification SEM image of $VBSO_2$ 0Ca after 7 days and EDX spectra of deposition detected by point analysis using SEM-EDX. The hemispherical deposition was composed of primary particles which had the scale-like shape. The peaks of P, Ca and Mg were detected in the EDX spectra of the deposition. The molar ratio of Ca/P was 1.60. Thus, the morphology and the moral ratio of deposition were similar to the apatite formed in simulated body environment.

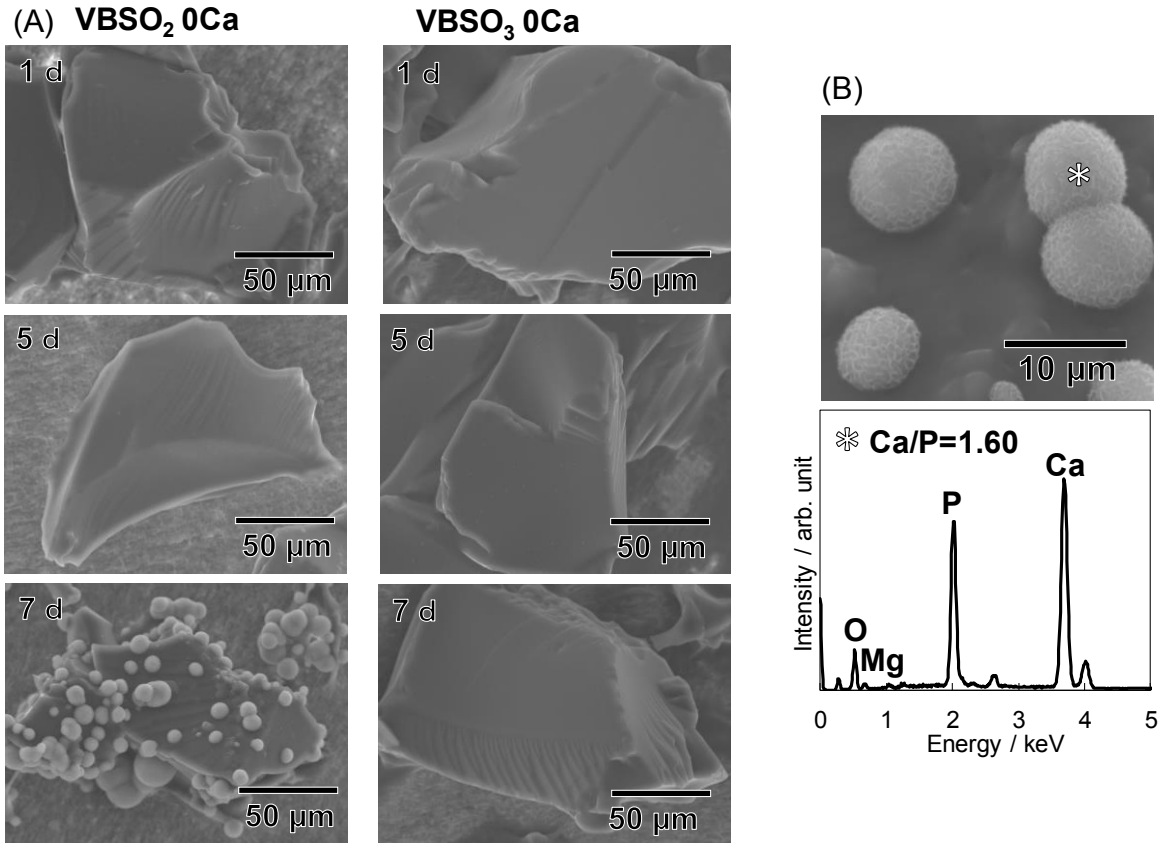

Figure 5 SEM images of the powdered copolymer specimens after soaking in SBF1.5Ca for various periods (A) and EDX spectra of deposition on the $VBSO_2$ 0Ca after soaking for 5 days observed at high magnification (B).

Figure 6 shows the change in concentration of Ca and P in SBF1.5Ca after soaking the powdered specimens of $VBSO_2$ 0Ca and $VBSO_3$ 0Ca for various periods. The decrease in Ca concentration was observed after soaking of both specimens. Subsequently, the Ca concentration was gradually decreased after soaking of $VBSO_2$ 0Ca, but it was almost constant after soaking of $VBSO_3$ 0Ca. After soaking of $VBSO_2$ 0Ca for 3 days, consumption of P concentration was observed. On the other hand, the P was slightly decreased after soaking of $VBSO_3$ 0Ca after 5 days.

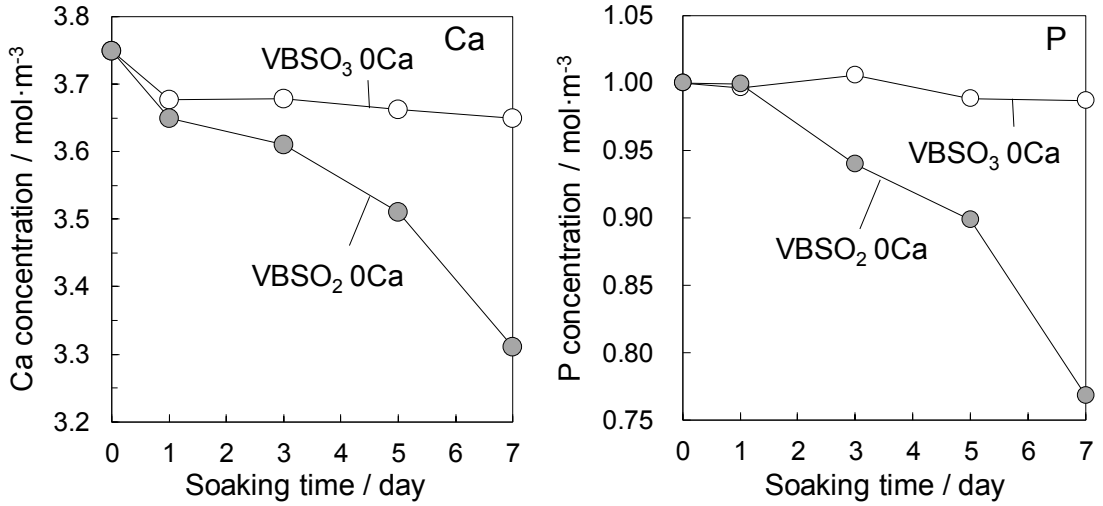

Figure 6 Change in concentration of Ca and P in SBF1.5Ca after soaking of the powdered copolymer specimens for various periods.

Table 1 shows ζ potential of powdered copolymer specimens after soaking in Tris-NaCl buffer and the stability constant of Ca^{2+} complex for the ionized *p*-toluenesulfinic acid and *p*-toluenesulfonic acid. The $VBSO_2$ 0Ca and $VBSO_3$ 0Ca had negatively potential and these values were near equivalent level at ion strength of physiological condition. The constant increased in this order: *p*-toluenesulfonic acid < *p*-toluenesulfinic acid.

Table 1 ζ potential of powdered copolymer specimens (n = 3) and stability constant (β) of Ca^{2+} complex consisting each acidic functional group at μ = 0.16.

	$VBSO_3$ 0Ca, $-SO_3H$	$VBSO_2$ 0Ca , $-SO_2H$
ζ potential / mV	-18.5±5.4	-16.8±2.3
log β	1.31	1.61

4. Discussion

The copolymers incorporated nearly equivalent amount of different acidic functional groups were prepared under the same method (see Figure 2(A)). The analysis of FT-IR spectra confirmed that $VBSO_2$ and $VBSO_3$ contained $-SO_2H$ and $-SO_3H$, respectively, as evidenced by the result that $VBSO_3$ displayed the peaks of O=S=O, but not $VBSO_2$ (see Figure 1). The composites of $VBSO_3$ 2.5Ca formed apatite after soaking in SBF within 1day, but not $VBSO_2$ (see Figure 4). This result revealed that $-SO_3H$ incorporated in the composites had more effective on the apatite formation on the composites than $-SO_2H$.

The apatite formation on the substrate depends on the condition of the substrate surface and supersaturation degree with respect to apatite in SBF [13]. Especially, the release of Ca^{2+} from the substrate accelerates the apatite formation due to the increase in the supersaturation degree [3]. It was confirmed by Ca^{2+} concentration measurement in Tris-NaCl buffer that $VBSO_3$ 2.5Ca could release more amount of Ca^{2+} than $VBSO_3$ 2.5Ca under the physiological condition (see Figure 3). It suggests that $VBSO_3$ 2.5Ca was able to increase the supersaturation degree to induce apatite formation in a short time.

However, the content of Ca in the $VBSO_3$ 2.5Ca was lower than that in the $VBSO_2$ 2.5Ca after soaking in $CaCl_2$ solution (see Figure 2 (B)). The Ca^{2+} release from composites into SBF was governed by not only Ca content, but also the binding with anionic functional groups. Previously, it has been reported that Ca^{2+} release was inhibited by increase in the amount of $-SO_3H$ in the nanocomposites *via* formation of complex such as $(-SO_3^-)_2\cdots Ca^{2+}$ [14]. In contrast, the composites were composed of different structure of acidic functional groups in this study. The stability constant of Ca^{2+} complex (see Table 1) indicates that $(-SO_2^-)_2\cdots Ca^{2+}$ showed more stable interaction than $(-SO_3^-)_2\cdots Ca^{2+}$. It is assumed that the effect of $-SO_3H$ on trapping the Ca^{2+} in the composites was weak for promoting the Ca^{2+} release in to the SBF *via* ion-ion interaction. Therefore, these results revealed that modification with $-SO_3H$ had advantage for apatite formation, because the low stability of the complex led to acceleration of Ca^{2+} release into SBF.

In the case of copolymer specimens without incorporation of Ca^{2+}, $VBSO_2$ 0Ca formed apatite faster than $VBSO_3$ 0Ca in SBF1.5Ca (see Figure 5). $VBSO_2$ 0Ca adsorbed larger amount of Ca and P than $VBSO_3$ 0Ca after they were soaked in SBF1.5Ca (see Figure 6). Thus, these results were considered that $-SO_2H$ on the surface of copolymer formed more amount of apatite nuclei or precursors than $-SO_3H$, when they were under the same level of supersaturation degree with respect to apatite in simulated body environment.

According to the mechanism of heterogeneous nucleation of apatite in previous reports, substrate initially adsorbs Ca^{2+}, and then phosphate ion on their surface to induce formation of calcium phosphate as apatite precursor in SBF [15-16]. Yamashita *et al.* reported that hydroxyapatite, which had the high negatively charged surface induced by electric poling, promoted apatite formation, because the adsorbed amount of Ca^{2+} increased on its surface [17]. Judging from these reports and higher rate of decrease in Ca concentration at initial stage of soaking (see Figure 6), it is assumed that $VBSO_2$ 0Ca had favorable surface for Ca^{2+} adsorption rather than $VBSO_3$ 0Ca and it enhanced reaction between Ca^{2+} on its surface and phosphate ion in SBF1.5Ca.

On the other hand, not only negatively surface charge [16-17] but also ion-ion interaction with Ca^{2+} [18] were considered as the factor of the Ca^{2+} adsorption for apatite formation. There was no difference in the ζ potential on each specimen, whereas stability constants of complex were changed by the modification with the different structure of acidic functional groups (see Table 1). It means that the structural difference contributed to the chemical interaction with Ca^{2+} significantly more than the surface potential for Ca^{2+} adsorption. Therefore, it is assumed that ionized $-SO_2H$ which bound to Ca^{2+} *via* stable chemical interaction enhanced Ca^{2+} adsorption for their higher ability to induce the apatite nucleation in simulated body environment.

In conclusion, the results of this study revealed that low stability of $-SO_3^-\cdots Ca^{2+}$ improves the apatite-forming ability of the polymer-$CaCl_2$ composites, although the stability of $-SO_2^-\cdots Ca^{2+}$ had higher ability of the inducing heterogeneous nucleation. The

reason for this phenomenon is considered that increase in the supersaturation degree contributed strongly to not only decrease in activation free energy for heterogeneous nucleation, but also subsequent crystal growth. On the other hand, the Ca^{2+} bound to the Ti surface played a role as adsorbed site of the proteins leading to the osteoblast adhesion [19-20]. Thus, it is also expected that the structure of sulfur-containing functional groups affects the bone-bonding ability through the state of binding with Ca^{2+}. To reveal this point, the behavior of protein adsorption and the activity of the osteoblast-like cells on the composites modified with these groups should be investigated in future work.

5. Conclusion

The apatite-forming behavior of polymer-$CaCl_2$ composites and copolymers modified with $-SO_2H$ or $-SO_3H$ was examined in simulated body environment. When composites released Ca^{2+}, $-SO_3H$ formed apatite faster than $-SO_2H$ on the surface, because low stability of $-SO_3^-\cdots Ca^{2+}$ had advantage for Ca^{2+} release to increase the supersaturation degree with respect to apatite in SBF. In contrast, high stability of interaction of $-SO_2^-\cdots Ca^{2+}$ enhanced the ability of heterogeneous nucleation of apatite on the polymer which did not released Ca^{2+} into the fluid. It was revealed that the lower stability of interaction with Ca^{2+} attributed to the structure of these groups is an important factor for preparation of composites exhibiting bone-bonding ability in terms of the apatite formation.

Reference

[1] L.L Hench, "Bioceramics," *J. Am. Ceram. Soc.*, **81**, 1707-1728 (1998).

[2] T. Kokubo, H.-M. Kim, M. Kawashita, "Novel bioactive materials with different mechanical properties," *Biomaterials*, **24**, 2161-2175 (2003).

[3] C. Ohtsuki, T. Kokubo, T. Yamamuro, "Mechanism of apatite formation on CaO-SiO_2-P_2O_5 glass in a simulated body fluid," *J. Non-Cryst. Solids*, **143**, 84-92 (1992).

[4] R. Nakata, T. Miyazaki, Y. Morita, E. Ishida, R. Iwatsuki, C. Ohtsuki, "Apatite formation abilities of various carrageenan gels in simulated body environment," *J. Ceram. Soc. Jpn.*, **118**, 487-490 (2010).

[5] I.Y. Kim, R. Iwatsuki, K. Kikuta, Y. Morita, T. Miyazaki, C. Ohtsuki, "Thermoreversible behavior of κ-carrageenan and its apatite-forming ability in simulated body fluid," *Mater. Sci. Eng. C,* 31, 1472-1476 (2011).

[6] P.M. López-Pérez, R.M. Silva, R.A. Sousa, I. Pashkuleva, R.L. Reis, "Plasma-induced polymerization as a tool for surface functionalization of polymer scaffolds for bone tissue engineering: An in vitro study," *Acta Biomater.*, 6, 3704-3721 (2010).

[7] D.D. Perrin, B. Dempesy, E.P. Serjeant, "Molecular factor that modify pK_a value," *pK_a prediction for organic acid and bases* (D.D. Perrin, B. Dempsey, E.P. Serjeant ed.), Springer, 12-20 (1981).

[8] T. Kokubo, H. Takadama, "How useful is SBF in predicting in vitro bone bioactivity?," *Biomaterials*, **27**, 2907-2915 (2006).

[9] S.B Cho, F. Miyaji, T. Kokubo, N. Nakanishi, N. Soga, T. Nakamura, "Apatite formation on various silica gels in a simulated body fluid containing excessive calcium ion," *J. Cream. Soc. Jpn.*, **104**, 399-404 (1996).

[10] L. Ferreira, M.M. Vidal, M.H. Gil, "Evaluation of poly(2-hydroxyethyl methacrylate) gels as drug delivery system at different pH value," *Int. J. Pharm.*, **194**, 169-180 (2000).

[11] C. Halm, J. Evarts, M.J. Kurth, "A new attachment / cleavage strategy: polymer-bound allylic sulfones in a solid-phase route to trisubstituted olefins," *Tetrahedron. Lett.*, **38**, 7709-7712 (1997).

[12] V. Chiono, I. Carmagnola, P. Gentile, F. Boccafoschi, C. Tonda-Turo, M. Ballarini, V. Georgieva, G. Georgiev, G. Ciardelli, "Layer-by-layer coating of photoactive polymers for biomedical applications," *Surf. Coat. Tech.*, **206**, 2446-2453 (2012).

[13] T. Kawai, C. Ohtsuki, M. Kamitakahara, M. Tanihara, T. Miyazaki, Y. Sakaguchi, S.

Konagaya, “A comparative study of apatite deposition on polyamide films containing different functional groups under a biomimetic condition,” *J. Ceram. Soc. Jpn.*, **113**, 588-592 (2005).

[14] T. Miyazaki, M. Imamura, E. Ishida, M. Ashizuka and C. Ohtsuki, “Apatite formation abilities and mechanical poperties of hydroxyethylmethacrylate-based organic-inorganic hybrids incorporated with sulfonic groups and calcium ions,” *J. Mater. Sci: Mater. Med.*, **20**, 157-161 (2009).

[15] H. Takadama, H.-M Kim, T. Kokubo, T. Nakamura, “An X-ray photoelectron spectroscopy study of the process of apatite formation on bioactive titanium metal,” *J. Biomed. Mater. Res.*, **55**, 158-193 (2001).

[16] H.-M. Kim, T. Himeno, T. Kokubo, T. Nakamura, “Process and kinetics of bonelike apatite formation on sintered hydroxyapatite in a simulated body fluid,” *Biomaterials*, **26**, 4366-4373 (2005).

[17] K. Yamashita, N. Oikawa, T. Umegaki, “Acceleration and deceleration of bone-like crystal growth on ceramic hydroxyapatite by electric poling,” *Chem. Mater.*, **8**, 2697-2700 (1996).

[18] M. Tanahashi, T. Matsuda, “Surface functional group dependence on apatite formation on self-assembled monolayers in a simulated body fluid,” *J. Biomed Mater. Res.*, **34**, 305-315 (1997).

[19] B. Feng, J. Weng, B.C. Yang, S.X. Qu, X.D. Zhang, “Characterization of titanium surface with calcium and phosphate and osteoblast adhesion,” *Biomaterials*, **25**, 3421-3428 (2004).

[20] L. Zhang, Y. Ayukawa, R.Z. LeGeros, S. Matsuya, K. Koyano, K. Ishikawa, “Tissue-response to calcium-bonded titanium surface,” *J. Biomed. Mater. Res. A.*, **95A**, 33-39 (2010).

General Summary

This thesis has described a fundamental investigation of apatite-forming behavior on the surface of the organic-inorganic composites modified with phosphorus- or sulfur-containing acidic functional groups to design novel bone substitutes showing bone-bonding ability. Apatite-forming ability has been considered as one of the essential properties of bone substitutes to be able to bond with bone tissue. The relationship between apatite formation in simulated body fluid (SBF) and chemical structure variations of the copolymer modified with these acidic functional groups as matrix of composites was discussed. In each Chapter, the results of this study were summarized as follows.

In Chapter 1, effects of polymerization accelerator on chemical durability and apatite formation of the copolymer modified with phosphonic acid were examined in SBF. The various amount of sodium *p*-toluenesulfinate (*p*-TSS) as the accelerator were added, while vinylphosphonic acid (VPA) and triethylene glycol dimethacrylate (TEGDMA) were copolymerized *via* photo induced radical polymerization. Increase in additive amount of *p*-TSS increased the phosphate group content and molecular weight in VPA-TEGDMA copolymer. The addition of 0.1-1.0 wt% of *p*-TSS relative to total amount of monomers inhibited the dissolution of the copolymer and decreased the pH in SBF. In contrast, phosphate groups-containing polymers were dissolved when adding with 3.0-5.0 of *p*-TSS, because increase in the phosphate content led to the hydrolysis of polymer chain. All copolymers formed no apatite in SBF, despite that the 0.1-1.0 wt% of *p*-TSS could improve the chemical durability of the copolymer. These results suggest that the existence of phosphate groups provided by VPA was insufficient to induce apatite formation on the surface of the organic matrix in SBF.

In Chapter 2, effects of phosphate group content on apatite-forming behavior of poly(VPA-2-hydroxyethylmethacrylate (HEMA)-TEGDMA)-$CaCl_2$ composites modified with different amounts of phosphate groups were examined in SBF. When the

additive amount of TEGDMA was fixed at 5 mol% relative to total amount of monomers in molar ratio, the Ca content was increased as increase in molar ratio of VPA/HEMA, after the copolymers were treated with $CaCl_2$ solution. Although the released amount of Ca into SBF also increased with the increase in VPA. Apatite was formed only on the composites added with less than 1 mol% of VPA in SBF. Surface ζ potential of the composites added with 1 mol% of VPA converted negative into positive in SBF. However, such conversion did not occur on the surface of composites added with 10 mol% of VPA. These phenomena was reflected by the formation of $-PO_3^{2-}\cdots Ca^{2+}$ and suppression of phosphate ion adsorption on the surface of composites added with. These results indicate that phosphate group content governed apatite formation on the poly(VPA-HEMA-TEGDMA)-$CaCl_2$ composites via surface state rather than the Ca^{2+} release.

In Chapter 3, the structural effects of phosphate groups on apatite-forming behavior of polymer-$CaCl_2$ composites were examined and clarified why the phosphate groups provided from VPA suppressed apatite formation in SBF. The composites modified with $-O-PO_3H_2$ and $-C-PO_3H_2$ were synthesized from poly(methacryloyloxyethyl phosphate-HEMA-TEGDMA) and poly(VPA-HEMA-TEGDMA), respectively. The composites modified with $-O-PO_3H_2$ formed apatite in SBF, but not those modified with $-C-PO_3H_2$, even if both consisted of equivalent amount of each type of phosphate group and released similar amounts of Ca^{2+} into the SBF. In SBF, adsorption of HPO_4^{2-} is followed by adsorption of Ca^{2+} only on the composites consisting of $-O-PO_3H_2$. The measurement of the stability constant of Ca^{2+} complex revealed that $CaHPO_4$ was formed on the surface of composites, because $-O-PO_3^{2-}\cdots Ca^{2+}$ complex was more unstable than that of $Ca^{2+}\cdots HPO_4^{2-}$. On the other hand, the $-C-PO_3^{2-}\cdots Ca^{2+}$ complex was too stable to form $CaHPO_4$. These results conclude that formation of $CaHPO_4$-based clusters was a key factor for heterogeneous nucleation of apatite on the surface of polymer-$CaCl_2$ composites.

In Chapter 4, the apatite-forming ability of sulfinic acid ($-SO_2H$) groups on the surface of polymer-$CaCl_2$ composites was investigated in SBF. The composites were

prepared from sodium 4-vinylbenzene sulfinate ($NaVBSO_2$) and HEMA. The composites of poly($NaVBSO_2$-HEMA)-$CaCl_2$ formed an apatite layer showing tight adhesion to their surface. In contrast, poly(HEMA)-$CaCl_2$ formed spherical depositions of apatite which were easily peeled from the substrate. The apatite-forming behavior of the composite incorporated with -SO_2H was similar to that of polymer film modified with -COOH groups. These results found that ionized -SO_2H groups which bound to Ca^{2+} *via* ion-ion interaction were also able to induce heterogeneous nucleation of apatite in SBF.

In Chapter 5, effects of structural difference in sulfur-containing acidic functional groups on the polymer-$CaCl_2$ composites were examined in SBF. The composites modified with -SO_3H and -SO_2H were prepared from poly(4-vinylbenzene sulfononic acid-HEMA) or poly(4-vinylbenzene sulfinic acid-HEMA), respectively. The difference in magnitude of the stability constant of complex indicates that the thermodynamic stability of $(-SO_2^-)_2\cdots Ca^{2+}$ was higher than that of $(-SO_3^-)_2\cdots Ca^{2+}$ under physiological condition. Although the Ca^{2+} content in the composites consisting of -SO_3H was lower than that of -SO_2H, this lower stability of interaction led to acceleration of Ca^{2+} release and apatite formation on them. When all copolymers did not contain Ca^{2+}, the high stability contributed to high ability to induce apatite formation on the surface modified with -SO_2H. The reason why the different nucleation behavior was different is that more amount of Ca^{2+} adsorbed on the surface with -SO_2H than that with -SO_3H. These results indicate that the stability of interaction with Ca^{2+} was depended on the difference in the structure of the sulfur-containing functional groups and it affected not only the formation of apatite nuclei, but also the Ca^{2+} release to promote crystal growth of apatite on the composites in SBF.

From these results, it was revealed that the stability of interaction between Ca^{2+} and ionized acidic functional groups depended on the modification amount and chemical structure of the acidic functional groups affects apatite formation on the composites in SBF. Especially, difference in specific structure of phosphate groups governs the ability to induce heterogeneous nucleation of apatite. When comparing the stability constant of

Ca^{2+} complex in phosphorus- or sulfur-containing acidic functional groups and HPO_4^{2-}, the stability to bind with Ca^{2+} increase in this order: $-SO_3^-$ < $-SO_2^-$ << $-O-PO_3^{2-}$ < HPO_4^{2-} < $-C-PO_3^{2-}$. The apatite nucleation occurred on the surface modified with $-O-PO_3^{2-}$, $-SO_2^-$ and $-SO_3^-$ whose stability constant of complex were lower than that of HPO_4^{2-} under physiological condition. On the other hand, the polymer surface modified with $-C-PO_3H_2$ and $-SO_2H$ had a near level of the initial ζ potential in physiological condition, but only the latter formed apatite. This means that this magnitude of biding stability with Ca^{2+} based on $CaHPO_4$ complex is considered as an important factor of surface condition to form apatite induced by existence of acidic functional groups on the composite in SBF.

The obtained results in this study provide the information to design the chemical structure of the bone-bonding bioactive composite applied as bone substitutes in terms of apatite formation in body environment. On the other hand, the adsorption of proteins in serum and subsequent osteoblast adhesion on the materials through the Ca^{2+} existing on the surface of the materials are expected to be a factor of expression of bone-binding ability. If the effects of the binding stability between Ca^{2+} and functional groups on the protein adsorption are also clarified, it would be a guideline to select the chemical structure of composite showing high activity to bond with bone tissue.

List of Publications

The present thesis "**Apatite Formation on Organic-inorganic Composites Modified with Phosphorus- or Sulfur-containing Functional Groups in Simulated Body Environment**" is based on the following publication.

Journal Papers

Chapter 1

R. Hamai, Y. Shirosaki, T. Miyazaki, "Biomineralization Behavior of a Vinylphosphonic Acid-based Copolymer added with Polymerization Accelerator in Simulated Body Fluid," *Journal of Asian Ceramic Societies*, **3**, 407-411 (2015).

Chapter 2

R. Hamai, Y. Shirosaki, T. Miyazaki, "Apatite-forming Ability of Vinylphosphonic Acid-based Copolymer in Simulated Body Fluid: Effects of Phosphate Group Content," *Journal of Materials Science: Materials in Medicine*, **27**, 152 (2016).

Chapter 3

R. Hamai, H. Maeda, H. Sawai, Y. Shirosaki, T. Kasuga and T. Miyazaki, "Structural Effects of Phosphate Groups on Apatite Formation in Copolymer Modified with Ca^{2+} in a Simulated Body Fluid" *Journal of Materials Chemistry B*, **6**, 174-182 (2018).

Chapter 4

R. Hamai, Y. Shirosaki, T. Miyazaki, "Apatite Formation on a Hydrogel Containing Sulfinic Acid Group under Physiological Conditions", *Journal of Biomedical Materials Research: Part B - Applied Biomaterials*, **105B**, 1924-1929 (2017).

Chapter 5

R. Hamai, Y. Shirosaki, T. Miyazaki, "Structural Effects of Sulfur-containing Functional Groups on Apatite Formation on a Polymer-Ca^{2+} Hybrids in a Simulated Body Environment," *ACS Biomaterials Science & Engineering*, submitted.

Acknowledgments

The present studies in this thesis has been carried out under the direction of Professor Dr. Toshiki Miyazaki, Graduate School of Life Science and Systems Engineering, Kyushu Institute of Technology. The author would like to express his sincere gratitude to Professor Toshiki Miyazaki for his encouragement and valuable advice all through the present works.

The author is sincerely grateful to Professor Dr. Yuki Shirosaki, Graduate School of Engineering, Kyushu Institute of Technology for her helpful advices and discussions, and students in Laboratory of Biofunctional Materials, Graduate school of Life Science and Systems Engineering, Kyushu Institute of Technology for helpful supports.

The author is also deeply grateful to Professor Dr. Hidenori Era, Graduate school of Engineering, Kyushu Institute of Technology, Professor Dr. Satoshi Iikubo and Professor Dr. Toshinari Maeda, Graduate School of Life Science and Systems Engineering, Kyushu Institute of Technology for their helpful support and suggestion.

The author's deeply gratitude goes to Professor Dr. Toshihiro Kasuga and Professor Dr. Hirotaka Maeda, Department of Life Science and Applied Chemistry, Nagoya Institute of Technology for their support in chemical calculation and valuable advice, Dr. Hikaru Sawai, Fukushima Prefectural Centre for Environmental Creation and Institute of Environment Radioactivity for his technical supports of analytical experiments, Mr. Masatoshi Takeo at Center for Instrumental Analysis, Kyushu Institute of Technology for his support of XPS analysis, Professor Dr. Masakazu Kawashita, Graduate School of Biomedical Engineering, Tohoku University for his valuable suggestions and supports in the experiments, and Professor Dr. Chikara Ohtsuki, Graduate School of Engineering, Nagoya University for his helpful advice, The professors, Doctors and students,

Division of Ceramics in Medicine, Biology and Biomimetics, The Ceramic Society of Japan for their helpful advice and suggestions.

Finally, the author expresses his hearty gratitude to his parents and sister for their warn understanding and continuing encouragement during long year.

March 2018

Ryo Hamai